

# **High-resolution characterization of structural changes involved in prion diseases and dialysis-related amyloidosis**

Dissertation

zur Erlangung des mathematisch-naturwissenschaftlichen Doktorgrades

"Doctor rerum naturalium"

der Georg-August-Universität Göttingen

vorgelegt von

Lukasz Skora

aus Gdansk, Polen

Göttingen 2009

Referent:

Prof. Dr. Markus Zweckstetter, Max-Planck-Institut für biophysikalische Chemie

Koreferent:

Prof. Dr. Reinhard Jahn, Max-Planck-Institut für biophysikalische Chemie

Mitglied des Betreuungsausschusses:

Prof. Dr. Christian Griesinger, Max-Planck-Institut für biophysikalische Chemie

Mitglied des Betreuungsausschusses:

Dr. Thomas M. Jovin, Max-Planck-Institut für biophysikalische Chemie

Tag der mündlichen Prüfung:

## **Declaration**

I hereby declare that the thesis “High-resolution characterization of structural changes involved in prion diseases and dialysis-related amyloidosis” has been written independently and with no other sources and aids than quoted.

Lukasz Skora  
Göttingen, June 2009

# Acknowledgements

I would like to thank everyone who by their friendliness and help supported me during the time spent in Goettingen, in particular:

My supervisor, **Prof. Dr. Markus Zweckstetter**, for his support and guidance and for giving me the possibility to work independently in his group.

The director of the department, **Prof. Dr. Christian Griesinger**, for the opportunity to conduct my studies in an excellent scientific environment, stimulating discussions and for his constant interest in my projects.

**Prof. Dr. Reinhard Jahn** and **Dr. Thomas M. Jovin** for agreeing to be members of my thesis committee and for valuable feedback during the thesis committee meetings.

**NEUREST** and **Dr. Joachim Bormann** for providing excellent financial support of my work.

My collaborators at the Department of Neuropathology of the Georg August University in Goettingen, **Dr. Jens Watzlawik**, **Dr. Michael Kramer** and **Dr. Walter Schulz-Schaeffer**, for initiating the prion project and the great cooperation.

**Dr. Dietmar Riedel** for acquiring electron micrographs and **Dr. Gerhard Wolf** for assistance in peptide synthesis and mass spectrometry.

**Dr. Stefan Becker** and **Karin Giller** for training in protein expression and purification and invaluable help in the bio-labs.

**Dr. Vinesh Vijayan**, **Dr. Christophe Fares** and **Dr. Min-Kyu Cho** for sharing their extensive knowledge in NMR spectroscopy, and the long but exciting hours spent on troubleshooting the spectrometers.

**Dr. Dirk Bockelmann** and **Raghavendran Lakshmi** for their thorough help with software and scripting and for being there whenever the computers failed to do what I wanted.

**Elisabeth Kaehler** and **Carsten Siebenhaar**, who provided huge help by taking over some of my duties during their internships.

**Mrs. Siegrid Silberer** and **Eva Strehler** for assistance in dealing with bureaucracy and any paper work.

All the former and present members of the group and the colleagues at the institute, who in various ways contributed to the nice working atmosphere and made my stay in Goettingen a very pleasant one. I would especially like to mention: **Nicolas, Min-Kyu, Hai-Young, Donghan, Sebastian, Stefan, Pierre, Fernando, Laura, Mitch, Christophe, Pinar, Elif, Soledad, Valeria, Vinesh, Shyamala, Kamila, Adema, ShengQi and Ulli.**

Very special thanks go to **Ola, Julia, Pawel, Tomek and Dorian** for their friendship, continuous support despite the many kilometers in between, and their tolerance and understanding when I was ‘too busy to call’.

**Evelina and Blago** for sharing their time with me, lots of moral support and all the great fun we had together in and out of Goettingen.

I would like to express my gratitude to **my parents** and **my brother** for always supporting my education, motivating me to reach higher and set new goals, and giving me the strength to survive the long years away from home and finish this thesis.

Finally, I would like to thank **Petya** for her love and enormous inner strength to put up with me and always stand by my side.

## Summary

Protein aggregation is the cause of several human diseases such as diabetes mellitus type 2, Parkinson's disease, Alzheimer's disease, Huntington's disease, spongiform encephalopathies, congestive heart failure or dialysis-related amyloidosis. All of these disorders result from protein misfolding which leads to fibrillization and deposition of amyloid plaques in different parts of the body.

Due to high molecular weight of the amyloid fibrils and intrinsic heterogeneity of the intermediate states, protein aggregation is a very challenging field of study for the structural biologist. However, nuclear magnetic resonance (NMR) provides a unique possibility to investigate aggregation at all stages, from the monomer to the fibrils.

In this work, structural changes involved in prion diseases and dialysis-related amyloidosis are investigated with the help of various NMR techniques.

Prion diseases are caused by the aggregation of the natively  $\alpha$ -helical prion protein PrP<sup>C</sup> into its pathological  $\beta$ -sheet-rich isoform PrP<sup>Sc</sup>. While the mechanism of conversion remains unclear, several models of PrP<sup>Sc</sup> have been proposed. Most of them originate from the assumption that, upon aggregation of the prion protein, helix 1 is converted into  $\beta$ -sheet. In **Chapter 3**, using different stop mutants of the human prion protein, it is shown that no such conversion occurs. Moreover, evidence is provided that while helix 1 region promotes aggregation of the protein, it is not resistant to proteinase K digestion and therefore not converted into a  $\beta$ -strand. Investigation of solvent protection of PrP fibrils reveals increased flexibility of helix 1 and  $\beta$ -strand 2 regions and identifies a small, rigid fibrillar core comprising four  $\beta$ -strands. Importantly, residues responsible for the species barrier and the M/V polymorphism at codon 129 are found to be deeply buried in the core of humPrP fibrils. Furthermore, it is shown that the fibrillar forms of different stop mutants of the human prion protein share common structural features. Finally, based on the available data a model for PrP<sup>Sc</sup> is proposed.

The second protein misfolding diseases studied here is dialysis related amyloidosis. The disease is observed in patients with chronic renal failure undergoing long-term hemodialysis and is caused by aggregation of beta-2-microglobulin (h $\beta$ 2m) - the light chain of the type I major histocompatibility complex. Due to its low molecular weight (11kDa) and a well-defined seven-stranded  $\beta$ -sandwich native fold, h $\beta$ 2m is considered a very good model

for studying all amyloid disorders. In **Chapter 4**, structural differences between two acid-denatured intermediate states of h $\beta$ 2m are shown, and experimental data is presented that strongly suggests an effect of the dynamics of the precursor ensembles on the morphology of the resulting fibrils. Furthermore, new information on solvent protection of the amyloid aggregates is provided and flexible regions within the fibrils of h $\beta$ 2m are identified.

Independent of the above-mentioned projects, a study on the effects of electrostatic interactions on molecular alignment of intrinsically unstructured proteins is presented in form of a reprint in **Appendix A**. Weak molecular alignment is required in NMR for observation of dipolar couplings, which are a sensitive probe of the structure and dynamics of biomolecules. It is demonstrated that alignment of disordered proteins depends critically on electrostatic interactions, is scaled with the ionic strength of the solution, and can be predicted using a simplified electrostatic model.

# Table of Contents

<b>Acknowledgements</b> .....	i
<b>Summary</b> .....	iii
<b>Table of Contents</b> .....	v
<b>List of Figures</b> .....	vii
<b>List of Tables</b> .....	ix
<b>Abbreviations</b> .....	x
<b>1. Introduction</b> .....	1
<b>1.1. Protein folding, misfolding and aggregation</b> .....	1
<b>1.2. NMR methods to study amyloid disorders</b> .....	5
1.2.1. Quenched H/D exchange .....	6
1.2.2. HR-MAS .....	8
<b>2. Materials and Methods</b> .....	10
<b>2.1. Materials</b> .....	10
2.1.1. Chemicals .....	10
2.1.2. Enzymes and DNA-Kits .....	10
2.1.3. Oligonucleotides .....	10
2.1.4. Plasmids .....	11
2.1.5. <i>Escherichia coli</i> strains .....	11
2.1.6. Chromatography resins .....	12
2.1.7. Software .....	12
2.1.8. Buffers and solutions .....	13
<b>2.2. Prion protein methods</b> .....	14
2.2.1. Safety considerations .....	14
2.2.2. Cloning of His6-tagged humPrP <sub>23-159</sub> .....	14
2.2.3. Cloning of shPrP <sub>23-159</sub> .....	15
2.2.4. Expression of prion protein mutants for NMR .....	16
2.2.5. Purification of non-tagged prion protein .....	16
2.2.6. Fast purification of non-tagged prion proteins .....	18
2.2.7. Purification of His6-tagged humPrP <sub>23-159</sub> .....	18
2.2.8. Aggregation .....	19
2.2.9. H/D exchange .....	19
<b>2.3. Beta-2-microglobulin methods</b> .....	19
2.3.1. Cloning of h $\beta$ 2m into pET32a .....	19
2.3.2. Protein expression .....	21
2.3.3. Purification of h $\beta$ 2m .....	21
2.3.4. Preparation of amyloid fibrils .....	22
2.3.5. H/D exchange .....	22
<b>2.4. NMR spectroscopy</b> .....	23
2.4.1. Backbone resonance assignments .....	23
2.4.2. Secondary structure determination .....	25
2.4.3. High-resolution magic angle spinning .....	25
2.4.4. Measurement of diffusion coefficients .....	26
2.4.5. Residual dipolar couplings .....	26
2.4.6. NMR-detection of H/D exchange rates .....	27
2.4.7. Structural predictions with CS-Rosetta .....	27
<b>3. Human prion protein</b> .....	29
<b>3.1. Introduction</b> .....	29



3.1.1. Transmissible spongiform encephalopathies.....	29
3.1.2. The “protein only” hypothesis .....	31
3.1.3. The species barrier.....	33
3.1.4. Prion protein .....	34
3.1.5. Structural models of PrP <sup>SC</sup> .....	36
<b>3.2. Results</b> .....	<b>39</b>
3.2.1. Secondary structure analysis of human prion protein mutants.....	39
3.2.2. Aggregation and proteinase K digestion of amyloid fibrils of the prion protein.....	43
3.2.3. NMR-detected H/D exchange studies of the prion protein mutants.....	47
3.2.4. Structural models of the core of human prion protein fibrils .....	53
<b>3.3. Discussion</b> .....	<b>58</b>
3.3.1. The role of helix 1 in the aggregation of human prion protein.....	58
3.3.2. Evaluation of structural models of PrP <sup>SC</sup> .....	59
3.3.3. Core of amyloid fibrils of human prion protein stop mutants .....	61
3.3.4. Implications for prion protein polymorphism and the species barrier.....	63
3.3.5. Conclusions and outlook .....	65
<b>4. Human beta-2-microglobulin</b> .....	<b>66</b>
<b>4.1. Introduction</b> .....	<b>66</b>
4.1.1. $\beta$ -2-microglobulin and dialysis-related amyloidosis.....	66
4.1.2. Folding, unfolding and aggregation of h $\beta$ 2m.....	67
4.1.3. Variants of h $\beta$ 2m.....	69
<b>4.2. Results</b> .....	<b>70</b>
4.2.1. Acid denaturation of h $\beta$ 2m .....	70
4.2.2. Structural analysis of the unfolded states.....	72
4.2.3. Observation of flexible regions in h $\beta$ 2m fibrils .....	77
4.2.4. Mapping the core of h $\beta$ 2m fibrils by H/D exchange .....	79
<b>4.3. Discussion</b> .....	<b>81</b>
<b>Literature</b> .....	<b>88</b>
<b>Appendix A. Charge-induced molecular alignment of intrinsically disordered proteins</b> .....	<b>100</b>
<b>Appendix B. Chemical shift lists</b> .....	<b>105</b>
<b>Appendix C. H/D exchange data of humPrP<sub>23-159</sub></b> .....	<b>115</b>
<b>Appendix D. CS-Rosetta output table</b> .....	<b>116</b>
<b>Curriculum vitae</b> .....	<b>122</b>
<b>Publications</b> .....	<b>123</b>

## List of Figures

Figure 1-1. Schematic representation of folding energy landscapes.....	1
Figure 1-2. Factors influencing protein folding and aggregation <i>in vivo</i> .....	2
Figure 1-3. Characteristics of amyloid proteins.....	4
Figure 1-4. Schematic representation of the NMR-detected H/D exchange experiment.....	7
Figure 1-5. High-resolution magic angle spinning.....	8
Figure 2-1. Vector map of pET14b plasmid coding for humPrP <sub>23-159</sub> .....	15
Figure 2-2. Vector map of pET26b plasmid coding for shPrP <sub>23-159</sub> .....	16
Figure 2-3. Vector map of pET32a plasmid coding for human beta-2-microglobulin.....	20
Figure 2-4. HNN pulse sequence.....	24
Figure 2-5. Pulse sequence of <sup>13</sup> C-detected CON-IPAP.....	25
Figure 2-6. Pulse sequence of LED sequence with bipolar gradients.....	26
Figure 3-1. Comparison of the incidence of BSE in cattle and vCJD in humans.....	31
Figure 3-2. Mechanistic models for PrP <sup>SC</sup> formation.....	32
Figure 3-3. Cross species transmission modelled by seeded aggregation.....	34
Figure 3-4. Structure of the human prion protein.....	35
Figure 3-5. Structural models of PrP <sup>SC</sup> .....	38
Figure 3-6. Schematic representation of the human prion protein stop mutants.....	39
Figure 3-7. Assignment of PrP stop mutants.....	40
Figure 3-8. Secondary chemical shifts of humPrP <sub>23-159</sub> .....	41
Figure 3-9. <sup>1</sup> H- <sup>15</sup> N dipolar couplings of humPrP <sub>23-159</sub> .....	42
Figure 3-10. Long-range interaction between the N-terminus and the helix 1 region.....	43
Figure 3-11. Aggregation of human prion protein stop mutants.....	44
Figure 3-12. Helix 1 region is not resistant to digestion by proteinase K.....	45
Figure 3-13. Molecular weight estimation of humPrP <sub>23-173</sub> fibrils.....	46
Figure 3-14. Dissolution of amyloid fibrils of humPrP <sub>23-159</sub> .....	48
Figure 3-15. NMR-based detection of H/D exchange.....	49
Figure 3-16. Protection map of humPrP <sub>23-159</sub> fibrils after 3 days of H/D exchange.....	50
Figure 3-17. Time dependence of deuterium incorporation into humPrP <sub>23-159</sub> fibrils.....	50
Figure 3-18. Residue specific H/D exchange profiles for residues 111-141.....	52
Figure 3-19. Fibrils of different humPrP stop mutants share common structural features.....	53
Figure 3-20. Flight maps for the 10 best 9-residue fragment candidates.....	54
Figure 3-21. Flight map of the 10 best 9-residue fragments for the “triplicated” peptide.....	55

Figure 3-22. Flight maps of the best 9-residue fragments selected with the hybrid approach.	56
Figure 3-23. Structures of Gly-rich regions in fragments selected by CS-Rosetta.	57
Figure 3-24. Flight map of the best 10 fragments assembled for residues 113-126 of the amyloid forming peptide 106-126.	62
Figure 3-25. Structural architecture of humPrP fibrils.	63
Figure 4-1. Aggregation of $\beta$ -2-microglobulin causes dialysis-related amyloidosis.	66
Figure 4-2. Schematic representation of amyloid fibril formation by h $\beta$ 2m.	68
Figure 4-3. 3D structure of K3 fibrils.	70
Figure 4-4. Unfolding of human $\beta$ -2-microglobulin followed by NMR.	71
Figure 4-5. Changes in hydrodynamic radius of h $\beta$ 2m upon acid denaturation.	72
Figure 4-6. Direct carbon detection allows for observation of highly dynamic regions of h $\beta$ 2m at pH 3.6.	73
Figure 4-7. Structural properties of h $\beta$ 2m at pH 3.6.	75
Figure 4-8. Secondary chemical shifts of h $\beta$ 2m at pH 2.5.	77
Figure 4-9. Amyloid fibril formation by h $\beta$ 2m.	78
Figure 4-10. NMR spectra of h $\beta$ 2m fibrils under high-resolution magic angle spinning.	78
Figure 4-11. Identification of flexible regions in amyloid fibrils of h $\beta$ 2m.	79
Figure 4-12. H/D exchange map for fibrils of human $\beta$ -2-microglobulin.	80
Figure 4-13. Secondary chemical shifts report $\alpha$ -helical propensities in h $\beta$ 2m at pH 2.5.	81
Figure 4-14. Residue-specific $R_2$ relaxation rates for h $\beta$ 2m at pH 2.5.	83
Figure 4-15. Deuterium incorporation into amyloid fibrils of h $\beta$ 2m.	84
Figure 4-16. Relationship between the dynamics of the h $\beta$ 2m intermediate and structural architecture of the fibrils.	85
Figure 4-17. Mapping of h $\beta$ 2m amyloid fibril solvent protection levels onto the native fold.	86

## List of Tables

Table 1-1. Examples of amyloidoses. ....	3
Table 2-1. Constructs .....	11
Table 2-2. Software .....	12
Table 2-3. Experiments used for backbone resonance assignments .....	23
Table 3-1. Prion diseases in animals .....	29
Table 3-2. Human prion diseases .....	30
Table 3-3. Properties of normal and “scrapie” forms of the prion protein.....	36

## Abbreviations

<b>1D, 2D, 3D</b>	1-, 2-, 3-dimensional
<b>APS</b>	ammonium persulfate
<b>BMRB</b>	biological magnetic resonance bank
<b>BSA</b>	bovine serum albumin
<b>BSE</b>	bovine spongiform encephalopathy
<b>C12E5</b>	<i>n</i> -dodecyl-penta(ethylene glycol)
<b>CD</b>	circular dichroism
<b>CIAP</b>	calf intestinal alkaline phosphatase
<b>CJD</b>	Creutzfeldt-Jacob disease
<b>CSA</b>	chemical shift anisotropy
<b>CWD</b>	chronic wasting disease
<b>C<math>\alpha</math>, C'</b>	carbon-alpha, carbonyl carbon
<b>DCA</b>	dichloroacetate
<b>DMSO</b>	dimethyl sulfoxide
<b>DNA</b>	deoxyribonucleic acid
<b>DOSY</b>	diffusion ordered spectroscopy
<b>DRA</b>	dialysis-related amyloidosis
<b>DTT</b>	dithiotreitol
<b>EDTA</b>	ethylenediaminetetraacetic acid
<b>FFI</b>	fatal familial insomnia
<b>FPLC</b>	fast protein liquid chromatography
<b>FSE</b>	feline spongiform encephalopathy
<b>FTIR</b>	Fourier transform infrared spectroscopy
<b>GdnSCN</b>	guanidinium thiocyanate
<b>GPI</b>	glycophosphatidylinositol
<b>GSS</b>	Gerstmann-Sträussler-Scheinker syndrome
<b>H/D</b>	hydrogen / deuterium
<b>HEPES</b>	4-(2-hydroxyethyl)-1-piperazineethanesulfonic acid
<b>HET-s</b>	prion protein of the fungus <i>Podospora anserina</i>
<b>HR-MAS</b>	high-resolution magic angle spinning
<b>Hsp</b>	heat shock proteins (molecular chaperones)
<b>HSQC</b>	heteronuclear single quantum coherence

<b>humPrP</b>	human prion protein
<b>hβ2m</b>	human beta-2-microglobulin
<b>INEPT</b>	insensitive nuclei enhanced polarization transfer
<b>IPAP</b>	in-phase anti-phase
<b>IPTG</b>	isopropyl-beta-D-thiogalactopyranoside
<b>K3</b>	peptide encompassing residues 20-41 of human β-2-microglobulin
<b>MAS</b>	magic angle spinning
<b>MCS</b>	multiple cloning site
<b>MD</b>	molecular dynamics
<b>MFR</b>	molecular fragment replacement
<b>MHC-I</b>	major histocompatibility complex I
<b>moPrP</b>	mouse prion protein
<b>MWCO</b>	molecular weight cut off
<b>Ni-NTA</b>	nickel-nitrilo triacetic acid
<b>NMR</b>	nuclear magnetic resonance
<b>NR</b>	database of non-redundant sequences
<b>OD<sub>600</sub></b>	optical density at 600 nm
<b>ORF</b>	open reading frame
<b>PAGE</b>	polyacrylamide gel electrophoresis
<b>PCR</b>	polymerase chain reaction
<b>PK</b>	proteinase K
<b>PMSF</b>	phenylmethanesulphonyl fluoride
<b>ppm</b>	parts per million
<b><i>Prnp</i></b>	gene coding for the prion protein
<b>PrP</b>	prion protein
<b>PrP27-30</b>	27-30 kDa product of digestion of PrP <sup>SC</sup> with proteinase K
<b>PrP<sup>C</sup></b>	normal cellular prion protein
<b>PrP<sup>SC</sup></b>	abnormal “scrapie” prion protein
<b>RDC</b>	residual dipolar coupling
<b>RNA</b>	ribonucleic acid
<b>SCS</b>	secondary chemical shift
<b>SDS</b>	sodium dodecyl sulfate
<b>shPrP</b>	Syrian hamster prion protein
<b>TEM</b>	transmission electron microscopy

<b>TEMED</b>	N,N,N',N'-tetramethylethylenediamine
<b>TLCK</b>	tosyl-lysine chloromethyl ketone
<b>TME</b>	transmissible mink encephalopathy
<b>TOCSY</b>	total correlation spectroscopy
<b>TPCK</b>	tosyl-phenylalanine chloromethyl ketone
<b>Tris</b>	tris(hydroxymethyl)aminomethane
<b>TSE</b>	transmissible spongiform encephalopathy
<b>U</b>	unit
<b>Ub</b>	ubiquitin
<b>w/v</b>	weight per volume
<b><math>\Delta</math>N6-h<math>\beta</math>2m</b>	mutant of human beta-2-microglobulin lacking the N-terminal hexapeptide
<b><math>\delta</math></b>	chemical shift

# 1. Introduction

## 1.1. Protein folding, misfolding and aggregation

Protein folding is a process in which a newly expressed and post-translationally modified polypeptide chain adopts a structural conformation in which the hydrophobic elements are buried inside the fold while the hydrophilic ones are exposed on the surface (Crick, 1970). This transition is crucial as the right fold is a prerequisite for a protein's long term stability and the ability to selectively interact with its partners (Dobson, 2003). But what is the mechanism of folding and how is the native structure adopted? The pioneering work on protein folding in the 1970s (Anfinsen, 1973) concluded that the three-dimensional structure is encoded in the amino acid sequence of the polypeptide chain and that this functional fold should represent a global minimum on the energy landscape. Based on this finding, enormous effort has been put in order to understand the process of folding and how the minimum energy state is achieved. It became evident that a random search for the right conformation cannot be performed on a microsecond to millisecond biological timescale of protein folding, and that the protein is rather “funneled” down the energy landscape by energy barriers, kinetic traps and narrow pathways (**Figure 1-1**) (Wolynes et al., 1995; Dill and Chan, 1997).

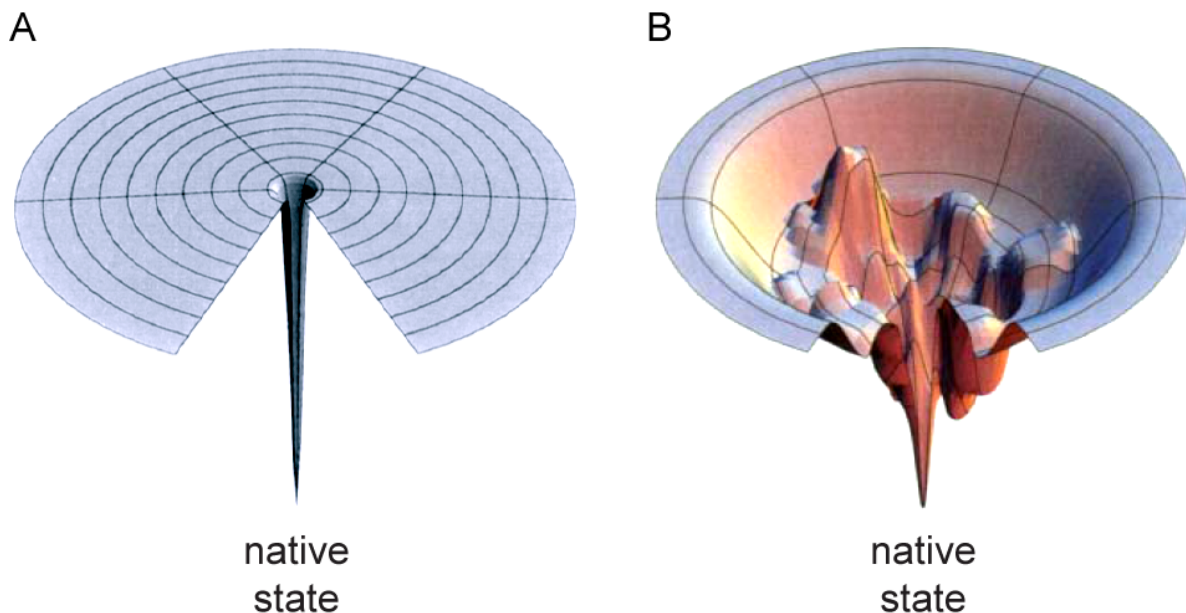


**Figure 1-1.** Schematic representation of folding energy landscapes.  
(a) Folding is achieved by a random search through all possible conformations.  
(b) Protein is funneled down the energy landscape through intermediate stages  
(adapted from Dill and Chan, 1997).



The presence of metastable intermediates may lead to intermolecular interactions between the partially unfolded states and self association into large assemblies known as aggregates (Dobson, 2003; Brockwell and Radford, 2007). Therefore, it is necessary for the cell that folding is controlled in order to prevent misfolding (**Figure 1-2**). In a normal biological state this is accomplished by molecular chaperones (Hsp) and the ubiquitin-proteasome pathway which prevent protein unfolding and aggregation by facilitating refolding and degradation, respectively (Jahn and Radford, 2005). Impairment of these factors results in malfunctioning of the living organism and hence in disease (Thomas et al., 1995; Dobson, 2001; Horwich, 2002).

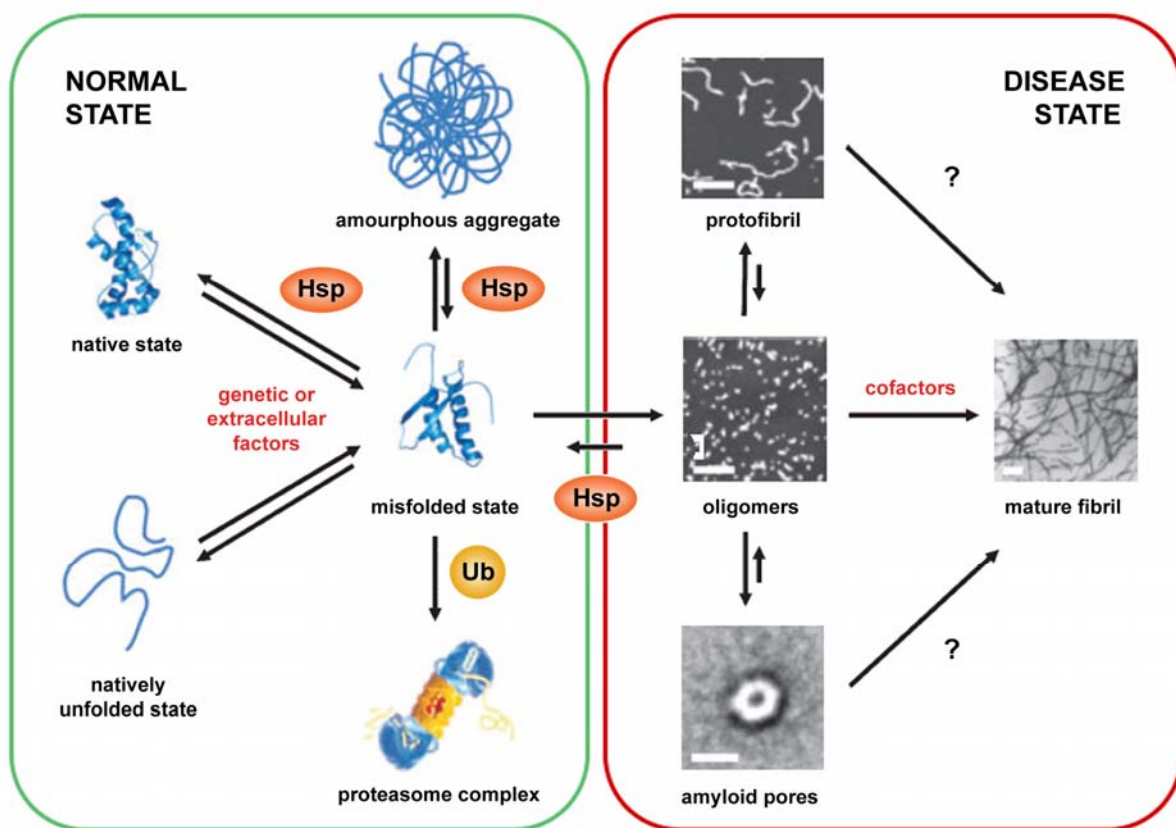


**Figure 1-2.** Factors influencing protein folding and aggregation *in vivo*.

In normal state, molecular chaperones (Hsp) and proteasomal degradation pathway prevent protein unfolding or misfolding. Failure of this mechanisms results in increased protein aggregation. By self-association of partially folded proteins small oligomers are formed which may further assemble into pores, protofibrils and mature fibril deposits (adapted from Jahn and Radford, 2005).

To current knowledge, more than a 100 diseases in both humans and animals involve aggregation of any of twenty non-homologous proteins (Kisilevsky, 1983; Pepys, 1988; Jacobson and Buxbaum, 1991; Selkoe, 1997; Kisilevsky, 2000). One of the classes of protein aggregation disorders are amyloidoses (see **Table 1-1**). This group of diseases is directly associated with deposition of proteinaceous aggregates in tissues, including the brain, heart, spleen, pancreas and skeletal tissue (Kelly and Lansbury, 1994; Tan and Pepys, 1994; Horwich, 2002). In many cases, the protein assemblies found *in vivo* contain a variety of other molecules, such as carbohydrates or additional proteins (Dobson, 2003).

**Table 1-1.** Examples of amyloidoses.

<b>disease</b>	<b>related protein</b>
Alzheimer's disease	$\beta$ -amyloid peptide, tau
Parkinson's disease	$\alpha$ -synuclein
familial amyloid polyneuropathy	transthyretin
transmissible spongiform encephalopathies	prion protein
Huntington's disease	huntingtin
frontotemporal dementia	tau
dialysis related amyloidosis	$\beta$ -2-microglobulin
diabetes mellitus type II	islet amyloid polypeptide

Even though the monomeric soluble forms of disease related proteins range from compact globular folds to intrinsically unstructured polypeptides, the aggregated forms share many common features. They are able to bind certain dyes such as Thioflavin T or Congo red (Elghetany and Saleem, 1988) and exhibit similar morphologies – namely long, unbranched and often twisted fibers a few nanometers in diameter, which show a characteristic X-ray diffraction pattern. These patterns display typical meridional reflections at  $\sim 4.7$  Å and equatorial reflections at  $\sim 10$  Å, indicative of a silk-like structure composed of stacked  $\beta$ -sheets with the strands running perpendicular to the axis of the fibril (cross- $\beta$  structure). The common features of amyloid fibrils are summarized in **Figure 1-3**.

Alternative to the cross- $\beta$  structure,  $\beta$ -helix and nanotube models have been proposed, in which one or more  $\beta$ -sheets wrap around a hollow core in a helical manner. The  $\beta$ -helical model was first suggested for fibrils of a short model peptide and showed a cylindrical antiparallel  $\beta$ -helix 20 Å in diameter (Lazo and Downing, 1997). The nanotube model, based on absence of the 10 Å equatorial reflection, suggested a water filled tube with internal and

external diameters of 12 Å and 32 Å, respectively (Perutz et al., 2002). Beta-helical models have also been proposed for the prion protein, based on 2D crystals of the protein extracted from brain tissue (Govaerts et al., 2004), and for amyloid-beta peptide, based on hydrogen-deuterium exchange data and a proline scan experiment (Kheterpal et al., 2000; Williams et al., 2004).

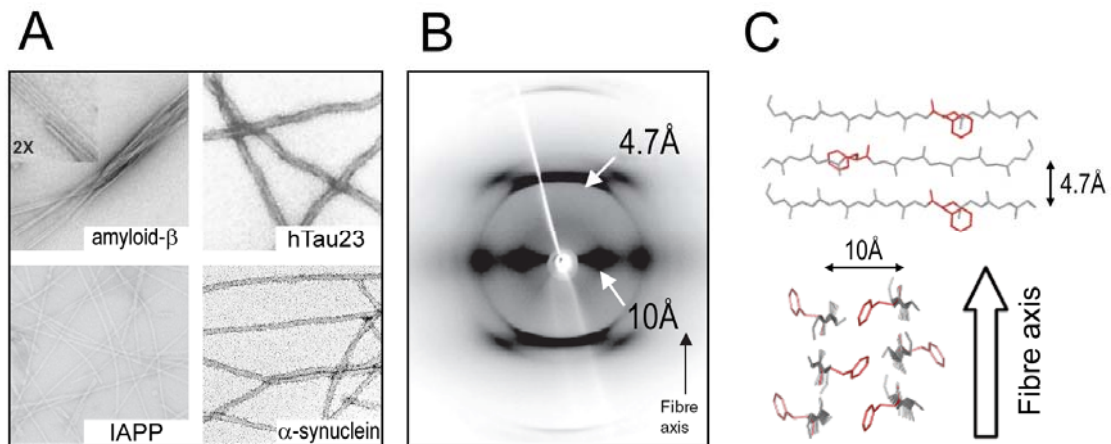


**Figure 1-3.** Characteristics of amyloid proteins.

(a) EM images of negatively stained amyloid fibrils. (b) X-ray fibre diffraction pattern from aligned fibrils formed by islet amyloid polypeptide showing the 4.7 Å and ~10 Å reflections (adapted from Makin and Serpell, 2005). (c) A model of the cross-β architecture showing the interstrand distance of 4.7 Å and intersheet distance of 10 Å (modified from Jack et al., 2006).

Regarding the origin of the structure of the fibrillar state, the ability to form aggregates is regarded an intrinsic physicochemical property of the polypeptide chain, as the amyloid structures are mostly stabilized by hydrogen bonds involving the protein backbone (Dobson, 1999). This is supported by evidence that under specific conditions also non-disease related proteins can form fibrils (Gujjarro et al., 1998; Chiti et al., 1999).

Evidence emerges that low molecular weight aggregates are indeed causing the toxicity, while appearance of mature fibril deposits is suggested to play a protective role as a removal mechanism for the toxic oligomeric intermediates (Snyder et al., 1994; Harper et al., 1997; Lambert et al., 1998; Klein et al., 2001; Bucciantini et al., 2002; Walsh et al., 2002; Yong et al., 2002). In fact, by targeting regions of the protein responsible for further self-association of oligomeric and protofibrillar species, it is possible to generate mutants with increased toxicity which do not form amyloid fibrils (Karpinar DP, unpublished data).

However, irrespective of whether the amyloid fibrils or intermediates are the toxic species, it is of extreme importance to investigate the structural properties of all stages on the aggregation pathway, in order to fully understand the process of amyloid formation and enable the development of treatment strategies. It is also very likely, that the structure of mature fibrils will shed light on the structure of their precursors.

## 1.2. NMR methods to study amyloid disorders

Due to the large size of the aggregates, dynamic conformational exchange during the aggregation process and intrinsic heterogeneity of the high molecular weight assemblies and their precursors, studies of protein aggregation present a great challenge to the structural biologist. While X-ray crystallography struggles with the insolubility and complexity of the fibrils and cryo electron microscopy fails to provide images at atomic resolution, nuclear magnetic resonance (NMR) remains the method of choice in investigation of amyloidoses.

However, in solution-state NMR spectroscopy, signals originating from fibrils are broadened beyond detection and therefore not directly observable. This is caused by increased relaxation rates due to contributions from dipolar couplings and chemical shift anisotropy (CSA). The dipolar coupling Hamiltonian for a heteronuclear case is given as:

$$\hat{H}_D = \frac{-\mu_0\gamma_1\gamma_2\hbar^2}{16\pi^3r^3} (3\cos^2\theta - 1) \hat{I}_{1z} \hat{I}_{2z}$$

while the chemical shift Hamiltonian is:

$$\hat{H}_{CS} = \gamma B_0 \left[ 1 - \left( \sigma_{iso} + \Delta\sigma (3\cos^2\theta - 1) + \eta_{CS} \sin^2\theta \cos 2\phi \right) \right] \hat{I}_z$$

where  $\Delta\sigma$  is the chemical shift anisotropy.

As can be seen from the above equations, both dipolar couplings and CSA depend on the term  $(3\cos^2\theta - 1)$ , which in an isotropic solution is time averaged to 0 as a result of Brownian motions. In a rigid amyloid fibril, lack of this free tumbling results in severe line broadening. Solid state NMR can overcome these problems, as during the experiment the sample is being spun at an angle  $\theta_m \sim 54.7^\circ$ , also called the ‘‘magic angle’’, where  $(3\cos^2\theta - 1)$  equals zero. Therefore, under magic angle spinning (MAS), CSA and dipolar couplings are removed (if the sample is spinning ‘‘fast enough’’) and spectra with relatively narrow lines can be recorded.

Numerous solid state NMR spectroscopy studies on amyloid fibrils have been performed and provided valuable information about the structure of the aggregates (see Heise, 2008 and references therein). Nevertheless, solid-state NMR spectroscopy has also its

drawbacks. As opposed to NMR in solution, where protons are the observed nucleus, in solid state NMR proton lines are still too broad and the spectra need to be detected on heteronuclei. The complexity of solid-state NMR spectra of amyloid fibrils frequently leads to problems with completing the assignment, which reflects onto the chemical shift based analysis of secondary structure. Although secondary chemical shifts provide useful direct information, it may be hard to determine the boundaries of secondary structure elements, especially in case of incompletely assigned spectra. Furthermore, selective and site-specific labeling is often required to decrease the complexity of the spectrum and since such labeling is not easily achievable in recombinantly expressed proteins, many of the solid state studies on amyloid fibrils were actually performed on short synthetic peptides rather than the full length protein (Jaroniec et al., 2004; Iwata et al., 2006; Walsh et al., 2009). Such approach raises questions regarding the preparation of aggregates and selection of the “minimal fragment” still able to form fibrils.

It may be therefore preferable to work with full-length proteins and use special solution-state-NMR-based techniques to get indirect information on the amyloid structure. In the past years, two such approaches have proven to be especially useful: quenched hydrogen/deuterium (H/D) exchange followed by fibril dissolving and high-resolution magic angle spinning (HR-MAS).

### 1.2.1. Quenched H/D exchange

The quenched H/D exchange method uses standard solution-state NMR experiments to detect residues found in the core of the fibril. It is based on partial solvent protection of the hydrogen bonded amide protons throughout the length of the fibril. Backbone amide groups located inside the amyloid structure experience lower solvent exchange rates than the ones present on the exterior of the fibril (Ippel et al., 2002). A crucial step in the procedure is the dissolving of fibrils to monomers, which are observable in the NMR experiment. The dissolution needs to be fast and complete in order to prevent back-exchange during the time of sample preparation. Commonly used solvents comprise mixtures of DMSO and dichloroacetate, which were found to rapidly dissociate amyloid fibrils formed by various proteins (Hoshino et al., 2007). An additional convenient feature of DMSO/DCA mixtures is that the acidic environment provided by addition of dichloroacetate slows down any exchange processes occurring after dissolution of fibrils, therefore allowing for longer NMR measurements.

Practically, the experiment is performed as follows. The fully protonated fibrils are collected, washed to remove residual monomer and incubated in D<sub>2</sub>O over a given period of time. The exchange process is quenched by freezing of the sample in liquid nitrogen and subsequent lyophilization. This allows for storage of the partially exchanged fibrils until the start of the NMR measurement. The fibrils are converted to monomer by addition of ice-cold DMSO/DCA mixture and a set of two-dimensional <sup>1</sup>H,<sup>15</sup>N-HSQC spectra is recorded. A schematic representation of the procedure is shown in **Figure 1-4**.

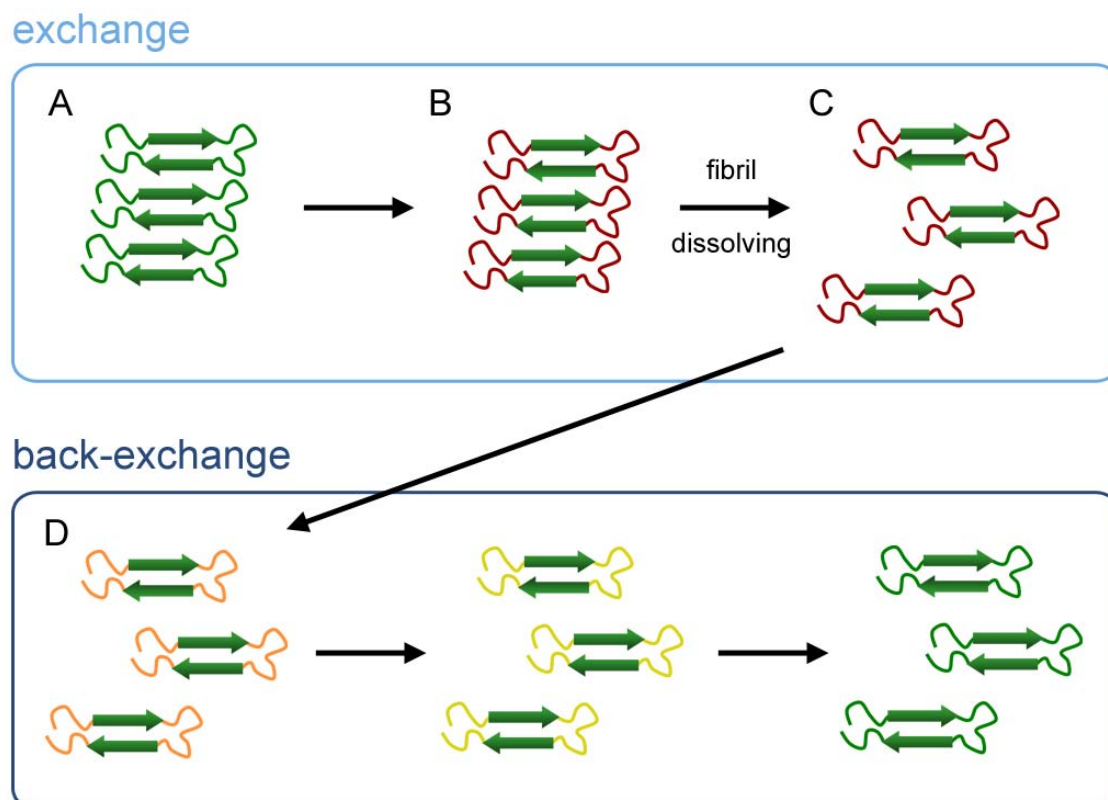


**Figure 1-4.** Schematic representation of the NMR-detected H/D exchange experiment. **(a)** During the exchange period fully protonated fibrils are incubated with D<sub>2</sub>O. **(b)** Hydrogen bonded protons in the core (green) are protected from the exchange, while protons in flexible parts exchange to deuterium (red). **(c)** Dissolving of fibrils leads to NMR-observable monomers. **(d)** During the back-exchange period a set of NMR spectra is recorded over time while the deuterons exchange back to protons.

The quenched H/D experiment has been successfully performed on amyloid fibrils of  $\beta$ -2-microglobulin (Hoshino et al., 2002), transthyretin (Olofsson et al., 2004) and amyloid- $\beta$ -(1-42) peptide (Olofsson et al., 2006). Even though the method does not provide a high-resolution structural model, it leads to residue-specific information on which amino acids are involved in the hydrogen-bonding network within the fibril. Detection of the H/D exchange

can alternatively be accomplished by mass spectrometry (Lu et al., 2007), however data collected in this way is less accurate and relies heavily on the fragmentation of the polypeptide chain. NMR-detected experiments have a strong advantage of providing data with single residue resolution.

### 1.2.2. HR-MAS

A second technique gaining popularity in studies of amyloid fibrils is high-resolution magic angle spinning. Similarly to solid-state NMR, the sample is spun at a speed of up to 19 kHz in order to remove relaxation contributions from dipolar couplings and CSA. The effect of spinning on the observed signal is depicted in **Figure 1-5**.

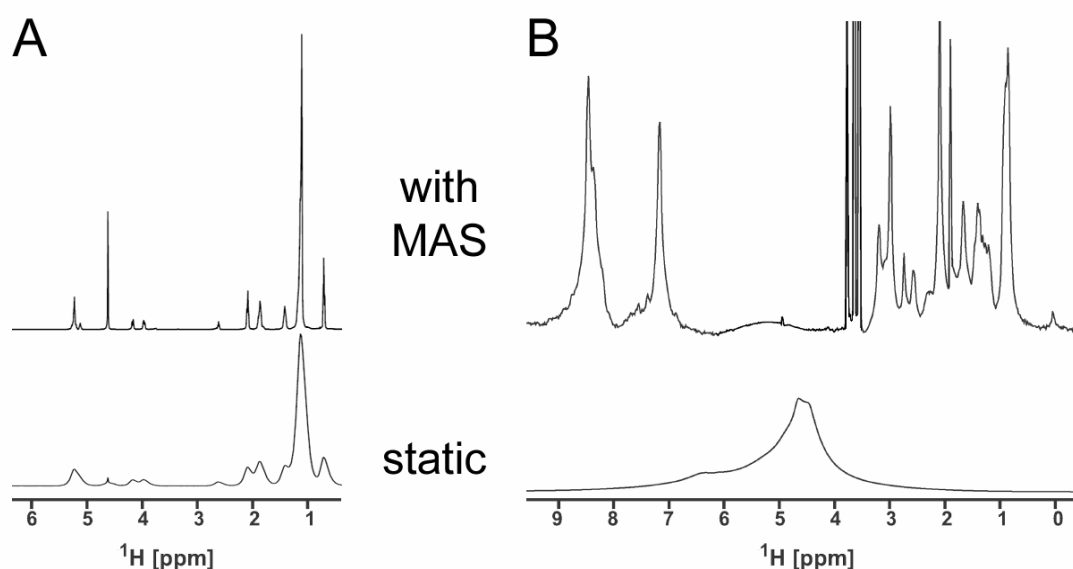


**Figure 1-5.** High-resolution magic angle spinning.

One-dimensional  $^1\text{H}$  spectra of (a) human Lipoma tissue (modified from Bruker Biospin HR-MAS manual) and (b) amyloid fibrils of the HET-s(218-289) prion protein (adapted from Siemer et al., 2006) recorded with (top) and without (bottom) magic angle spinning.

HR-MAS experiments utilize the INEPT transfer commonly found in heteronuclear pulse schemes for NMR in solution. As a result, in rigid regions of the protein, strong dipolar couplings lead to fast relaxation of the magnetization during the transfer and evolution periods, and only signals originating from flexible regions are observed in the spectrum. Therefore, an HR-MAS spectrum provides information complementary to a dipolar-based solid state NMR experiment in which only rigid residues contribute to the recorded signal

(Andronesi et al., 2005). Another important consideration in this respect are potential problems with obtaining sequence specific assignments. In case of very rigid and compact fibrils, only a few resonances may be observable and only chemical shift based assignment of residue types may be possible. However in a recent study on the HET-s prion protein, complementation of the HR-MAS data by solid state NMR experiments led to partial assignment of the flexible regions (Siemer et al., 2006).

High-resolution MAS has also the potential to become a powerful tool in metabonomics and diagnostic tests of neurodegenerative diseases (Holmes et al., 2006). With sample requirements as low as 12  $\mu$ L for liquid- or  $\sim$ 10 mg in case of solid-type material, HR-MAS can easily be used on cerebrospinal fluid or tissues from biopsies. The technique has already been utilized in cancer studies (Moka et al., 1998; Tate et al., 2000) and very recently in the model worm *C.elegans*, which (if necessary) can be kept alive during the experiment (Blaise et al., 2007).



## 2. Materials and Methods

### 2.1. Materials

#### 2.1.1. Chemicals

*Cambridge Isotope Laboratories* (Andover, USA):  $^{15}\text{N-NH}_4\text{Cl}$

*Spectra Stable Isotopes* (Columbia, USA):  $^{13}\text{C}$ -[C<sub>6</sub>]-D-glucose, D<sub>2</sub>O

*Sigma-Aldrich* (Deisenhofen, Germany): guanidinium thiocyanate, *n*-dodecyl-penta(ethylene glycol) (C12E5), hexanol

*Invitrogen* (Karlsruhe, Germany): agarose, Bench Mark protein ladder

*Serva* (Heidelberg, Germany): SDS

*Roth* (Karlsruhe, Germany): acrylamid, ampicillin sodium salt, APS, dipotassium hydrogen phosphate, ethidium bromide, EDTA, guanidinium hydrochloride, HEPES, IPTG, kanamycin, potassium dihydrogen phosphate, sodium acetate, sodium deoxycholate, TEMED, tryptone, yeast extract

*Roche Diagnostics* (Mannheim, Germany): Complete<sup>TM</sup> protease inhibitors, Complete<sup>TM</sup> protease inhibitors EDTA-free, proteinase K

*Merck* (Darmstadt, Germany): acetic acid,  $\alpha$ -D(+)-glucose monohydrate, ammonium chloride, disodium hydrogen phosphate, ethanol, formic acid, glycerol, hydrochloric acid, magnesium sulfate heptahydrate, sodium chloride, sodium dihydrogen phosphate, sodium hydroxide, thiaminechloride hydrochloride, Tris, urea

#### 2.1.2. Enzymes and DNA-Kits

*Fermentas* (Burlington, Canada): *Nde*I, *Bam*HI, *Xho*I, T4-DNA ligase, Pfu DNA polymerase, CIA phosphatase

*Finnzymes* (Espoo, Finland): Phusion High Fidelity PCR Master Mix

*Qiagen* (Hilden, Germany): Qiagen Plasmid Midi Kit, QIAquick Gel Extraction Kit, QIAquick PCR Purification Kit

*Macherey-Nagel* (Dueren, Germany): NucleoSpin Extract II Kit, NucleoBond PC 100 Midi Kit

#### 2.1.3. Oligonucleotides

**B2M3** (wt h $\beta$ 2m, forward, *Nde*I)

5'- GTC TCT AGA CAT ATG ATC CAG CGT ACT CCA AAG ATT CAG G -3'

**B2M2** (wt h $\beta$ 2m, reverse, *Bam*HI)

5'- GCT AAG CTT GGA TCC TTA CAT GTC TCG ATC CCA CTT AAC TAT C -3'

**KM9** (shPrP<sub>23-159</sub>, forward, *Nde*I)

5'- GTC TCT AGA CAT ATG AAG AAG CGG CCA AAG CCT GG -3'

**KM10** (shPrP<sub>23-159</sub>, reverse, *Bam*HI)

5'- GCT AAG CTT GGA TCC TCA GTT AGG GTA GCG GTT CAT GTT TTC -3'

All oligonucleotides were purchased from Invitrogen (Karlsruhe, Germany).

#### 2.1.4. Plasmids

pET26b(+), [ pelB leader; **MCS**; His-Tag ], 5360 bp, Kan<sup>r</sup>

pET27b(+), [ pelB leader; **MCS**; HSV-Tag; His-Tag ], 5414 bp, Kan<sup>r</sup>

pET32a(+), [ Trx-Tag; His-Tag (thrombin); S-Tag (Ek); **MCS** ], 5900 bp, Amp<sup>r</sup>

All vectors were purchased from Novagen (Darmstadt, Germany).

**Table 2-1.** Constructs

Plasmid	Coding for	Source
pET27b / humPrP <sub>23-159</sub>	human prion protein, fragment 23-159	kindly provided by Dr. W. Schulz-Schaeffer, University Hospital, Goettingen, Germany
pET27b / humPrP <sub>23-173</sub>	human prion protein, fragment 23-173	
pQE80LSN_h $\beta$ 2m	human beta-2-microglobulin	purchased from RZPD, Berlin, Germany
pGX2T-shPrP <sup>C</sup> (23-231)	Syrian hamster prion protein, full length	kindly provided by Dr. S. Weiss, GenCenter, LMU Munich, Germany
pET14b / humPrP <sub>23-159</sub>	human prion protein, fragment 23-159	this work, Figure 2-1
pET26b / shPrP <sub>23-159</sub>	Syrian hamster prion protein, fragment 23-159	this work, Figure 2-2
pET32a / h $\beta$ 2m	human beta-2-microglobulin	this work, Figure 2-3

#### 2.1.5. *Escherichia coli* strains

**XL2-Blue** (*Stratagene*, La Jolla, USA)

*recA1 endA1 gyrA96 thi-1 hsdR17 supE44 relA1 lac* [F' *proAB lacI<sup>q</sup>Z $\Delta$ M15 Tn10* (Tet<sup>r</sup>) Amy Cam<sup>r</sup>]

**BL21(DE3)** (*Novagen*, Darmstadt, Germany)

$F^- ompT hsdSB(r_B^-, m_B^-) gal dcm$  (DE3)

### 2.1.6. Chromatography resins

**Ni-NTA agarose**, affinity chromatography resin (*Qiagen*, Hilden, Germany)

**EMD-TMAE Fractogel**, anion exchange chromatography resin (*Merck*, Darmstadt, Germany)

**EMD-COO<sup>-</sup> Fractogel**, cation exchange chromatography resin (*Merck*, Darmstadt, Germany)

**HiLoad 16/60 Superdex 200 prep grade**, size-exclusion chromatography column (*GE Healthcare*, Chalfont St. Giles, UK)

### 2.1.7. Software

The software used for acquisition of NMR experiments, data analysis and visualization is listed in Table 2-2.

**Table 2-2.** Software

<b>Name and version</b>	<b>Source / Reference</b>
XWIN-NMR 3.5	<i>Bruker Biospin</i> , Karlsruhe, Germany
TopSpin 1.0 ~ 2.1	<i>Bruker Biospin</i> , Karlsruhe, Germany
NMRPipe	spin.niddk.nih.gov/NMRPipe (Delaglio et al., 1995)
Sparky 3	www.cgl.ucsf.edu/home/sparky (Goddard and Kneller)
MacPyMol	<i>DeLano Scientific LLC</i> , Palo Alto, USA
IgorPro 5.0	<i>WaveMetrics</i> , Portland, USA
Rosetta++	www.rosettacommons.org
CS-ROSETTA	spin.niddk.nih.gov/bax/software/CSROSETTA (Shen et al., 2008; Shen et al., 2009)
PALES	www.mpibpc.mpg.de/groups/griesinger/zweckstetter/_links/software_pales.htm

### 2.1.8. Buffers and solutions

#### 2.1.8.1. Prion protein purification

##### **Lysis buffer**

100 mM Tris-HCl, 1 M NaCl, 1 mM EDTA, 1 % Triton-X-100, 1 mM benzamidine-HCl, pH 8.0

##### **Protease Inhibitor mix**

0.1 mM PMSF, 10  $\mu$ M TPCK, and 10  $\mu$ M TLCK in dry methanol

##### **Inclusion Body wash (IB-wash) buffer**

50 mM Tris-HCl, 23 % sucrose, 1 mM EDTA, 1 mM benzamidine-HCl, 1 % Triton-X-100, pH 8.5

##### **Buffer A**

6 M guanidinium-HCl, 10 mM Tris-HCl, 100 mM sodium phosphate, 15 mM  $\beta$ -mercaptoethanol, pH 8.0

##### **Buffer B**

10 mM Tris-HCl, 100 mM sodium phosphate, pH 8.0

##### **Buffer C**

10 mM Tris-HCl, 100 mM sodium phosphate, pH 5.8

##### **Buffer E**

10 mM Tris-HCl, 100 mM sodium phosphate, 0.5 M imidazole, pH 5.8

##### **Buffer W**

20 mM sodium phosphate, 10 mM  $\beta$ -mercaptoethanol, pH 6.0

#### 2.1.8.2. Beta-2-microglobulin purification

##### **Buffer S1**

50 mM Tris-HCl, 5 % v/v glycerol, 0.1 mM EDTA, 0.1 mM DTT, 50 mM NaCl, pH 7.9

##### **Buffer W1**

10 mM Tris-HCl, pH 8.0

##### **Buffer U1**

8 M urea, 10 mM Tris-HCl, pH 8.0

##### **Buffer GF**

10 mM Tris-HCl, 150 mM NaCl, pH 9.0

##### **Buffer 10xAG**

250 mM sodium acetate, 250 mM sodium phosphate, pH 2.5

**NaDOC**

20 % sodium deoxycholate in ddH<sub>2</sub>O

**2.1.8.3. Cell culture media****Luria-Bertani (LB) broth**

10 g tryptone, 5 g yeast extract, 10 g NaCl, H<sub>2</sub>O up to 1 L

**M9 minimal medium (per 1 L)**

6.8 g Na<sub>2</sub>HPO<sub>4</sub>, 3 g KH<sub>2</sub>PO<sub>4</sub>, 0.5 g NaCl, 1 g NH<sub>4</sub>Cl or <sup>15</sup>N-NH<sub>4</sub>Cl, 4 g α-D-glucose or <sup>13</sup>C-[C<sub>6</sub>]-glucose, 2 mM MgSO<sub>4</sub>, 0.1 mM CaCl<sub>2</sub>, 30 mg thiamine-HCl, H<sub>2</sub>O up to 1 L

**2.2. Prion protein methods****2.2.1. Safety considerations**

All expression and purification of human prion protein mutants was carried out under S3 conditions, in the laboratory of Dr. Walter Schulz-Schaeffer at the Department of Neuropathology of the University Hospital in Goettingen, Germany. Samples of Syrian hamster PrP were prepared in the S1 laboratory of the Department of NMR-based Structural Biology at the Max-Planck-Institute for Biophysical Chemistry, Goettingen, Germany.

**2.2.2. Cloning of His6-tagged humPrP<sub>23-159</sub>**

The pET27b/humPrP<sub>23-159</sub> (see **Table 2-1**) and target pET14b plasmid DNA were digested with 2 units of *Nde*I endonuclease per μg of DNA. The reaction was carried out at 37 °C overnight. The digestion products were purified using the MN Nucleospin Extract II Kit following the PCR Product Purification protocol of the supplier, and further cleaved for 2 hours at 37 °C with 2 units of *Xho*I endonuclease per μg of DNA. After digestion, 1 μL of CIA (Calf intestinal alkaline) phosphatase was added to the pET14b vector sample and incubated for 30 minutes at 37 °C, while the digested pET27b/humPrP<sub>23-159</sub> DNA was stored on ice. The reaction mixtures were separated on a 1 % agarose gel for 1 hour at 70 V. Bands of pET14b vector and humPrP<sub>23-159</sub> insert were excised from the gel and DNA was purified using the MN Nucleospin Extract II Kit following the Gel Extraction protocol of the supplier. The insert and vector DNA were ligated overnight at 14 °C in presence of 1 Weiss unit of T4 DNA ligase. Afterwards the ligation mixture was transformed into XL2-Blue CaCl<sub>2</sub>-competent *E.coli* strain and the cells were plated out onto an agar plate containing 100 μg/ml

Ampicillin. After an overnight incubation at 37 °C, six colonies were picked from the plate to start 20 ml cultures from which plasmid DNA was isolated using the MN NucleoBond PC 100 Midi Kit and controlled by DNA-sequencing (*SeqLab*, Goettingen, Germany). Vector map of the pET14b-humPrP<sub>23-159</sub> construct is shown in **Figure 2-1**.

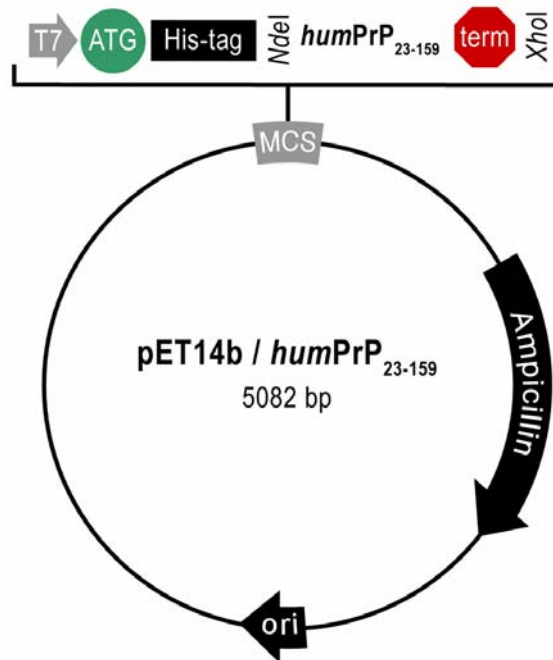


**Figure 2-1.** Vector map of pET14b plasmid coding for humPrP<sub>23-159</sub>.

### 2.2.3. Cloning of shPrP<sub>23-159</sub>

The open reading frame (ORF) coding for shPrP<sub>23-159</sub> was amplified from the plasmid pGX2T-shPrP<sup>C</sup>(23-231) using the primers KM9 and KM10 and the Phusion High Fidelity PCR Master Mix. The PCR amplification was done on a Hybaid PCR Sprint thermal cycler (*Thermo Fisher Scientific*, Waltham, USA) using the following cycling conditions:

94 °C - 2 min

94 °C - 30 sec; 55°C - 30 sec; 72°C - 1 min / 30 cycles

72 °C - 10 min

PCR products were separated on a 1 % agarose gel at 70 V and purified using the MN NucleoSpin Extract II Kit. The amplified ORF and pET26b vector were then digested with *NdeI* and *BamHI* restriction endonucleases, ligated, and transformed into XL2-Blue as described in 2.2.2. Six clones were picked from the agar plate (containing 50 µg/ml Kanamycin) and tested by colony PCR using the HotStarTaq Kit (*Qiagen*, Hilden, Germany).

Two positive clones were selected and verified by DNA sequencing (*SeqLab*, Goettingen, Germany). Vector map of the pET26b-shPrP<sub>23-159</sub> is shown in **Figure 2-2**.

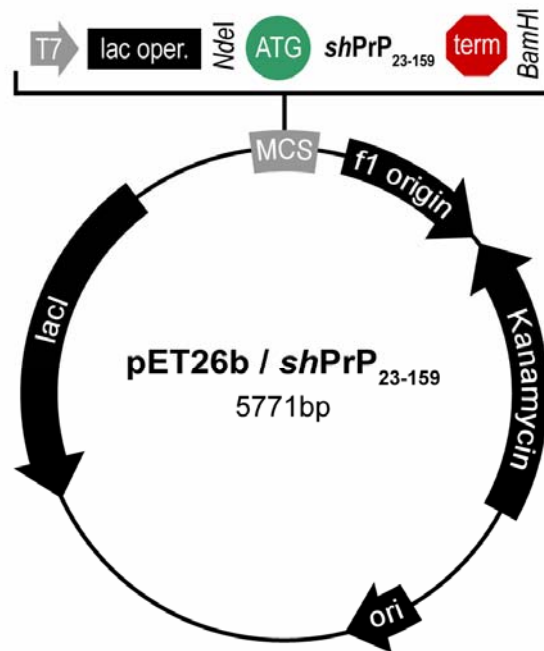


**Figure 2-2.** Vector map of pET26b plasmid coding for shPrP<sub>23-159</sub>.

#### 2.2.4. Expression of prion protein mutants for NMR

Independent of the construct used, plasmid DNA was freshly transformed into BL21 (DE3) and cells were grown on selective agar plates. A single colony was picked from the plate and a 10 ml overnight culture in LB was started. Next morning cells were pelleted at 3000 x g, 4 °C for 10 minutes (Beckmann JA17) and resuspended in 1 liter of M9 minimal medium containing (if required) <sup>15</sup>N-NH<sub>4</sub>Cl and <sup>13</sup>C-[C<sub>6</sub>]-glucose to obtain uniformly <sup>13</sup>C and/or <sup>15</sup>N labeled proteins. Protein expression was induced at OD<sub>600</sub> = 1.0-1.1 by addition of IPTG to a final concentration of 1 mM. After induction, the cells were grown for 8 hours, spun down at 8000 x g, 4 °C for 15 minutes (Kendro Multifuge 3R) and stored at -80 °C.

#### 2.2.5. Purification of non-tagged prion protein

Non-tagged prion protein constructs (both human and Syrian hamster) were purified according to a common protocol as follows:

### 2.2.5.1. Isolation of inclusion bodies

The bacterial pellet was resuspended in 30 ml of Lysis buffer supplemented with 300  $\mu$ l Protease Inhibitor mix, 3 mg DNase I, 3 mg RNase A, 10 mM CaCl<sub>2</sub> and 10 mM MgCl<sub>2</sub> (per liter of M9 medium). Cells were disrupted by three freeze/thaw cycles in liquid nitrogen and inclusion bodies were pelleted at 30000 x g, 4 °C for 30 minutes (Beckmann JA17). The inclusion bodies were then washed (2-3 times) in a homogenizer with IB-wash buffer supplemented with 2 M NaCl and centrifuged at 30000 x g, 4 °C for 30 minutes. Finally, the inclusion bodies were washed once with IB-wash buffer supplemented with 0.5 % Sulfobetaine 14.

### 2.2.5.2. Extraction of protein from inclusion bodies

Purified inclusion bodies were resolubilized in buffer A and centrifuged at 30000 x g, 4 °C for 30 minutes in order to remove any guanidinium-insoluble particles. The supernatant was then transferred into a new tube and a second centrifugation round was performed. The prion protein was found solely in the supernatant.

### 2.2.5.3. Purification by chromatography methods

#### A. Affinity chromatography

Ni-NTA agarose resin was equilibrated with buffer A and the prion protein was bound to the resin by incubation at room temperature for 30 minutes. N-terminally truncated protein not containing the histidine-rich octarepeat region and nucleic acids were removed by washing the resin with buffer A containing 10 mM imidazole and prion protein was eluted in a 1:1 mixture of buffers A and 1 M imidazole, pH 7.5. The protein was precipitated by addition of 4 volumes of methanol and an overnight incubation at -20 °C.

#### B. Anion exchange chromatography

After centrifugation at 7800 x g, 4 °C for 10 minutes, the protein was resolubilized in 8 M urea, 20 mM sodium phosphate, 10 mM  $\beta$ -mercaptoethanol, pH 8.0 and loaded onto a EMD-TMAE Fractogel anion exchange resin (*Merck*, Darmstadt, Germany) equilibrated with the same buffer. Under this conditions, no binding of the prion protein to the resin occurred.

#### C. Cation exchange chromatography

The PrP-containing flow-through from the anion exchanger was subjected to a EMD-COO<sup>-</sup> Fractogel cation exchange resin (*Merck*, Darmstadt, Germany) equilibrated with 8 M urea in 20 mM sodium phosphate, 10 mM  $\beta$ -mercaptoethanol, pH 8.0. Urea was removed by



washing the resin with buffer W and the protein was eluted with increasing concentrations (0.5 M, 1 M, 6 M) of guanidinium-hydrochloride (GdnHCl) in buffer W. Fractions containing prion protein were combined, solid GdnHCl was added to a final concentration of 6 M and the pH was adjusted to 8.0.

### 2.2.5.4. Refolding of the prion protein

The purified prion protein was bound to Ni-NTA resin as described in 2.2.5.3.A and washed in batch mode with a gradient of buffer B in buffer A, such that the GdnHCl concentration was decreasing from 6 M to 0 M in 1 M steps. Next, the resin was washed with buffer C and the protein was finally eluted with buffer E. Immediately after elution, the protein was dialyzed 3 times against 5 liters of 5 mM sodium acetate, pH 4.5 to remove the aggregation inducing phosphate buffer.

### 2.2.6. Fast purification of non-tagged prion proteins

Since for many NMR experiments, protein purity of about 90% is satisfactory, a shorter purification protocol, omitting the ion-exchange chromatography steps, has been developed.

The bacterial pellets (see 2.2.4) were resuspended in 30 ml of buffer B containing 3 mg DNase I and 3 mg RNase A, and cells were disrupted by three freeze/thaw cycles. Inclusion bodies were pelleted by centrifugation for 30 minutes at 30000 x g, 4 °C, and washed twice with 30 ml buffer B. The protein was then extracted and preliminarily purified from DNA and RNA as described in 2.2.5.2 and 2.2.5.3.A. On the next day, the methanol-precipitated protein was resolubilized in buffer A, re-subjected to a fresh Ni-NTA resin, and refolded as outlined in 2.2.5.4.

### 2.2.7. Purification of His6-tagged humPrP<sub>23-159</sub>

#### 2.2.7.1. Refolding on an affinity column

The N-terminally tagged humPrP<sub>23-159</sub> protein was extracted from inclusion bodies as described in 2.2.5.1-2. The protein was then bound to ~5 ml of Ni-NTA resin (equilibrated with buffer A) by incubation at room temperature for 1 hour on a rocking shaker. In the first step, the resin was washed with 10 volumes of buffer A, and afterwards a 180 ml gradient of buffer A to buffer B was applied to refold the protein. Impurities were removed by washing

the resin with 50 ml of buffer B containing 50 mM imidazole. In the last step, the resin was washed with buffer C followed by elution of the His6-tagged protein in buffer E.

#### 2.2.7.2. Cleavage of the histidine tag

The eluate was dialysed twice against 10 mM sodium acetate pH 4.5 to remove phosphate buffer and decrease the ionic strength of the solution and then twice against 10 mM Tris-HCl, pH 8.0 to provide convenient conditions for the cleavage reaction. The histidine tail was completely cleaved off in one hour at room temperature with 10 units of thrombin (*GE Healthcare*, Chalfont St. Gilles, UK) per 1 mg of tagged protein, while no cleavage of humPrP<sub>23-159</sub> occurred under these conditions. After the reaction, solid GdnHCl was added to the solution to a final concentration of 6 M to denature thrombin and allow for binding to Ni-NTA resin. By repeating the refolding protocol described in 2.2.5.4, thrombin could be fully removed during the washing steps while humPrP<sub>23-159</sub> was eluted in buffer E and dialyzed against 5 mM sodium acetate, pH 4.5.

#### 2.2.8. Aggregation

The aggregation process was initiated by addition of a 10 times concentrated phosphate buffer (500 mM potassium phosphate, pH 6.5) to a 400  $\mu$ M prion protein solution. The pH was controlled with an Aldrich microelectrode (*Sigma-Aldrich*, Deisenhofen, Germany) and the reaction mixture was incubated at room temperature in a Stuart SB3 rotator (*Bibby Scientific*, Staffordshire, UK) operating at a speed of 8 rpm.

#### 2.2.9. H/D exchange

After the aggregation process was completed, fibrils were collected by centrifugation and washed twice with the aggregation buffer in order to remove residual monomeric protein. Finally, the fibrils were resuspended in 0.1 % formic acid in D<sub>2</sub>O, pD 2.5 and incubated for a given amount of time – 1, 2, 3 and 7 days for humPrP<sub>23-159</sub> and 7 days for humPrP<sub>23-173</sub>. The exchange was stopped by rapid freezing of the samples in liquid nitrogen and lyophilization.

### 2.3. Beta-2-microglobulin methods

#### 2.3.1. Cloning of h $\beta$ 2m into pET32a

cDNA coding for human  $\beta$ -2-microglobulin was amplified by PCR from the pQE80LSN\_h $\beta$ 2m vector (**Table 2-1**) using primers B2M2 and B2M3 and the following cycling conditions:

95 °C - 30 sec

95 °C - 30 sec; 57°C - 1 min; 72°C - 1 min / 25 cycles

72 °C - 5 min

The PCR product was separated in 1 % agarose gel at 70 V and purified using QIAquick PCR Purification Kit. The fragment was then digested with 2 U of *NdeI* endonuclease per  $\mu$ g DNA (37 °C overnight), purified again using the QIAquick Kit and digested with 2 U per  $\mu$ g DNA of *BamHI* restriction enzyme (2 hours at 37°C). The target pET32a vector was cleaved with *NdeI* and *BamHI* in the same manner, and subsequently incubated with 1  $\mu$ L of CIA phosphatase in order to dephosphorylate the 5' ends and prevent self religation of the vector. The vector and insert were then ligated overnight at 14 °C in the presence of 1 Weiss unit of T4 DNA Ligase, transformed into XL2-Blue and plated out onto agar plates containing 100  $\mu$ g/ml Ampicillin. Six colonies were picked from the plate to start 100 mL cultures in LB medium, and plasmid DNA was isolated using the QIAGEN Plasmid DNA Midi Kit. The DNA was verified by sequencing (*SeqLab*, Goettingen, Germany) and transformed into BL21(DE3) *E.coli* strain from which glycerol stocks were prepared and stored at -80 °C. Vector map of the pET32a-h $\beta$ 2m construct is depicted in **Figure 2-3**.

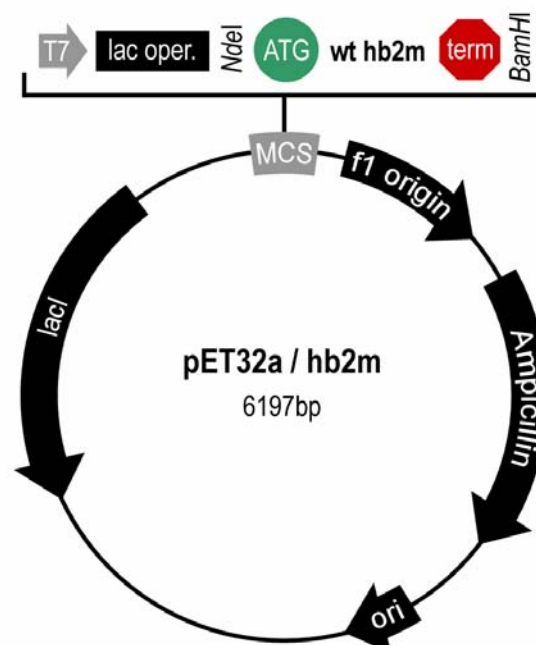


**Figure 2-3.** Vector map of pET32a plasmid coding for human beta-2-microglobulin.

### 2.3.2. Protein expression

#### 2.3.2.1. Expression in LB medium

The BL21(DE3) cells carrying the pET32a-h $\beta$ 2m construct were grown on a fresh agar/Ampicillin plate from the glycerol stock, and a single colony was picked to start a 20 mL overnight culture in LB, which was transferred into 750 mL of the medium the next morning. Cells were grown at 37 °C to an OD<sub>600</sub> of 0.6 and protein expression was induced by addition of IPTG to a final concentration of 1 mM. Following induction, the culture was incubated for 6 hours at 37 °C and cells were collected by centrifugation at 8000 x g, 4 °C, 15 minutes (Beckman J-20) and stored at -80 °C.

#### 2.3.2.2. Expression in M9 minimal medium

Similarly to the expression protocol in LB, the cells from the glycerol stock were grown on a fresh agar/Ampicillin plate and a single colony was picked to start a day culture in 2 mL of LB medium, which was then used to inoculate a 50 mL overnight culture in M9 medium. The next day, the overnight culture was transferred into 1 liter of M9 minimal medium, which contained <sup>15</sup>N-NH<sub>4</sub>Cl and if required <sup>13</sup>C-glucose in order to obtain uniformly <sup>15</sup>N- or <sup>13</sup>C<sup>15</sup>N-labeled protein. At an OD<sub>600</sub> = 0.7-0.8, protein expression was induced. Eight hours after induction the cells were harvested and stored at -80 °C.

### 2.3.3. Purification of h $\beta$ 2m

#### 2.3.3.1. Isolation from inclusion bodies

The frozen cell pellet was resuspended in 30 ml of buffer S1 and sonicated 5 times for 20 seconds using a Bandelin Sonopuls HD2200 sonicator equipped with a UW2200 horn, SH213G probe and a 12.7 mm TT13 sonotrode (*Bandelin electronic*, Berlin, Germany). After sonication, sodium deoxycholate was added to the sample to a final concentration of 2 % (w/v) and the mixture was incubated on ice for 10 minutes.  $\beta$ -2-microglobulin is secreted in the BL21(DE3) strain into inclusion bodies, which after disruption of the cells were collected by centrifugation at 20000 x g, 4 °C for 10 minutes (Beckman J-20) and washed three times with buffer W1. The inclusion body pellet was then resolubilized by stirring in 20 mL of buffer U1 for 1 hour at room temperature. The urea-denatured protein was cleared from any insoluble contaminants by centrifugation at 48000 x g, 4 °C for 30 minutes (Beckman Avanti J-30I).

### 2.3.3.2. Refolding by dialysis

Refolding of h $\beta$ 2m was achieved by removal of denaturant during dialysis. As more than 50-fold excess of buffer led to partial precipitation of the protein, dialysis was performed twice against 1 liter of 10 mM Tris, pH 8.0 using a Spectra/Por Cellulose Ester 3500 MWCO membrane (*Spectrum Laboratories*, Rancho Dominguez, USA).

### 2.3.3.3. Size-exclusion chromatography

After the removal of denaturant, the sample was dialyzed twice against 1 liter of buffer GF, sterile filtered and concentrated to <16 mL in a Vivaspin 20, 5000 MWCO concentrator (*Vivaproducts*, Littleton, USA). The protein was then loaded onto a HiLoad 16/60 Superdex 200 column installed on an ÄKTA purifier FPLC system (*GE Healthcare*, Chalfont St. Gilles, UK) and separated in a 0.5 mL/min flow of buffer GF. Fractions containing monomeric h $\beta$ 2m were pooled, concentrated to 200-250  $\mu$ M, dialyzed against water and stored at 4 °C.

### 2.3.4. Preparation of amyloid fibrils

Aggregation of h $\beta$ 2m was carried out at 37 °C in 25 mM phosphate, 25 mM acetate buffer, pH 2.5 with agitation at 500 rpm in an Eppendorf Thermomixer comfort (*Eppendorf*, Hamburg, Germany). The samples were prepared by addition of 10xAG buffer and water such that the final protein concentration was 100  $\mu$ M in 1xAG buffer. Prior to incubation, the solution was sterile filtered and the pH value was controlled with an Aldrich glass microelectrode (*Sigma-Aldrich*, Deisenhofen, Germany).

### 2.3.5. H/D exchange

Proton / deuterium exchange in the fibrillar state was performed as described in 2.2.9. The exchange time for h $\beta$ 2m fibrils was 7 days.

## 2.4. NMR spectroscopy

### 2.4.1. Backbone resonance assignments

During the course of this work, several backbone assignments of  $\beta$ -2-microglobulin and the prion protein mutants were obtained. The sample conditions and corresponding NMR experiments used for assignment are listed in **Table 2-3**.

**Table 2-3.** Experiments used for backbone resonance assignments

Protein	Sample conditions	NMR experiments	Comments
humPrP <sub>23-159</sub>	10 mM sodium acetate, pH 4.5	(HA)CANNH, HNCO	based on BMRB entry 4402
	10 mM sodium acetate, pH 6.5	(HA)CANNH	based on assignment at pH 4.5
	2 M GdnSCN, 0.1 % formic acid, 50% H <sub>2</sub> O / 50% D <sub>2</sub> O, pH 3.0	HNN, HNCACB	
humPrP <sub>23-173</sub>	10 mM sodium acetate, pH 4.5	(HA)CANNH	
	2 M GdnSCN, 0.1% formic acid, 50 % H <sub>2</sub> O / 50 % D <sub>2</sub> O, pH 3.0	HNN, HNCACB	
h $\beta$ 2m	in pure water, pH 2.5	(HA)CANNH, HNCO	based on assignment by Katou et al., 2002
	in pure water, pH 3.6	<sup>13</sup> C-detected CON	only <sup>13</sup> C' and <sup>15</sup> N resonances assigned
	25 mM sodium phosphate, pH 7.0	HNCA	based on BMRB entry 5169
	4 M GdnSCN, 0.1 % formic acid, 50% H <sub>2</sub> O, 50% D <sub>2</sub> O, pH 3.0	HNN, HNCACB, CBCA(CO)NH	
h $\beta$ 2m fibrils	25 mM sodium phosphate, 25 mM sodium acetate, pH 2.5	2D planes of HNCO and HNCA	

In general, conventional 3D experiments such as HNCACB, CBCA(CO)NH, HNCO and (HA)CANNH were applied. In case conditions facilitating unfolding were used and increased spectral overlap in the <sup>1</sup>H-<sup>15</sup>N plane was observed, the <sup>1</sup>H and <sup>15</sup>N backbone resonances were assigned with the HNN experiment shown in **Figure 2-4** (Panchal et al., 2001).

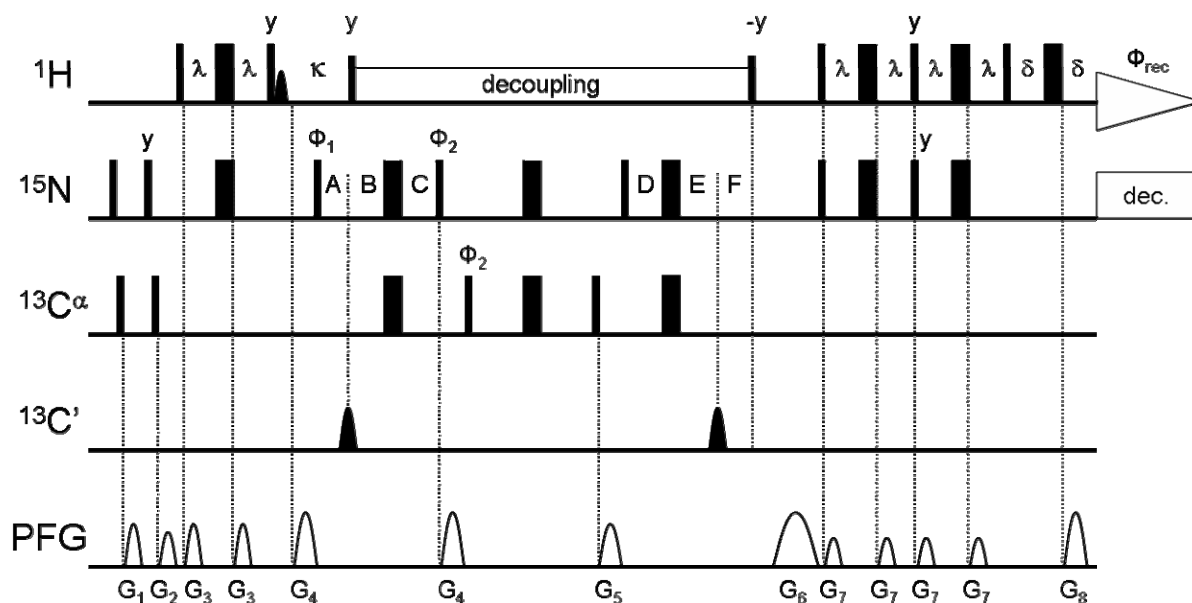


**Figure 2-4.** HNN pulse sequence.

Narrow and wide pulses correspond to  $90^\circ$  and  $180^\circ$  flip angles, respectively, with phase  $x$  unless indicated. Water suppression is achieved by a flip-back pulse in the first INEPT. The delays are:  $\lambda = 2.7$  ms,  $\kappa = 5.4$  ms,  $\delta = 0.35$  ms,  $A = t_1/2$ ,  $B = T_N$ ,  $C = T_N - t_1/2$ ,  $D = t_2/2$ ,  $E = T_N$ , and  $F = t_2/2$ . Phase cycling for the experiment is:  $\Phi_1 = 2(x), 2(-x)$ ;  $\Phi_2 = x, -x, -x, x$ ; and  $\Phi_{\text{rec}} = 2(x), 2(-x)$ ; (adapted from Panchal et al., 2001).

Assignments of human prion protein mutants at pH 4.5 were aided with the chemical shift list of humPrP<sub>23-230</sub> deposited in the Biological Magnetic Resonance Bank (BMRB, <http://www.bmrb.wisc.edu>) under accession number 4402.

Assignment of h $\beta$ 2m at pH 3.6 was obtained based on chemical shift changes in the  $^{13}\text{C}$ -detected CON experiment (**Figure 2-5**) (Bermel et al., 2006) upon a 6-step titration of NaOH from pH 2.5 to pH 3.6.

Signals of h $\beta$ 2m fibrils observed under HR-MAS were assigned from 2D projections of HNCA and HNCOC experiments, and by comparison of the fibril spectrum with the spectrum of monomeric h $\beta$ 2m at pH 2.5.

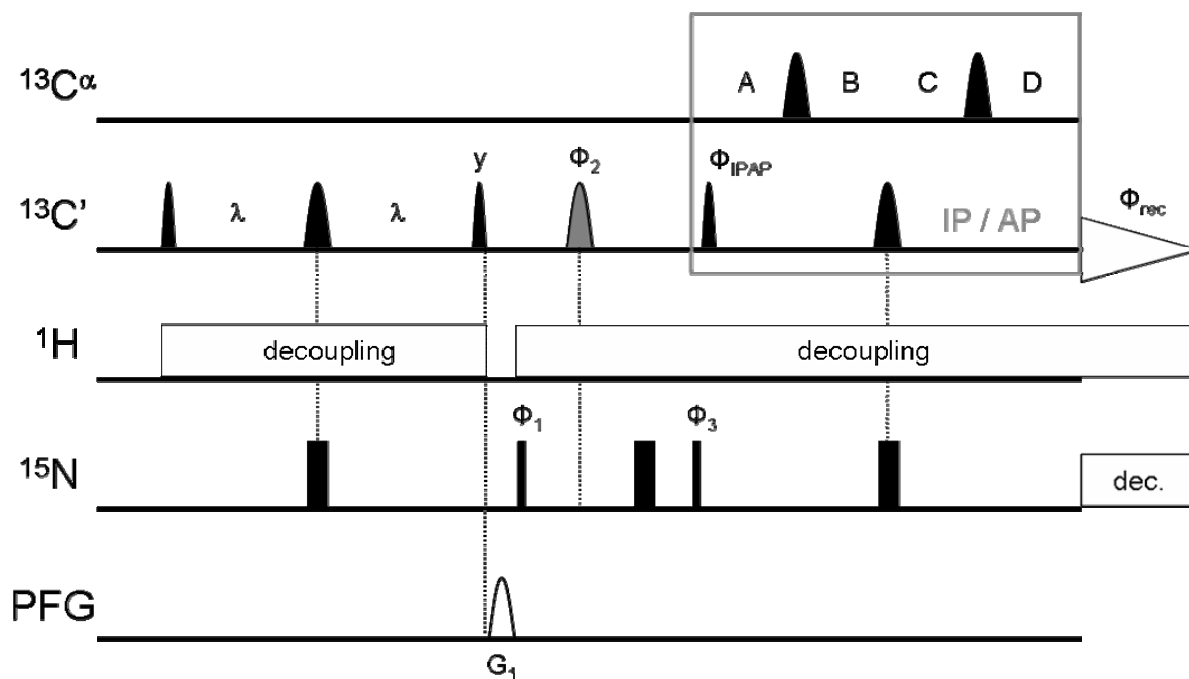


**Figure 2-5.** Pulse sequence of  $^{13}\text{C}$ -detected CON-IPAP.

Narrow and wide pulses correspond to  $90^\circ$  and  $180^\circ$  flip angles, respectively, with phase  $x$  unless indicated. The gray colored shape indicates an adiabatic pulse. The delay  $\lambda = 12.5$  ms. Selection of in-phase (IP) and anti-phase (AP) components is done by changing the duration of delays A, B, C, D. For IP spectrum the delays are: A = B = C = D = 6.25 ms, and for the AP spectrum: A = 4.5 ms; B = 8 ms; C = D = 6.25 ms. The phase cycle for the experiment is:  $\Phi_1 = x, -x$ ;  $\Phi_2 = 2(x), 2(-x)$ ;  $\Phi_3 = 4(x), 4(-x)$ ;  $\Phi_{\text{IPAP}}(\text{IP}) = x$ ;  $\Phi_{\text{IPAP}}(\text{AP}) = -y$ ; and  $\Phi_{\text{rec}} = x, -x, x, -x, -x, x, -x, x$ ; (adapted from Bermel et al., 2006).

#### 2.4.2. Secondary structure determination

Regions of secondary structure or propensities for adopting a certain conformation can be detected by secondary chemical shifts (SCS), which are calculated as the difference between the experimentally observed chemical shift and the random coil chemical shift. Random coil values used in the calculation were taken from literature (Wishart et al., 1995; Schwarzinger et al., 2001).

#### 2.4.3. High-resolution magic angle spinning

The sample for high-resolution magic angle spinning was prepared by placing 10 mg of uniformly  $^{13}\text{C}, ^{15}\text{N}$ -labeled h $\beta$ 2m fibrils in a BL4 50  $\mu\text{L}$  Teflon rotor (*Bruker Biospin*, Karlsruhe, Germany). All spectra were measured under MAS at 7.2 kHz on a 900 MHz Bruker AVANCE spectrometer equipped with a 4 mm HR-MAS probe with Z-gradients.



## 2.4.4. Measurement of diffusion coefficients

The diffusion coefficient of h $\beta$ 2m fibrils under HR-MAS was measured by pulse field gradient NMR using the LED pulse sequence with a bipolar gradient pulse pair and two spoil gradients (Figure 2-6). Residual water and 1,4-dioxane were used as the internal, and bovine serum albumin as the external reference. Signal decay curves for the protein were plotted after integration of both the amide and the aliphatic regions of the spectrum. The decay curves were fitted to a single exponential function and corresponding diffusion coefficients were calculated using the external reference values, while the internal reference was used to verify that no change in experimental conditions occurred in between the two measurements.

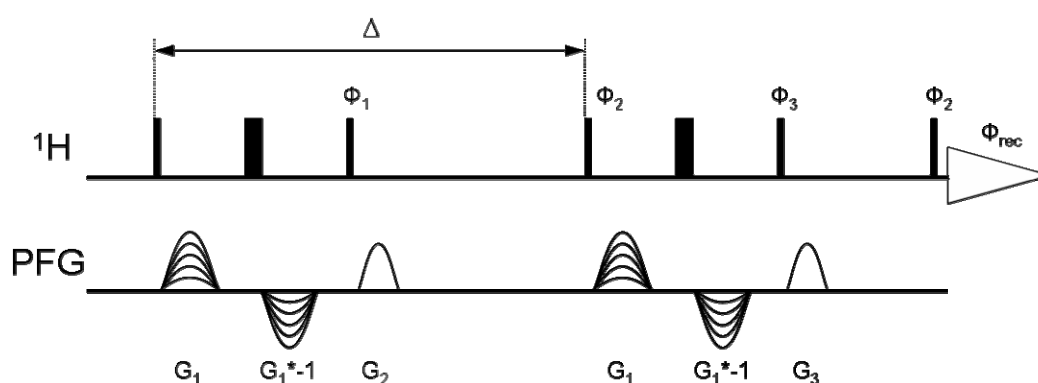


**Figure 2-6.** Pulse sequence of LED sequence with bipolar gradients.

Narrow and wide pulses correspond to  $90^\circ$  and  $180^\circ$  flip angles, respectively, with phase  $x$  unless indicated. The length of the diffusion labeling gradient  $G_1$  was 0.5 ms and its strength varied from 2 to 95 %, with the diffusion delay  $\Delta = 50$  ms and the eddy current delay  $T_e = 5$  ms. The phase cycle is:  $\Phi_1 = 2(x), 2(-x)$ ;  $\Phi_2 = 4(x), 4(-x), 4(y), 4(-y)$ ;  $\Phi_3 = 2(x, -x), 2(-x, x), 2(y, -y), 2(-y, y)$ ;  $\Phi_{rec} = x, -x, -x, x, -x, x, x, -x, y, -y, -y, y, -y, y, y, -y$ ; (adapted from Wu et al., 1995).

## 2.4.5. Residual dipolar couplings

Residual dipolar couplings were determined in presence of  $n$ -alkyl-poly(ethylene glycol) (C12E5) / hexanol mixture as cosolvent (Ruckert and Otting, 2000), using the IPAP-HSQC pulse sequence (Ottiger et al., 1998). First, the J-couplings were measured as splittings in the  $^{15}\text{N}$  dimension of the IPAP-HSQC in an isotropic solution of the protein. Then partial alignment was introduced by addition of C12E5 to a concentration of 5% (w/v) and subsequent titration of  $n$ -hexanol until a splitting in a 1D  $^2\text{H}$  spectrum was observed. The spectrum was remeasured and the  $^1\text{D}_{\text{NH}}$  dipolar couplings were calculated as the difference between the splitting measured in the anisotropic condition and the J-couplings measured in absence of alignment.

#### 2.4.6. NMR-detection of H/D exchange rates

Prior to the measurement of H/D exchange rates, the temperature in the sample chamber of the spectrometer was set to 278 K, and probehead tuning and matching was performed on an aliquot of precooled fibril dissolving buffer. The sample was then prepared by resolubilizing the lyophilized exchanged fibrils in 250  $\mu$ L of precooled dissolving buffer followed by a brief centrifugation for 10 seconds at top speed in a table-top centrifuge (*Eppendorf*, Hamburg, Germany). The sample was then transferred to a Shigemi NMR tube and transported on ice to the spectrometer. To monitor the back-exchange process in the monomeric state, a series of  $^1\text{H}, ^{15}\text{N}$ -HSQC spectra was recorded over a period of 24 hours with each spectrum acquired with 1024 x 512 complex points and 4 transients per increment (experiment time of 46 minutes). The “dead time” for sample preparation and experiment setup was typically 10-15 minutes.

Changes in peak intensity during the back-exchange process were then analyzed and fitted to a single exponential function. The protection map was subsequently generated by plotting the normalized intensity at the end of the experiment series ( $I_{24\text{h}}/I_0$ ) against the sequence.

#### 2.4.7. Structural predictions with CS-Rosetta

Predictions with CS-Rosetta were generally run according to the authors' manual provided at [spin.niddk.nih.gov/bax/software/CSROSETTA/index.html](http://spin.niddk.nih.gov/bax/software/CSROSETTA/index.html). Minor alterations in the executable scripts were necessary for proper functioning of the package. These included usage of “fasta” and “non-fasta” NR databases and changes in checkpoint definition for *psipred*.

##### 2.4.7.1. MFR fragment selection

In the MFR mode, 200 fragments were selected and used for the subsequent ROSETTA structure prediction, and all full-atom models were evaluated by chemical shift rescoring. In case of the “triplicate” fragment (see 3.2.4.1), the energy terms for residues in the Gly-Ser linkers were excluded from the ROSETTA full-atom energy. Finally, the chemical shift based energy rescoring was applied using the script *runCSrescore.com* provided in the installation package.

#### 2.4.7.2. Hybrid fragment selection

To run CS-Rosetta in hybrid mode, new databases of idealized protein structures (vall.dat.apr24), pdb files (PDBH.hyb), chemical shift lists (CS.hyb), and idealized backbone torsion angles (ANGLESS.hyb) needed to be modified by the authors. Due to problems with fragment assembly, the initial fragment candidate files containing 2000 hybrid fragments (`$TAG$PDB$CHAIN09_05.000_v1_3` and `$TAG$PDB$CHAIN03_05.000_v1_3`) were generated by Dr. Yang Shen at the National Institute for Diabetes and Digestive and Kidney Diseases, Maryland, USA. The fragment candidates were then scored with the script `rosettaFrag2csFrag` and 200 fragments with best chemical shift scores were kept for each 3- and 9-residue target fragment.

## 3. Human prion protein

### 3.1. Introduction

#### 3.1.1. Transmissible spongiform encephalopathies

Transmissible spongiform encephalopathies (TSE), also termed “prion diseases”, are a group of rare fatal neurodegenerative disorders in humans and animals (**Tables 3-1** and **3-2**). The first cases of TSEs were observed more than 200 years ago in sheep, however it was about 20 years ago when prion diseases attracted public attention due to an outbreak of bovine spongiform encephalopathy (BSE) or “mad cow disease” in the United Kingdom, and several other European countries.

Prion diseases are characterized by progressive lesions with vacuolation in the brain, massive loss of neuronal cells and appearance of activated astrocytes (astrogliosis) (Brown and Gajdusek, 1991). However, the most distinct hallmark of TSE diseases is the accumulation of proteinaceous fibrils or “prion rods” in the central nervous system (Merz et al., 1981; Prusiner et al., 1983). These deposits consist mainly of the scrapie form of prion protein, PrP<sup>Sc</sup>, which is an isoform of host-encoded PrP (Bueler et al., 1993). While the incubation periods of TSEs may range from months to several years, after occurrence of clinical symptoms the disease rapidly progresses and leads to death in 3-6 months (Chesebro, 2003).

Prion diseases in animals have been identified in sheep, goat, cattle, mink, deer, elk and wild cats living in captivity (see **Table 3-1**). In humans, TSE diseases such as Creutzfeldt-Jakob disease (CJD) (Creutzfeldt, 1920; Jakob, 1921), Gerstmann-Sträussler-Scheinker syndrome (GSS) (Gerstmann et al., 1936) or kuru (Gajdusek and Zigas, 1957) comprise three groups of disorders: familial, transmitted and sporadic ones (**Table 3-2**).

**Table 3-1.** Prion diseases in animals

Disease	Animal	Etiology	First case
Scrapie	sheep, goat	infection	1732
Transmissible Mink Encephalopathy (TME)	mink	infection	1947
Chronic Wasting Disease (CWD)	deer, elk	infection	1967
Bovine Spongiform Encephalopathy (BSE)	cow	infection	1985
Feline Spongiform Encephalopathy (FSE)	cats	infection	1990

Sporadic CJD (sCJD) occurs at an incidence of 1 in 1 million people worldwide and accounts for 90% of TSE cases in humans (Masters and Richardson, 1978). The origin of sCJD is unknown as no mutations in the PrP-coding gene were found, and there is no epidemiological evidence for contact with people or animals with TSE disease (Harries-Jones et al., 1988; Will, 1993).

In about 10% cases, the prion disease occurrence has been attributed to either a PrP point mutation or insertions of octapeptide repeats. At present, 42 mutations in the *Prnp* gene are known, 20 of which are causative. Mutation-associated TSE diseases include familial CJD, GSS and fatal familial insomnia (FFI). Interestingly, clinical variability occurs even in patients of the same family, which suggests that other genes or non-genetic factors may play a role in these diseases (Masters et al., 1981; Chapman et al., 1993).

**Table 3-2.** Human prion diseases

Disease	Etiology	First case
sporadic Creutzfeldt-Jakob disease (sCJD)	unknown	1920/21
familial Creutzfeldt-Jakob disease (fCJD)	PrP mutation	1924
Gerstmann-Sträussler-Scheinker syndrome (GSS)	PrP mutation	1928
Kuru	infection	1956
iatrogenic Creutzfeldt-Jakob disease (iCJD)	infection	1974
Fatal familial insomnia (FFI)	PrP mutation	1992
variant Creutzfeldt-Jakob disease (vCJD)	infection	1995

The group of transmitted TSEs includes kuru, iatrogenic (iCJD) and variant Creutzfeldt-Jakob disease (vCJD) and accounts to less than 1 % of all cases. Patients with iCJD develop the disease as a result of a surgical procedure during which they were infected with contaminated surgical instruments or received a tissue transplant from a donor with non diagnosed prion disease (Duffy et al., 1974; Bernoulli et al., 1977; Brown et al., 1992). About 90 cases of iCJD occurred after treatment with human growth hormone, which was pooled from large groups of individuals (Fradkin et al., 1991; Billette de Villemeur et al., 1996). Infectious prions in kuru disease were transmitted by ritualistic cannibalism and the disease disappeared when these rituals were ceased (Gajdusek and Zigas, 1957; Gajdusek, 1977). A few years after the epidemic occurrence of BSE in the UK, cases of a new variant of CJD have been observed (**Figure 3-1**) (Will et al., 1996). Experimental data indicated that this

variant CJD and BSE are caused by the same prion strain (Hill et al., 1997) and it is now believed that vCJD is the human counterpart of BSE.

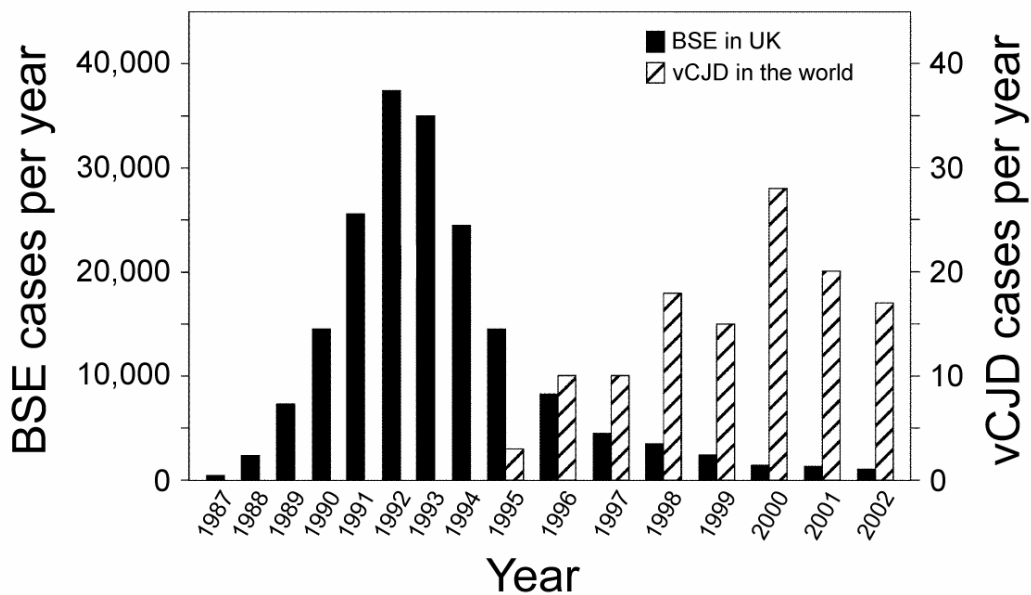


**Figure 3-1.** Comparison of the incidence of BSE in cattle and vCJD in humans (adapted from Chesebro, 2003).

### 3.1.2. The “protein only” hypothesis

For many years after the first description of TSE in humans by Creutzfeldt and Jakob, it was believed that prion diseases are caused by a “slow virus” (Sigurdsson, 1954; Hadlow, 1959; Klatzo et al., 1959; Gajdusek et al., 1966). With increasing knowledge of the diseases, it became clear that such a virus would need to have very special properties. Although short nucleic acid fragments have been found in scrapie prion preparations, no intact nucleic acid molecules of potential viral genome size have been identified. The virus would therefore need to be able to regenerate from small fragments. Additionally, the high correlation with PrP mutations in familial CJD would have to be explained. The virus should be rather common to account for almost 100% disease incidence in individuals carrying PrP mutations, and at the same time preferentially interact only with the mutant prion protein, in order to explain very low incidence of the disease in people lacking mutations in the *Prnp* gene (Chesebro, 2003). In spite of many efforts, no candidate viruses fulfilling all these criteria have been suggested.

The protein only hypothesis was first suggested by Griffith, who proposed that the infectious agent might be a self-replicating protein (Griffith, 1967). With the discovery of prion protein as the major component of scrapie, the altered pathogenic PrP<sup>Sc</sup> has been proposed to be the sole component of the infectious agent (Bolton et al., 1982; Prusiner,

1982). However, this theory has not been proven as the purified *in vivo* PrP aggregates contain traces of nucleic acids, and only one study reported that transgenic mice infected with synthetic prions developed clinical symptoms following lengthy incubation periods (Legname et al., 2004). This result is however highly controversial as the mice used in the study were aging, and it has been shown that transgenic mice overexpressing PrP<sup>C</sup> spontaneously develop the disease at late stages of life without prion inoculation (Westaway et al., 1994). As other trials of producing an infectious prion *in vitro* have been unsuccessful (Hill et al., 1999), the infectivity of synthetic prions remains questionable.

Two kinetic models for the conversion of PrP<sup>C</sup> to PrP<sup>SC</sup> have been proposed (Figure 3-2).

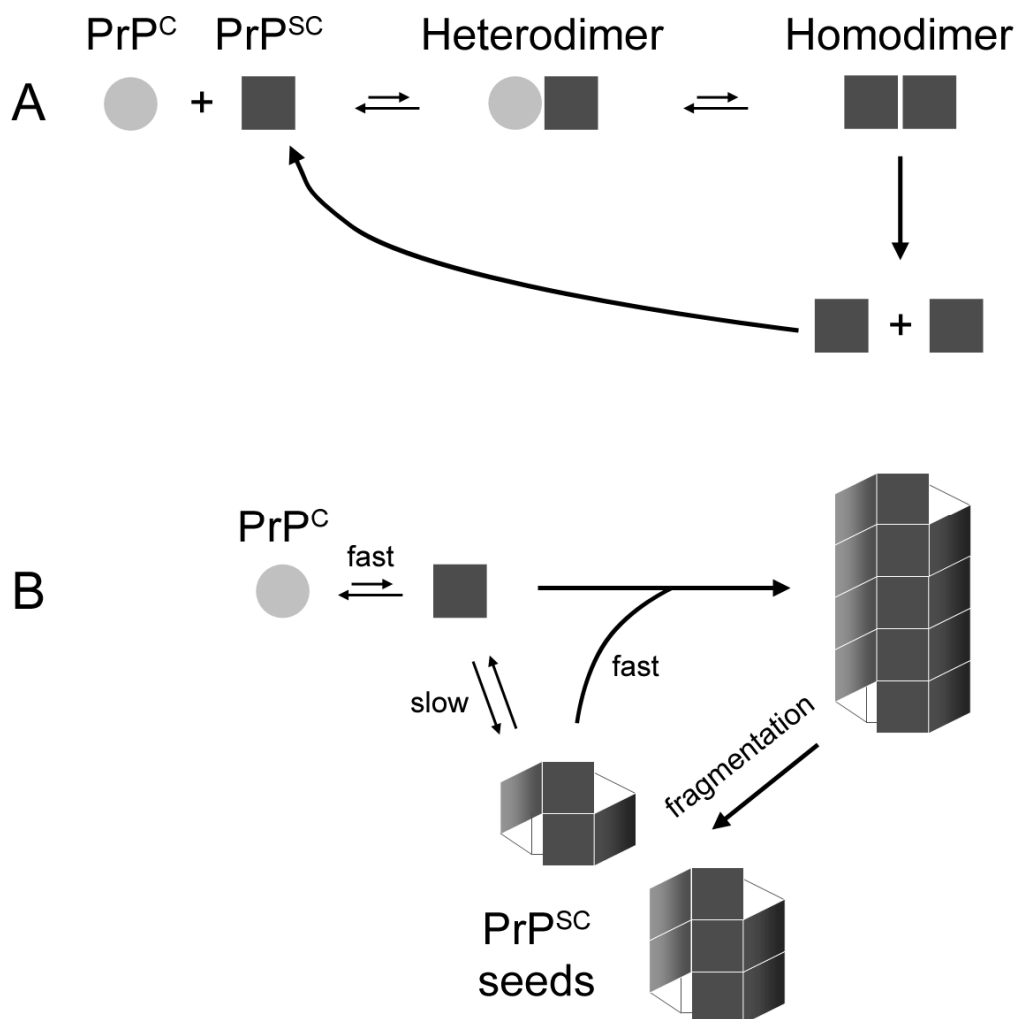


**Figure 3-2.** Mechanistic models for PrP<sup>SC</sup> formation. (a) PrP<sup>SC</sup> catalyzes the conversion of PrP<sup>C</sup> via a heterodimeric intermediate. (b) PrP<sup>SC</sup> serves as a seed for aggregation of PrP<sup>C</sup>. Fragmentation of the polymer leads to multiplication of PrP<sup>SC</sup> seeds (adapted from Caughey and Chesebro, 1997).

In the first model (Prusiner, 1991), monomeric PrP<sup>SC</sup> forms a heterodimer with PrP<sup>C</sup> (**Figure 3-2a**). With the help of another protein (called “protein X”) PrP<sup>C</sup> is then converted to the infectious form and dissociates from the complex to auto catalyze the formation of more PrP<sup>SC</sup> molecules. The second model (Caughey et al., 1995) proposes that conversion of the cellular form to the scrapie form takes place upon recruitment of PrP<sup>C</sup> by an aggregate of PrP<sup>SC</sup> (**Figure 3-2b**).

Another alternative to the “protein only” prion hypothesis is a bacterial infection activating prion protein on the cell surface. *Spiroplasma* bacteria are able to resist high temperatures and irradiation and have been isolated from brains of sheep with scrapie, deer with chronic wasting disease and CJD patients (Bastian, 2005). Furthermore, the isolated *Spiroplasma* bacteria from sheep and deer were shown to cause TSE disease when inoculated intracranially into the animals (Bastian et al., 2007). However, no *Spiroplasma* rRNA has been found in scrapie-infected hamster brain (Alexeeva et al., 2006), therefore if presence of bacteria is not essential for development of the disease, it makes bacterial infection very unlikely to be the cause.

### 3.1.3. The species barrier

One of the characteristic features of prion diseases is their transmissibility. In contrast to the relatively easy intra-species transmission, cross-species transmission of TSE, typically studied on laboratory rodents, is much less efficient as indicated by extended incubation times and incomplete spectrum of symptoms (Prusiner, 1996; Weissmann et al., 1996). This phenomenon, called the species barrier, can be overcome by a few passages in the new host, reflecting adaptation of the prion. Evidence exists that the adaptation depends on several factors, such as the pair of species involved and the direction of transmission.

The best example of the host related species barrier is the rabbit, which is resistant to prions from sheep scrapie, human CJD and BSE (Gibbs and Gajdusek, 1973). However, rabbits expressing ovine PrP gene, developed TSE upon infection with sheep scrapie (Sarradin, 2007). A similar observation was made in mice expressing mink and cervid PrP which made them susceptible to TME and CWD, respectively (Browning et al., 2004; Windl et al., 2005; LaFauci et al., 2006).

The dependence of species barrier upon the direction of transmission was well illustrated by experiments on recombinant C-terminally truncated mouse and hamster PrP (Vanik et al., 2004; Jones and Surewicz, 2005). The authors have shown that while



recombinant hamster PrP rapidly aggregates upon seeding with preformed hamster PrP fibrils, no polymerization is observed when hamster PrP is seeded with preformed mouse PrP fibrils (**Figure 3-3a**). In contrast, monomeric mouse PrP aggregates when seeded with either mouse or hamster PrP fibrils. However, the conformation of hamster-seeded mouse PrP fibrils is similar to those of pure hamster PrP, and the newly formed „2nd generation“ fibrils can be used to seed monomeric hamster PrP (**Figure 3-3b**).

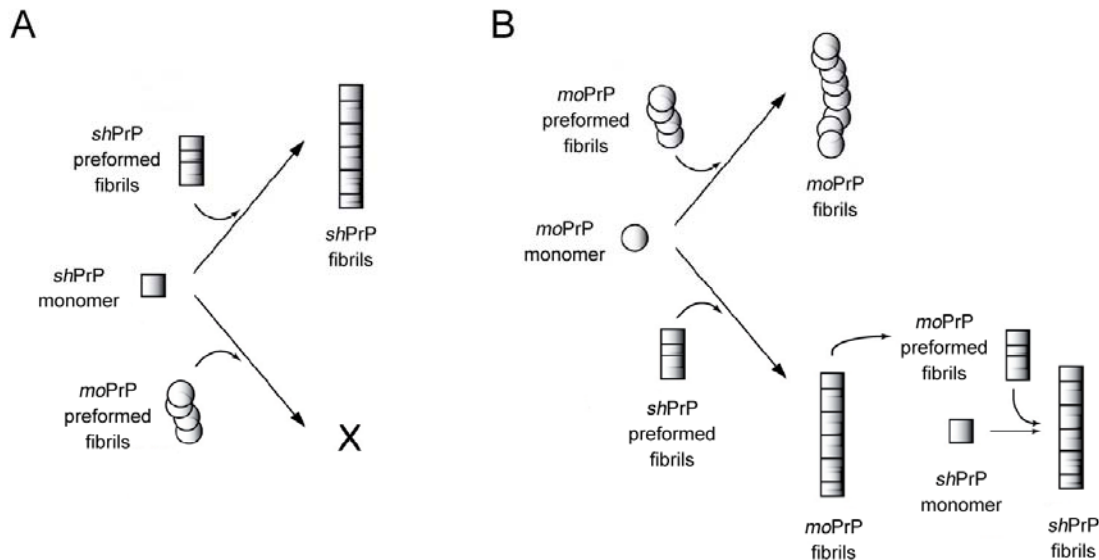


**Figure 3-3.** Cross species transmission modelled by seeded aggregation.

(a) shPrP aggregates rapidly when seeded with preformed shPrP fibrils. Seeds of moPrP cannot convert monomeric shPrP. (b) Monomeric moPrP can be seeded both by mouse and hamster preformed fibrils. If seeded with shPrP, resulting fibrils have morphology similar to parent seeds and can be used to seed shPrP monomer (adapted from Beringue et al., 2008).

These results strongly suggest that the species barrier is encoded in the structure of PrP<sup>SC</sup> and that some types of fibrils can be used to seed the monomeric PrP of a different species because they are within the spectrum of allowed conformations. Still, these data were obtained on truncated forms of the proteins that lack the C-terminal glycosylation and the GPI anchor, and could not be reproduced with full length PrP (Makarava et al., 2007). Further studies are therefore needed to understand the cause underlying the species barrier.

#### 3.1.4. Prion protein

The cellular form of the prion protein (PrP<sup>C</sup>) is synthesized as a family of four members, which include the major subset of glycosylphosphatidylinositol (GPI) anchored

protein, two transmembrane forms of opposite topologies ( $^{Ntm}PrP$  and  $^{Ctm}PrP$ ) and the minor soluble fraction ( $^{Cyt}PrP$ ) (Hegde et al., 1998; Holscher et al., 2001; Hegde and Rane, 2003). The prion protein is presented on the surface of neuronal cells (Kretzschmar et al., 1986) and through the interaction of the GPI-anchor with lipids associates with cholesterol- and glycosphingolipid-rich detergent resistant microdomains, called lipid rafts (Vey et al., 1996; Kaneko et al., 1997).

The structure of the prion protein comprises an unstructured N-terminal domain with five characteristic octapeptide repeats, and a globular C-terminus containing three helices, two short  $\beta$ -strands, a disulphide bridge and two glycosylation sites (**Figure 3-4**) (Zahn et al., 2000).

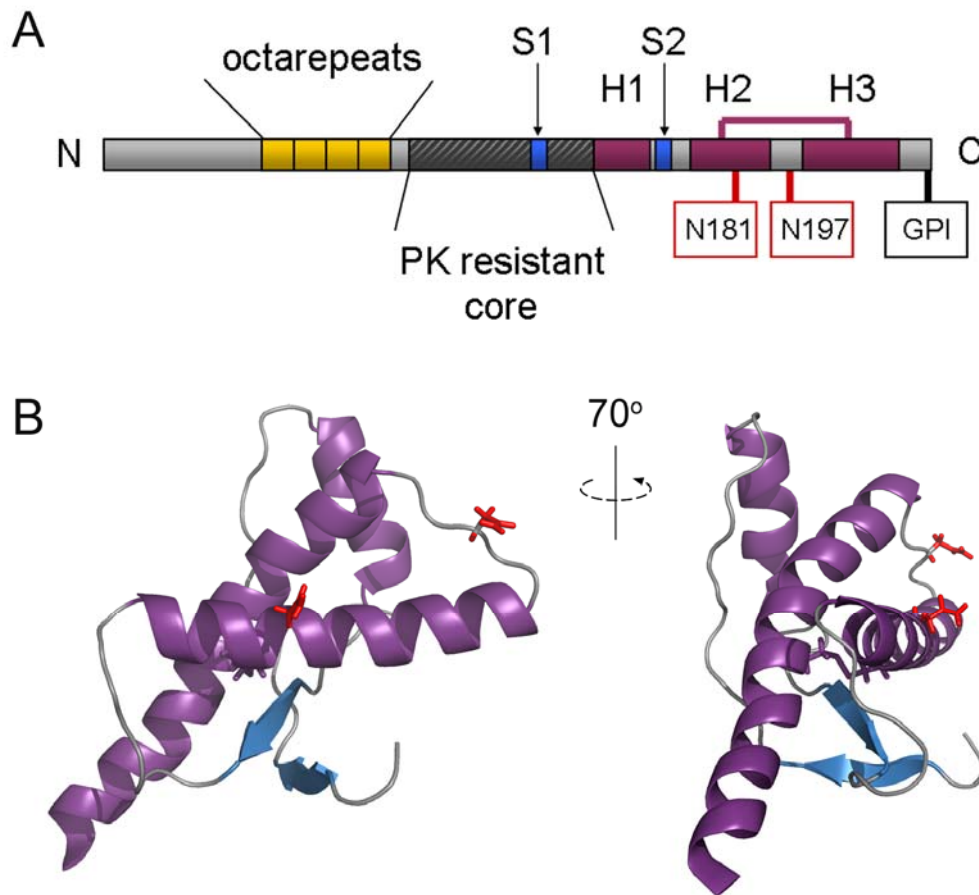


**Figure 3-4.** Structure of the human prion protein. (a) Schematic overview of the primary sequence; the octarepeat region (yellow),  $\alpha$ -helices (magenta),  $\beta$ -strands (blue), glycosylation sites (red) and the GPI anchor are indicated. (b) NMR structure of human prion protein fragment 121-230 (pdb entry 1QM0); structural elements are color coded as in a.

The hydrophobic helices 2 (residues 174-194) and 3 (200-228) are connected by a short loop and stabilized via a disulphide bridge between cysteins 179 and 214. Due to its polar amino acid sequence, helix 1 is not able to form hydrophobic interactions and is therefore isolated from the rest of the molecule (Morrissey and Shakhnovich, 1999) and thought to be stabilized by two arginine-aspartic acid salt bridges (Speare et al., 2003).

### 3.1.5. Structural models of PrP<sup>SC</sup>

The abnormal form of PrP<sup>C</sup>, denoted PrP<sup>SC</sup> was found to be the major component of the infectious TSE agent (Prusiner, 1982). Studies of the two forms of the protein show several differences, which are summarized in **Table 3-3**.

**Table 3-3.** Properties of normal and “scrapie” forms of the prion protein

normal PrP (PrP <sup>C</sup> )	abnormal PrP (PrP <sup>SC</sup> )
function unclear	TSE-specific
GPI-anchored glycoprotein	large aggregates and amyloid fibrils
soluble	insoluble in non-denaturing detergents
mostly $\alpha$ -helical	$\beta$ -sheet enriched
non-infectious	major component of infectious prion agent
proteinase K sensitive	partially resistant to proteinase K

PrP<sup>SC</sup> is insoluble in non-denaturing detergents, exists in an oligomeric or fibrillar form (Swietnicki et al., 2000) and shows partial resistance to digestion with proteinase K (Bolton et al., 1982). The molecule resulting from digestion of scrapie prions with proteinase K is termed PrP27-30 as in a SDS-PAGE gel it shows a band of 27-30 kDa. Many studies on *in vivo* isolated PrP<sup>SC</sup> are actually performed on PrP27-30, as the PrP<sup>SC</sup> preparations contain large amounts of PrP<sup>C</sup>. On a structural level PrP27-30 shows an increased  $\beta$ -sheet content of 32-37 % and 12-17 %  $\alpha$ -helix (Caughey et al., 1991; Gasset et al., 1993; Pan et al., 1993), in contrast to the predominantly helical PrP<sup>C</sup> (30 % helix and 4 %  $\beta$ -strand) (Zahn et al., 2000).

Several structural models of PrP<sup>SC</sup> that have been suggested so far (**Figure 3-5**) can be divided into two general categories: (i) structures in which helix 1 is converted to  $\beta$ -strand and (ii) structures in which helix 1 is retained.

One of the first models (**Figure 3-5a**) was proposed by Cohen and coworkers (Huang et al., 1995), one year before the first solution NMR structure of mouse prion protein was determined (Riek et al., 1996). The model bases on various spectroscopic and genetic data and shows a four-stranded beta-sheet covered on one side with two helices. The  $\beta$ -sheet would be formed by extended  $\beta$ -strands S1 and S2 (see **Figure 3-4**) and helix 1 converted into two strands. In this arrangement, residues implicated in the species barrier are found on the solvent accessible face of the  $\beta$ -sheet.

A more recent model (**Figure 3-5b**) from the same group suggests a left-handed  $\beta$ -helix as the structure of PrP<sup>SC</sup> (Govaerts et al., 2004). This model is based on electron crystallography projection maps of 2D crystals of mouse brain isolated PrP<sub>27-30</sub>. A simulation was performed for residues 89-175 of the mouse prion protein and the C-terminal helices were subsequently added to fit the EM images. In this model, helix 1 of the prion protein is also assumed to be converted to  $\beta$ -strand.

A model in which helix 1 is retained was proposed very recently as a result of a molecular dynamic simulation of human PrP<sub>90-230</sub> at low pH (DeMarco and Daggett, 2007). In this model, all three helices are retained and formation of six short  $\beta$ -strands is suggested in the region between residues 90 and 166, two of which originate from strands S1 and S2 present in PrP<sup>C</sup> (**Figure 3-5c**).

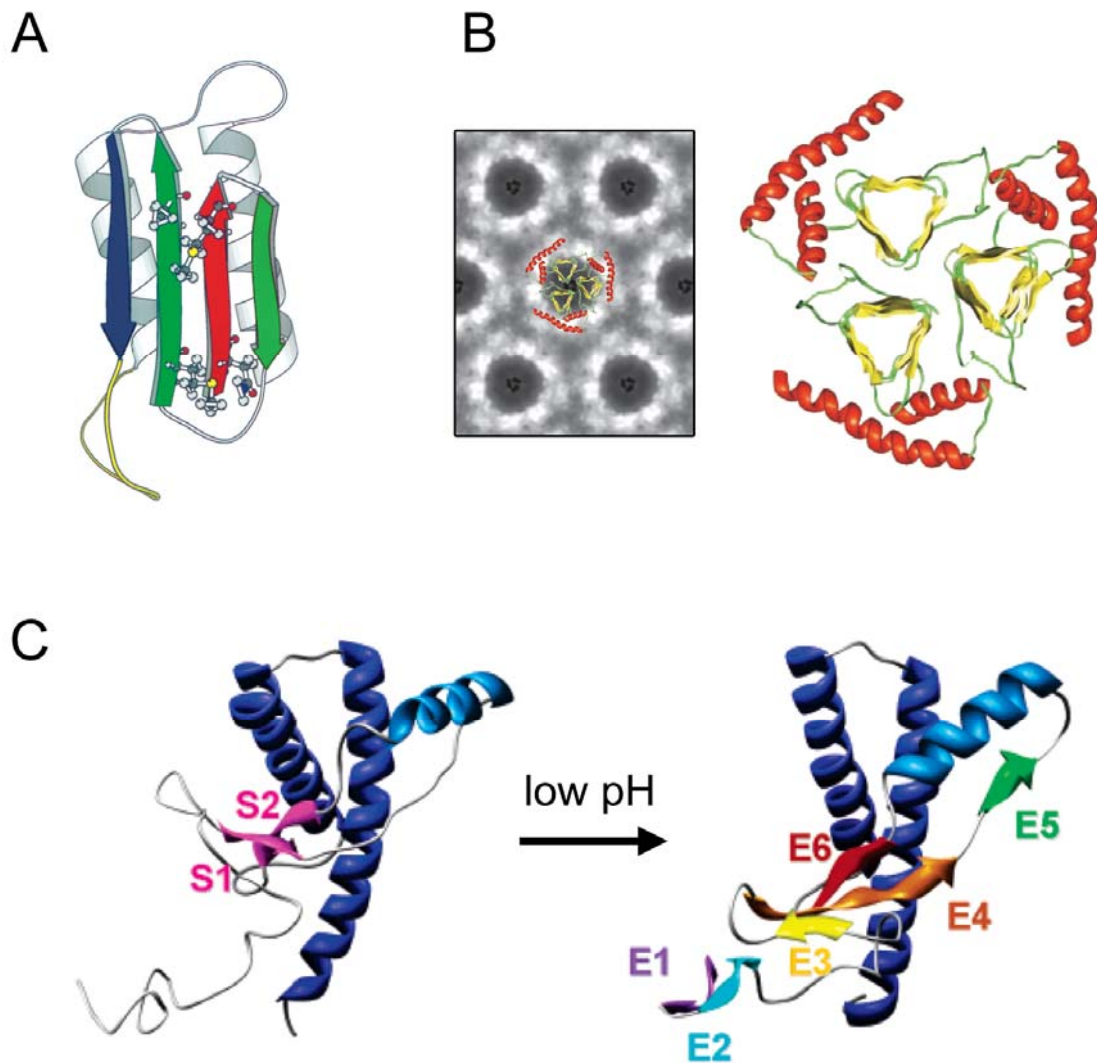


**Figure 3-5.** Structural models of PrP<sup>Sc</sup>.

(a) A four-stranded  $\beta$ -sheet is covered on one face with two helices; the four strands originate from  $\beta$ -strand 1 (red),  $\beta$ -strand 2 (blue), and converted helix 1 (green) (Huang et al., 1995). (b) A left-handed  $\beta$ -helix arrangement (Govaerts et al., 2004). (c) Six  $\beta$ -strands are formed between residues 90 and 166 (DeMarco and Daggett, 2007).

## 3.2. Results

### 3.2.1. Secondary structure analysis of human prion protein mutants

The various *Prnp*-gene mutants coding for fragments of the prion protein used in this study are schematically represented in **Figure 3-6** (see also **Table 2-1**). Expression and purification of the encoded proteins was performed as described in 2.2.4 – 2.2.7, and included isolation of inclusion bodies, purification by affinity chromatography and refolding of the protein fragments.

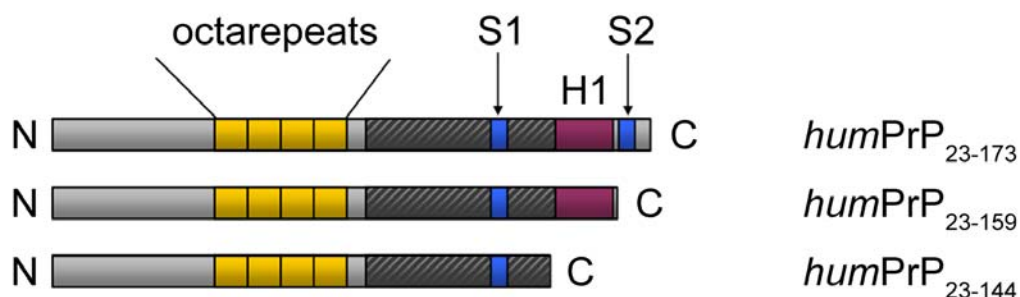


**Figure 3-6.** Schematic representation of the human prion protein stop mutants.

A preliminary structural analysis by circular dichroism (CD) spectroscopy showed spectra characteristic for largely unstructured proteins (Watzlawik et al., 2006). Deconvolution of the CD spectra was inconclusive and reported presence of small amounts of both  $\alpha$ -helical and  $\beta$ -sheet conformations in all of the mutant proteins (data not shown). Presence of secondary structure elements was detected by means of NMR secondary chemical shifts (SCS), which are defined as the differences between the observed chemical shift and the random coil chemical shift values. These small but distinct deviations are a very sensitive probe for secondary structure, especially in case of  $C\alpha$  and  $C'$  atoms (Dyson and Wright, 1998). A prerequisite for SCS analysis is the sequence specific assignment of resonances in an NMR spectrum. First, the backbone assignment of  $\text{humPrP}_{23-144}$  was obtained from standard three-dimensional NMR experiments (**Table 2-3**). The spectra of  $\text{humPrP}_{23-159}$  and  $\text{humPrP}_{23-173}$  were then compared to that of the shorter mutant in order to identify resonances originating from the C-terminal extensions of the polypeptide chain, which were then assigned from 3D spectra (**Figure 3-7**).

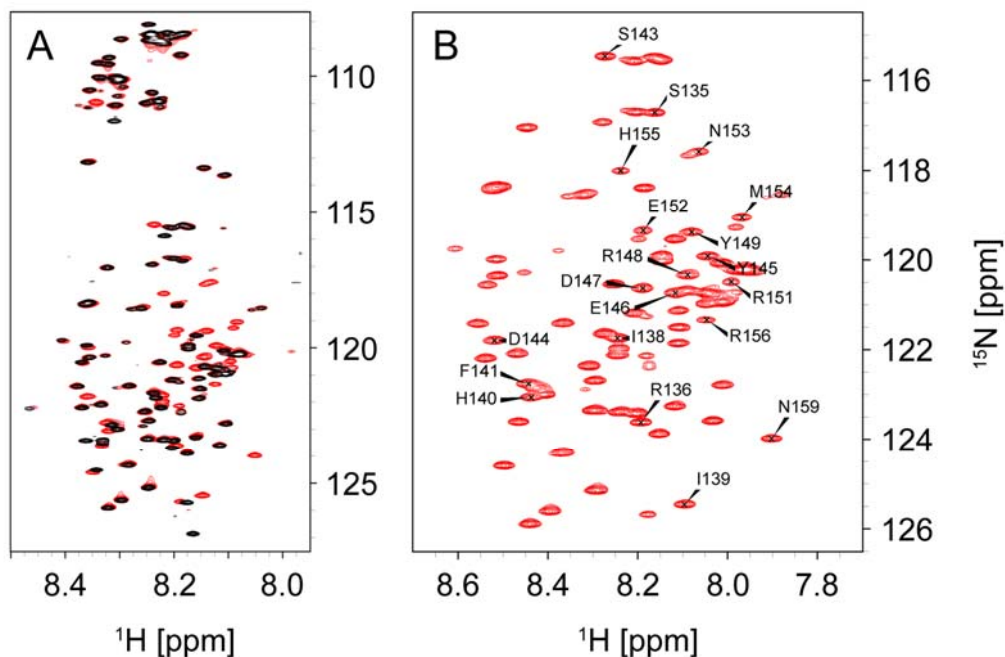


**Figure 3-7.** Assignment of PrP stop mutants.

(a) Overlay of  $^1\text{H}$ ,  $^{15}\text{N}$ -HSQC spectra of humPrP<sub>23-144</sub> (black) and humPrP<sub>23-159</sub> (red). (b) Assignment of resonance peaks of residues 136-159.

For the calculation of SCS, sequence corrected random coil values determined at pH 3.0 were used (Schwarzinger et al., 2001), except for prolines and aspartates where the random coil values were taken from Wishart and Sykes (Wishart and Sykes, 1994). Averaged secondary chemical shifts of  $\text{C}\alpha$  and  $\text{C}'$  atoms for humPrP<sub>23-159</sub> are depicted in **Figure 3-8**. Stretches of positive values are indicative of propensity for  $\alpha$ -helical conformation, which is clearly observed for residues 146-154. A comparison of the average SCS magnitude within the helix 1 region for humPrP<sub>23-159</sub> and humPrP<sub>23-230</sub> (based on BMRB entry 4402) reveals a helical content in the mutant of about 33 % with respect to the full length protein (data not shown). Interestingly, a propensity for extended structure is observed in the region 98-144 which forms the proteinase K resistant core in PrP<sup>SC</sup> (Peretz et al., 1997). Although the prion protein mutants spontaneously aggregate in presence of phosphate at pH 6.5, no change in secondary structure preference was observed under low ionic strength conditions at this pH.

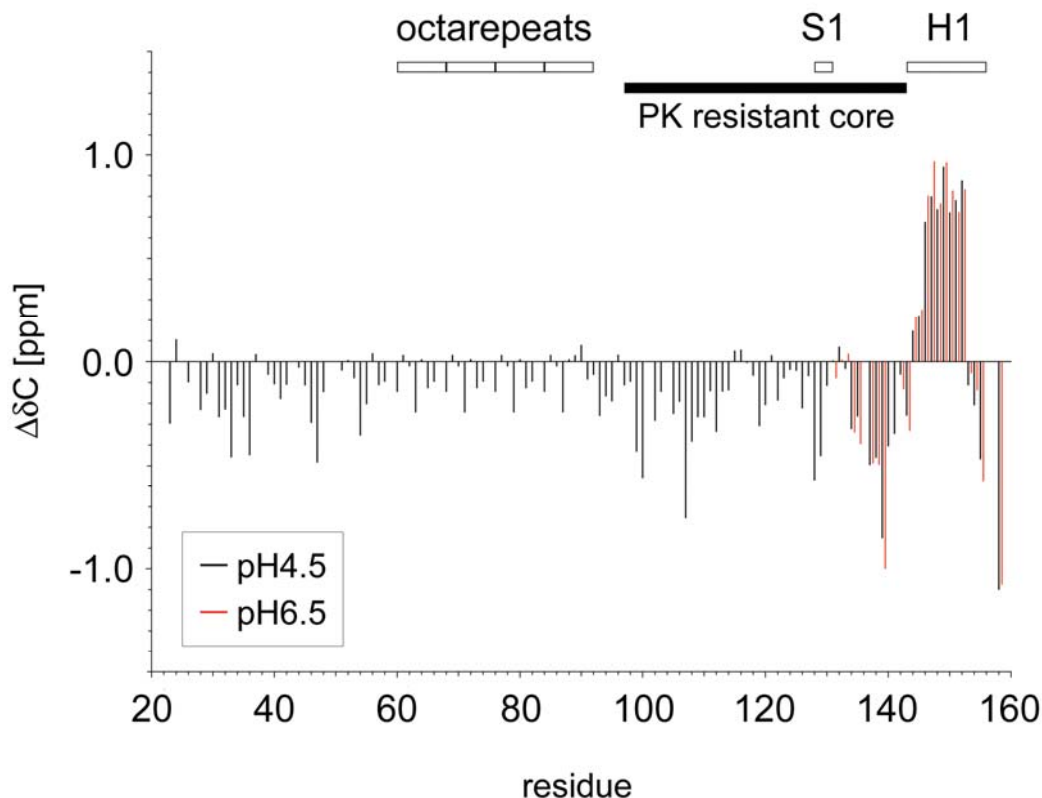


**Figure 3-8.** Secondary chemical shifts of humPrP<sub>23-159</sub>. SCSs were calculated as the difference between the observed chemical shift and the random coil values separately for C' and C $\alpha$  atoms and subsequently averaged to obtain  $\Delta\delta C$ . Structural elements found in the full-length prion protein are indicated by open and filled bars.

Additional information about the structure and dynamics can be obtained from residual dipolar couplings (RDCs) which can be measured for proteins weakly aligned in liquid-crystalline media. RDCs have proven especially useful in detection of local structure in denatured and intrinsically unfolded states where measurements of global dimensions suggest a random-coil behavior (Tanford et al., 1966). Since the stop mutants of the prion protein are indeed largely disordered and the humPrP<sub>23-159</sub> and humPrP<sub>23-173</sub> show local structural propensities, a measurement of RDCs was performed to support the SCS analysis. An important factor that needs to be considered in RDC measurements is the surface charge of the liquid-crystalline medium used (Skora et al., 2006). To prevent electrostatic interactions between the alignment medium and charged residues in the helix 1 region, a nonionic nematic phase comprising a mixture of *n*-alkyl-poly(ethylene glycol) and *n*-alkyl alcohol (Ruckert and Otting, 2000) was used. The RDC profile of humPrP<sub>23-159</sub> in C12E5 / *n*-hexanol is compared to the SCS data in **Figure 3-9**. A very good agreement is found within the helix 1 region and



the sign of RDCs for residues 23-50 and 90-135 reflects the structural tendencies observed with secondary chemical shifts. The inversion of the sign of residual dipolar couplings with respect to SCS seen for residues 135 and 139 suggests a change of the alignment tensor in this region. This might indicate that residues 135-143 align together with helix 1, however it should be noted that RDCs from only two residues in this region could be attained. Due to significant spectral overlap, no reliable RDCs could be obtained for the octarepeat region.

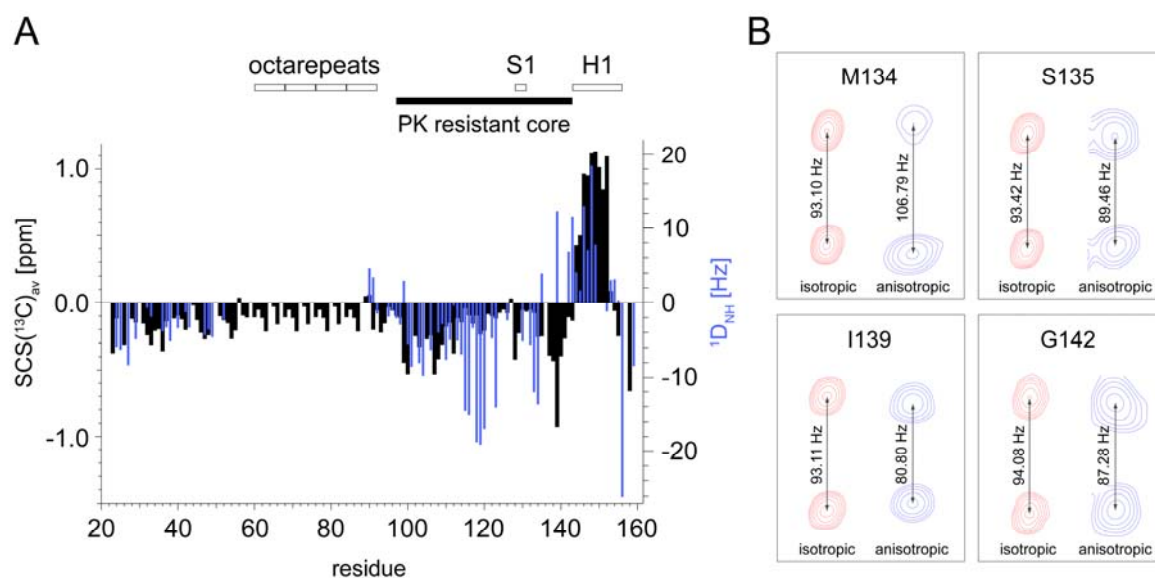


**Figure 3-9.**  $^1H$ - $^{15}N$  dipolar couplings of humPrP<sub>23-159</sub>.

(a) A comparison between secondary chemical shifts (black) and  $^1D_{NH}$  dipolar couplings (blue) measured in presence of 5% C12E5/hexanol alignment medium. (b) Excerpts from the  $^1H, ^{15}N$ -IPAP-HSQC spectra showing isotropic (red) and anisotropic (blue) couplings for the four observable residues in the 134-142 region. RDCs were calculated as differences between the isotropic and anisotropic couplings.

An interesting observation was made when comparing the chemical shifts between humPrP<sub>23-144</sub> and humPrP<sub>23-159</sub> spectra. Average shift differences were calculated according to Equation 3-1.

$$\Delta\delta_{AV} = \sqrt{(\delta_H)^2 + (\delta_N/5)^2} \quad (\text{Eq. 3-1})$$

As expected the extension of humPrP<sub>23-144</sub> by the C-terminal helix 1 region results in changes in the chemical environment of residues 130–144 which is reflected by a shift of those resonances in the NMR spectrum. However, such behavior is also observed for the N-terminal residues 23-25, which suggest a possible long-range interaction of the helix 1 region with the N-terminus (**Figure 3-10**). Another possible explanation for this finding might be a change in

pH since the N-terminal residues are charged and an increased change in the chemical shift is seen for His111, however no such behavior is observed for histidines in the octarepeat region, which makes pH an unlikely cause of the chemical shift changes reported for residues 23-25.

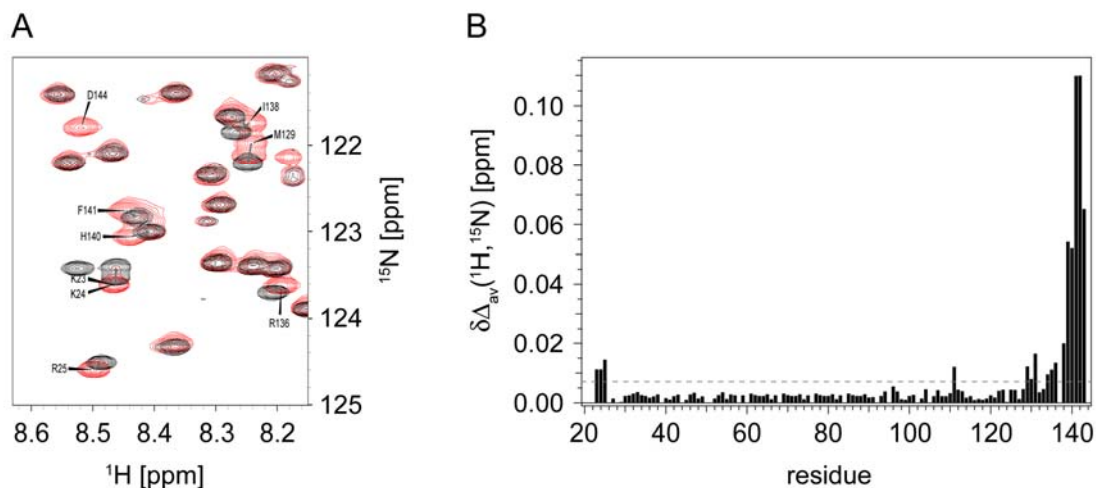


**Figure 3-10.** Long-range interaction between the N-terminus and the helix 1 region. (a) Selected region of HSQC spectra showing shifts of resonances in the spectrum of humPrP<sub>23-159</sub> (black) with respect to humPrP<sub>23-144</sub> (red). (b) Averaged chemical shift differences between the spectra of humPrP<sub>23-144</sub> and humPrP<sub>23-159</sub> calculated according to Eq.3-1.

In general, NMR investigations of secondary structure elements in mutants of the human prion protein confirmed the presence of helix 1 in the prion protein fragments 23-159 and 23-173. Furthermore, an increased propensity for extended structure was observed in the region corresponding to the proteinase K resistant core in the fibrils, and a possible long-range interaction involving helix 1 and the N-terminal residues was identified.

### 3.2.2. Aggregation and proteinase K digestion of amyloid fibrils of the prion protein

One of the advantages of using the stop mutants of the prion protein is that these fragments can be aggregated under physiologically relevant conditions (Kundu et al., 2003). The aggregation of these mutants was typically performed in a 50 mM potassium phosphate buffer at pH 6.5. However, under these conditions, the lag phase is significantly shortened and no difference in aggregation profiles of the prion protein variants was observed. The aggregation buffer was therefore changed to a 50 mM phosphate / acetate (1:1) solution and fibril formation was monitored by a standard Thioflavin T fluorescence assay. Surprisingly,

both in case of seeded and spontaneous aggregation, humPrP<sub>23-159</sub> mutant was found to form fibrils faster than humPrP<sub>23-144</sub>, in a concentration independent fashion (**Figure 3-11**). Such behavior is surprising as the polar helix 1 segment consists in 50 % of charged residues and would therefore be expected to have a hindering effect on fibril formation. The finding that humPrP<sub>23-159</sub> aggregates faster with respect to the variant lacking helix 1, suggests a promoting effect of this region on the aggregation of the human prion protein. Interestingly, the increased aggregation propensity of humPrP<sub>23-159</sub> correlates with a case study of one patient carrying the Q160stop mutation (Finckh et al., 2000) who presented clinical symptoms six years earlier than patients carrying the Y145stop mutation (Ghetti et al., 1996).

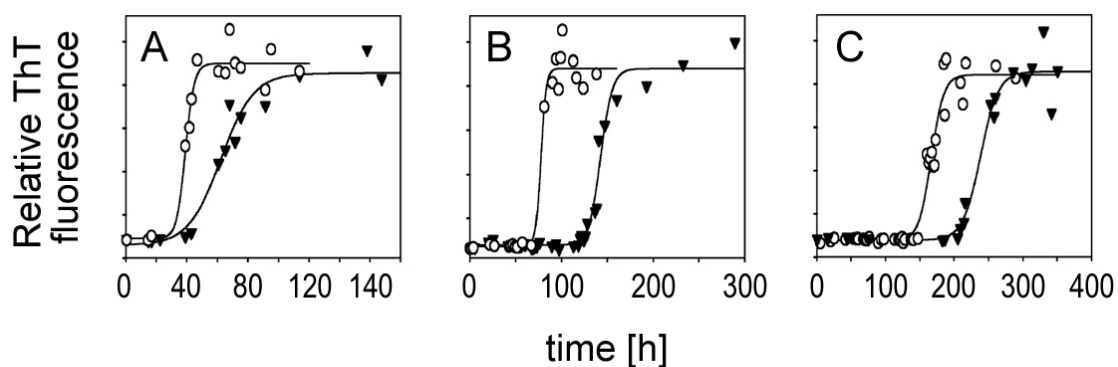


**Figure 3-11.** Aggregation of human prion protein stop mutants. Fibril formation by humPrP<sub>23-144</sub> (filled triangles) and humPrP<sub>23-159</sub> (open circles) was monitored by Thioflavin T fluorescence. The protein concentrations were: (a) 340 μM, (b) 200 μM and (c) 80 μM. The assay was carried out by Dr. Jens Watzlawik.

Digestion of amyloid fibrils formed by humPrP<sub>23-144</sub> and humPrP<sub>23-159</sub> with proteinase K resulted in a release of a 7-8 kDa fragment (**Figure 3-12a**), consistent with previous biochemical observations (Salmona et al., 2003). Subsequently, a Western Blot analysis was performed (**Figure 3-12b**) using antibodies 1E4 and 6H4 directed against residues 98-109 and the helix 1 region, respectively. The 1E4 antibody recognized the presence of the target region in the soluble forms of the proteins as well as in the PK-resistant fragments of the both mutants. Recognition by the 6H4 antibody was positive only for the soluble form of humPrP<sub>23-159</sub>, which strongly suggests that the helix 1 region is not resistant to proteinase K digestion in amyloid fibrils of this prion protein fragment.

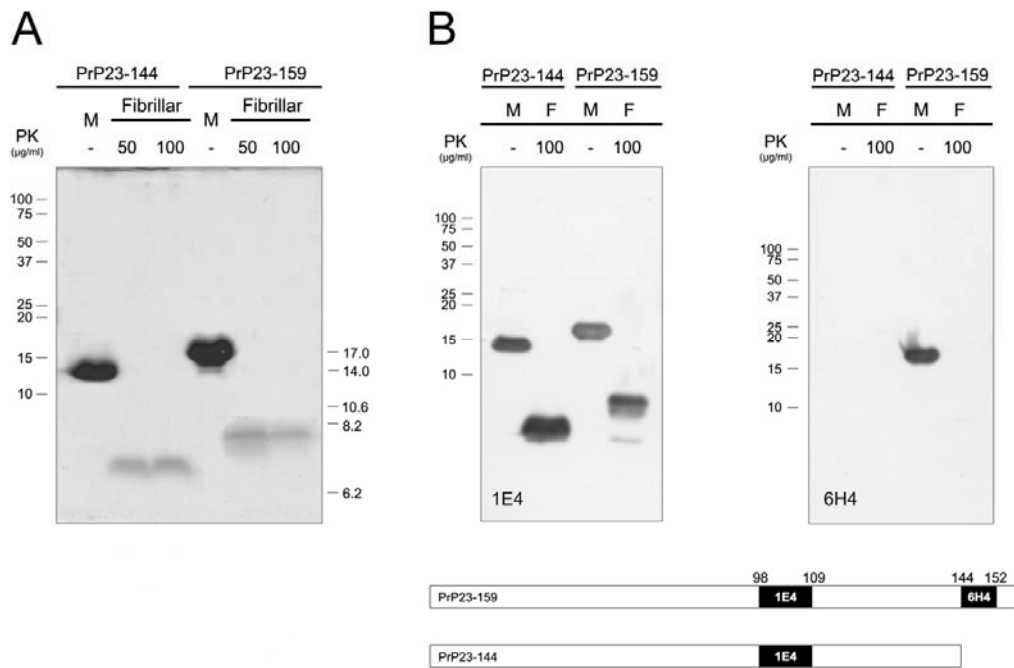


**Figure 3-12.** Helix 1 region is not resistant to digestion by proteinase K. (a) SDS-PAGE analysis of digestion products of humPrP<sub>23-144</sub> and humPrP<sub>23-159</sub> amyloid fibrils. (b) Western Blot analysis with the 1E4 antibody detects proteinase K digested fibrils of both mutants, while the helix 1-targeted antibody 6H4 recognizes only the monomeric form of humPrP<sub>23-159</sub> demonstrating that the helix 1 region is not resistant to proteinase K digestion. The epitope location for both antibodies is schematically depicted by black bars. SDS-PAGE and Western Blot analysis was performed by Dr. Jens Watzlawik.

The proteinase K resistant fragments released from the fibrils of humPrP<sub>23-144</sub> and humPrP<sub>23-159</sub> show a slightly different electrophoretic behavior suggesting either a N- or C-terminal extension of the PK-resistant fragment in humPrP<sub>23-159</sub>. Edman sequencing of the PK-resistant cores resulted in both cases in cleavage at residues 97-98 suggesting that the extension of the core of humPrP<sub>23-159</sub> is C-terminal. However, considering the fact that the helix 1-targeted antibody 6H4 did not recognize the PK-resistant core of humPrP<sub>23-159</sub> fibrils, and that the alternative SDS-PAGE system used here was shown to separate aggregation prone amyloid- $\beta$  peptides differing in size by a single amino acid (Wiltfang et al., 2001), it is very likely that the C-terminal extension in humPrP<sub>23-159</sub> proteinase K resistant core is only a few amino acids long and does not cover the entire helix 1 region.

The size of amyloid aggregates of the prion protein variants was determined by diffusion based NMR experiments for the humPrP<sub>23-173</sub> fragment. Because the signals originating from large assemblies such as amyloid fibrils are not observable in solution state NMR spectra, the diffusion measurement was performed under high-resolution magic angle spinning (see 1.2.2). Translational diffusion coefficient can be measured by spatial labeling of the molecules with a field gradient followed by a delay during which the molecules diffuse until their new position is decoded by another field gradient (Stejskal and Tanner, 1965). The resulting NMR signal is attenuated by the diffusion delay ( $\Delta$ ), and the length ( $\delta$ ) and strength ( $g$ ) of the field gradients. If  $\Delta$  and  $\delta$  are kept constant during the measurement, a series of 1D spectra is acquired in which the signal attenuation depends solely on the strength of the applied field gradient.

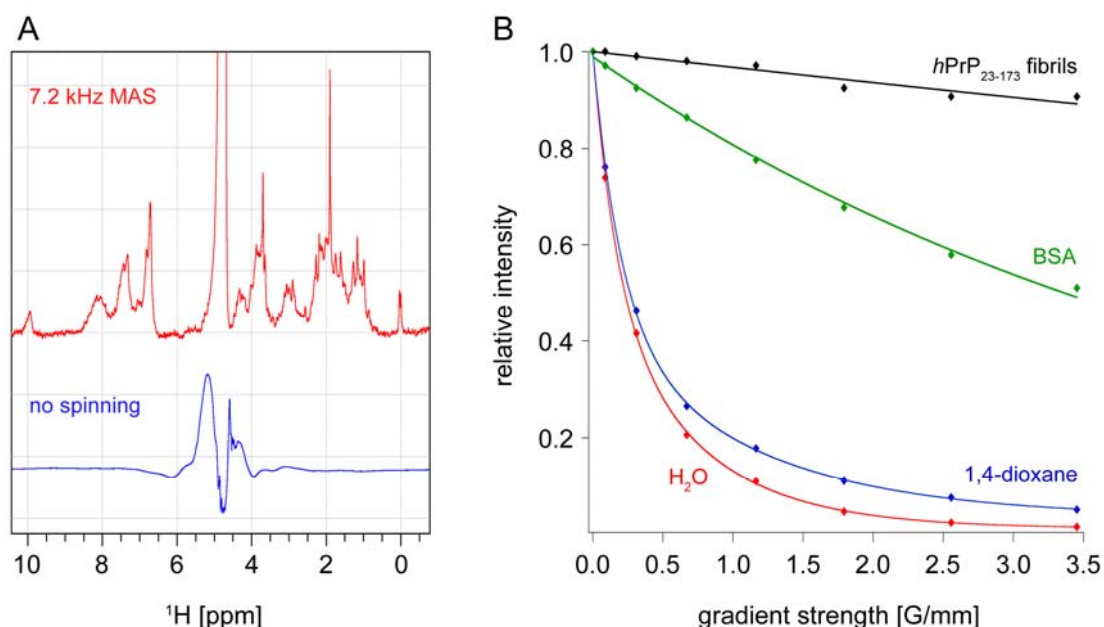


**Figure 3-13.** Molecular weight estimation of humPrP<sub>23-173</sub> fibrils. (a) 1D proton spectra recorded without (blue) and with (red) magic angle spinning. (b) Signal intensity decays under pulsed field gradients recorded for humPrP<sub>23-173</sub> fibrils (black), bovine serum albumin (green), 1,4-dioxane (blue) and water (red) measured using an LED pulse sequence.

The diffusion coefficient of humPrP<sub>23-173</sub> fibrils under HR-MAS (Figure 3-13a) was measured using a bipolar stimulated spin echo sequence (pulse program: ledbpgp2s, Bruker Biospin) as described in 2.4.4. The signal decay curves (Figure 3-13b) were fitted to a single exponential function and the experimental diffusion coefficient was calculated to be  $D = 3.3 \times$

$10^{-11}$  m<sup>2</sup>/s. Because of the non-spherical shape of the aggregates, this value cannot be directly used to calculate the molecular weight based on comparison of the diffusion coefficient between the fibrils and the reference molecule. A recent study by Baldwin and coworkers reported that for large molecules rotational diffusion might contribute to the signal attenuation measured in the NMR experiment (Baldwin et al., 2007). Here however, a simple diffusion theory for an ellipsoid of revolution (Perrin, 1934) was applied, which accounts for both translational and rotational diffusion. The theory allows to calculate the corresponding diffusion coefficient for a spherical molecule of the same molecular weight, which considering the average dimensions of humPrP<sub>23-173</sub> fibrils was found to be  $D_0 = 6 \times 10^{-11}$  m<sup>2</sup>/s. Based on the Stokes-Einstein equation and using bovine serum albumin (BSA) as reference the molecular weight of the fibrils was determined to be in the range of 8 MDa which corresponds to ~600 monomeric units per fibril.

### 3.2.3. NMR-detected H/D exchange studies of the prion protein mutants

#### 3.2.3.1. Optimization of experimental conditions

Due to the large size of amyloid fibrils, direct structural investigation of these assemblies is very challenging and experimentally difficult. However, the fibrils can be conveniently studied by H/D exchange experiments followed by dissociation of the aggregates and detection of solvent protection patterns in the monomeric state. A concept of such an experiment was introduced in 1.2.1. An important parameter that requires optimization in the quenched H/D exchange technique is the composition of the dissolving buffer, as the desolution of fibrils to monomer is fundamental for the success of the experiment. The ideal buffer should quickly and fully dissociate the fibrils and provide conditions under which exchange in the monomeric stage is slowed down. This is typically achieved by mixtures of dimethyl sulfoxide (DMSO) and dichloroacetate (DCA) (Hoshino et al., 2007). Several DMSO/DCA based solvents were tested, covering a concentration range of 92-98% for DMSO and 0.01-0.5% for DCA, and a pH range of 4.0-6.5. While none of these solutions was found to fully dissociate the fibrils of prion protein stop mutants (**Figure 3-14b**), a rapid and complete fibril dissolving was observed in 2 M guanidinium thiocyanate (GdnSCN) at pH 2.5 (**Figure 3-14c**). The GdnSCN buffer therefore fulfills all the requirements achieving fast and complete conversion of fibrils to monomers and slowing down the amide exchange rates due to the acidic pH of the solution.

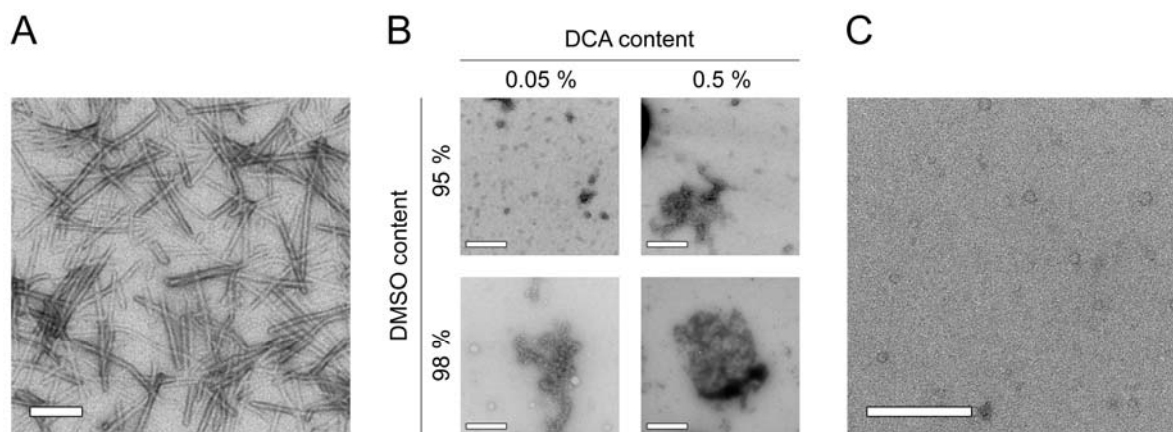


**Figure 3-14.** Dissolution of amyloid fibrils of humPrP<sub>23-159</sub>. (a) Mature fibrils of humPrP<sub>23-159</sub>. (b) Commonly used mixtures of dimethyl sulfoxide (DMSO) and dichloroacetate (DCA) fail to fully dissolve humPrP<sub>23-159</sub> fibrils. (c) A complete and rapid dissolution is achieved in a 2 M solution of guanidinium thiocyanate at pH 2.5. The white scale bars indicate a size of 200 nm.

### 3.2.3.2. Single residue detection of solvent protection in humPrP<sub>23-159</sub> fibrils

Fibrils of humPrP<sub>23-159</sub> (**Figure 3-14a**) were prepared as described in 2.2.8 and exchanged with 0.4 % formic acid in D<sub>2</sub>O, pD 2.5. Fibrils were dissolved in 2 M GdnSCN in 50% H<sub>2</sub>O / 50% D<sub>2</sub>O and a series of <sup>1</sup>H, <sup>15</sup>N correlation spectra were recorded at 278 K as outlined in 2.4.5. **Figure 3-15** shows a selected region of the <sup>1</sup>H, <sup>15</sup>N-HSQC spectra taken at 1 h, 6 h, and 24 h after the dissolution of fibrils. Due to the experimental setup used, if a residue is solvent accessible in the fibrillar form of the protein the amide proton will exchange with the solvent to deuterium and in the first spectrum no signal is observed. As the back-exchange in monomeric state is not absolutely quenched, over time the deuteron will experience partial back-exchange to proton, which in the NMR spectrum results in increase of signal intensity. This is the case for R25 and K104.

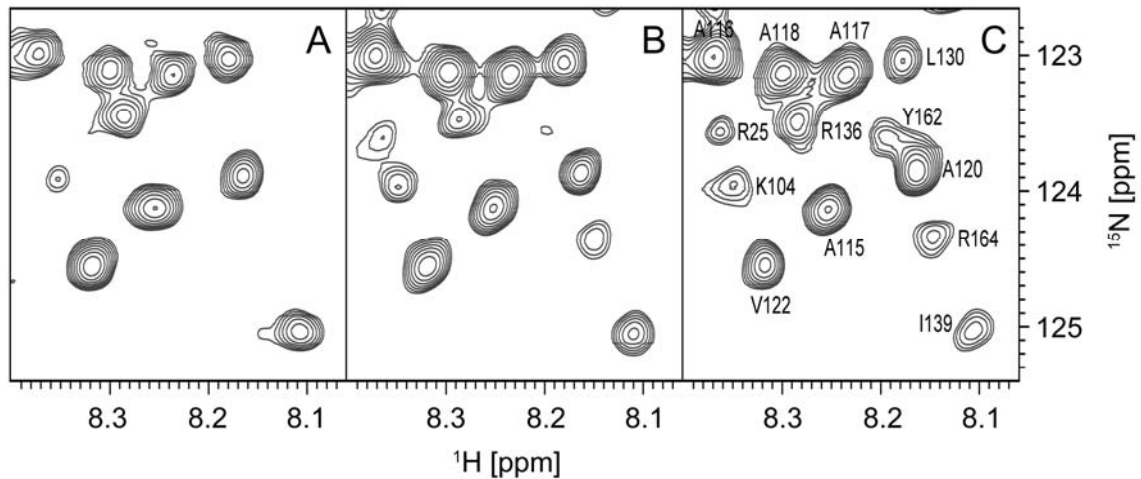


**Figure 3-15.** NMR-based detection of H/D exchange. The panels show selected regions of a  $^1\text{H}$ ,  $^{15}\text{N}$ -HSQC spectrum after (a) 1, (b) 6, and (c) 24 hours after the dissolution of fibrils.

A residue that is buried in the fibril core shows an opposite behavior in the H/D exchange experiment. As it is protected from solvent in the fibrillar state the amide group remains protonated during the exchange period and after dissolving yields a signal in the NMR spectrum. During the back-exchange process the signal will slowly decay as the proton partially exchanges to a deuteron as seen for V122 and I139.

By plotting the relative signal intensities at the end of the back-exchange period against the sequence, a solvent protection map is obtained. **Figure 3-16** shows a protection map for humPrP<sub>23-159</sub> fibrils after 3 days of deuterium exchange. As expected, the N-terminal part of the protein covering residues 23-97 remains unstructured in the fibril and is therefore not protected from the solvent, which is represented by relative intensity ratios above 1 (less than 50% protection). Interestingly, regions with different protection are observed within the proteinase K resistant region 98-144. The highest protection levels are seen for amino acids 121-139. Residues 111-120 are clearly less buried in the core and therefore experience lower solvent protection, while the region 98-110 shows similar solvent accessibility as the N-terminal part of the protein. Most importantly, helix 1 residues 147-157 show very high relative intensity ratios indicative of very low protection from solvent in the amyloid fibrils. This is in full agreement with the proteinase K digestion experiment confirming that helix 1 is not converted to  $\beta$ -sheet and does not contribute to the proteinase K resistant core of the prion protein fibrils. In fact, the very low protection factors may suggest that this segment is fully flexible in the fibril.



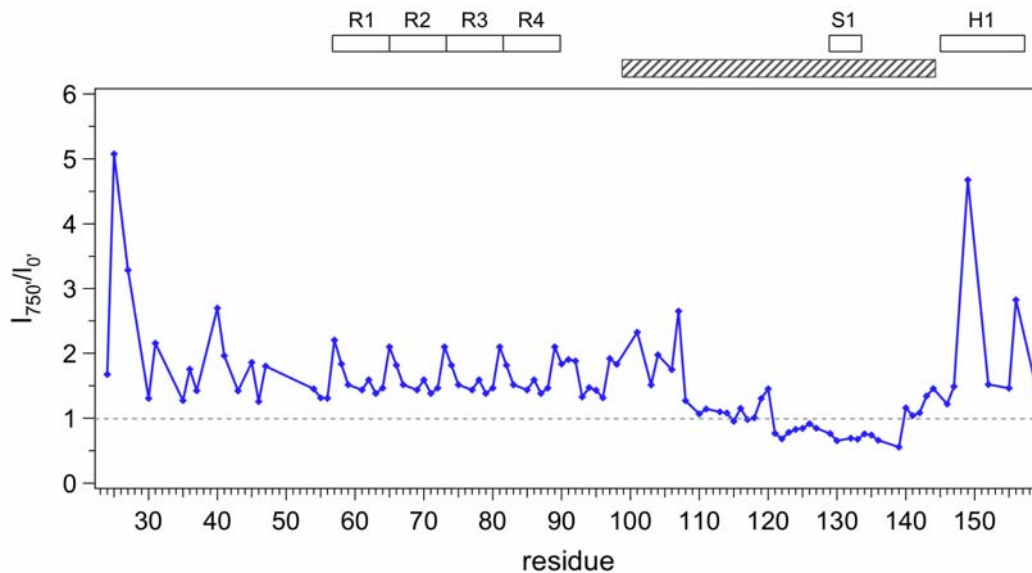


**Figure 3-16.** Protection map of humPrP<sub>23-159</sub> fibrils after 3 days of H/D exchange. Positions of octarepeats (R1-R4),  $\beta$ -strand 1 (S1) and helix 1 (H1) are indicated by open bars; the hatched bar marks the proteinase K resistant core in humPrP fibrils.

Additional information on the rigidity of various segments of humPrP<sub>23-159</sub> within the amyloid fibril structure can be obtained by comparing the H/D exchange profiles after different exchange times. Longer incubation of fibrils with D<sub>2</sub>O results in saturation of H/D exchange in the flexible regions and further incorporation of deuterium in the rigid parts. **Figure 3-17** shows a comparison between H/D exchange profiles of humPrP<sub>23-159</sub> fibrils obtained after a 3- and 7-day exchange with D<sub>2</sub>O.

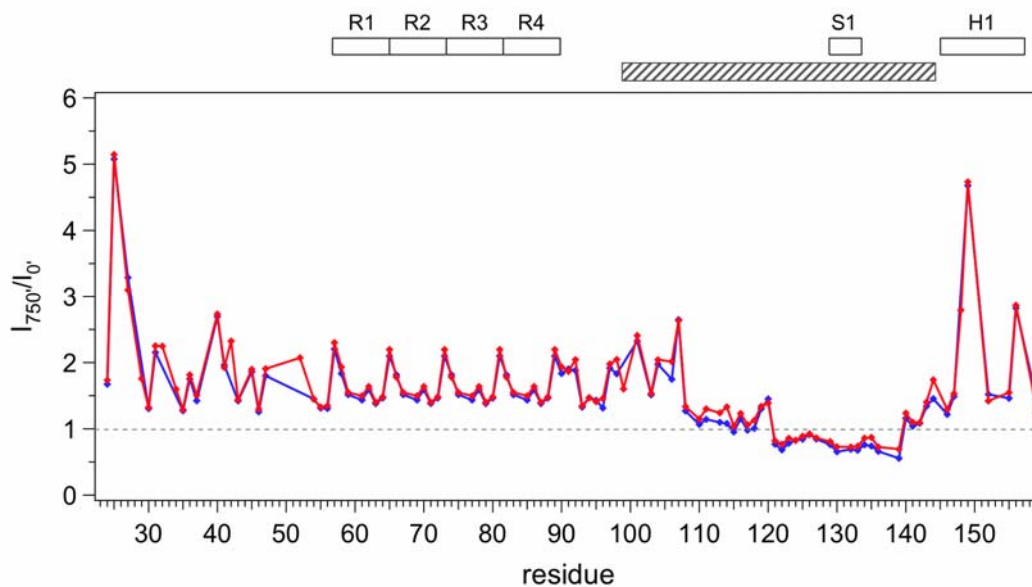


**Figure 3-17.** Time dependence of deuterium incorporation into humPrP<sub>23-159</sub> fibrils. The overlay of protection maps recorded after 3 days (blue) and 7 days (red) reveals two fragments with slower deuterium incorporation encompassing residues 111-116 and 133-139.

In the previously identified solvent accessible regions of the protein (residues 23-110 and 141-159), the exchange process is saturated after 3 days. Within the amino acids 110-140 two regions (111-116 and 133-139) are showing a significant change in deuterium incorporation between the 3- and 7-day time points.

Taken together, the collected H/D exchange data suggest at this stage that the core of the humPrP<sub>23-159</sub> consists of three regions with distinct solvent protection. The first would be located around residues 111-118 and to account for the observed level of deuterium incorporation, it would need to be located on the outside of the core. The other two regions would comprise residues 121-127 and 129-139 with the latter being the one most buried in the rigid core of the fibrils. A potential turn at residues 119-120 can also be concluded, and this hypothesis is further supported by the analysis of signal intensity changes during the back-exchange process for individual residues (**Figure 3-18**).

Out of a total of 31 residues in the H/D exchange-mapped fibril core, 24 signals could be unambiguously assigned in the <sup>1</sup>H, <sup>15</sup>N-HSQC spectra. Out of the 6 missing residues, one is a proline (Pro137) and the remaining five (M112, G123, G127, Y128, G131 and I138) were overlapping with other signals. Among all residues in the 111-141 region, G119 and A120 show the most pronounced increase in signal intensity after the dissolution of fibrils, which indicates that these two amino acids exhibit higher amide proton exchange with the solvent than the neighboring residues. The change in signal intensity over time for V121 shows a striking difference with respect to A120 and clearly indicates that the second proposed core region starts exactly at this residue.

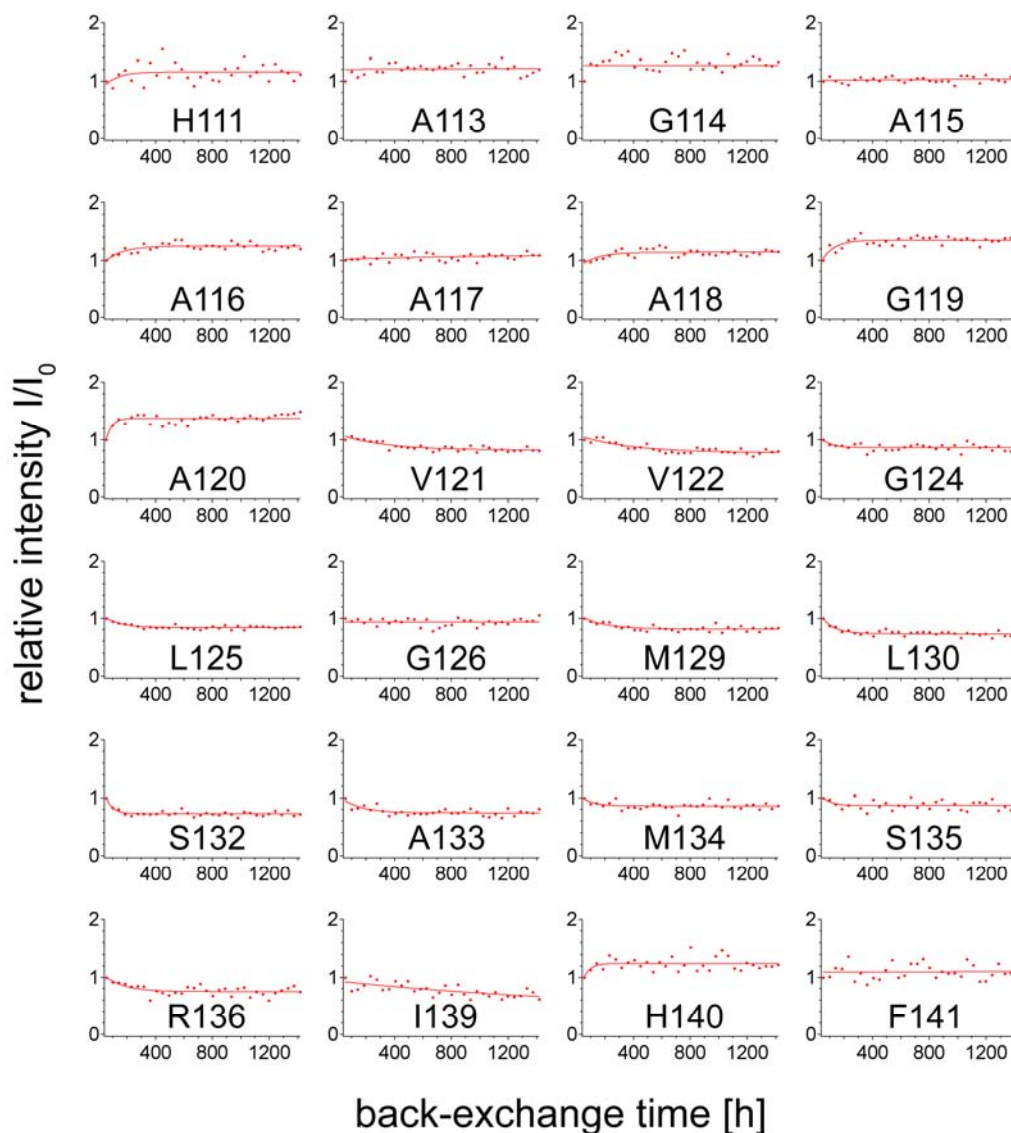


**Figure 3-18.** Residue specific H/D exchange profiles for residues 111-141. Changes in signal intensity during the back-exchange process were followed by a series of  $^1\text{H}$ ,  $^{15}\text{N}$ -HSQC experiments providing data with single residue resolution.

### 3.2.3.3. Fibrils of different stop mutants of the human prion protein show similar solvent protection

The observations made for fibrils of humPrP<sub>23-159</sub> are also seen in the longer fragment – humPrP<sub>23-173</sub>, which spans the  $\beta$ -sheet 2 region of the prion protein. The comparison of solvent protection patterns for the two mutants after 7 days of exchange is depicted in **Figure 3-19**. A remarkably good agreement between the relative intensities at the end of the back-exchange process is seen in all the regions of the two proteins.

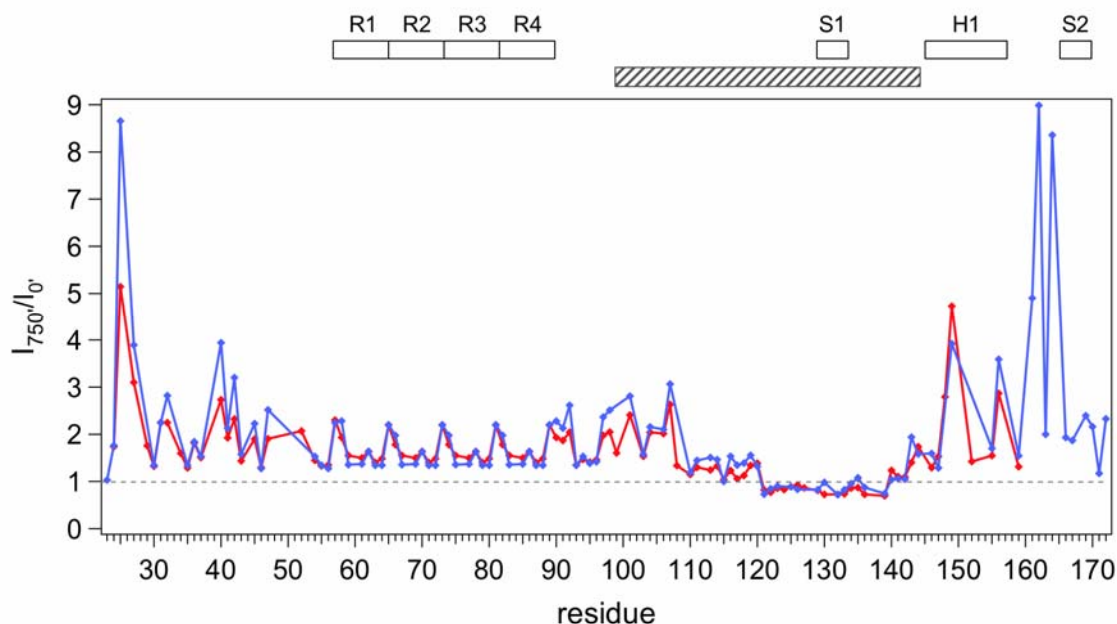


**Figure 3-19.** Fibrils of different humPrP stop mutants share common structural features. An overlay of protection maps of humPrP<sub>23-159</sub> (red) and humPrP<sub>23-173</sub> (blue) fibrils exchanged with D<sub>2</sub>O for 7 days shows a very good agreement throughout the entire sequence.

### 3.2.4. Structural models of the core of human prion protein fibrils

The H/D exchange profiles of human PrP mutants studied here consistently indicate the presence of a small fibril core comprising residues ~111-139. In order to suggest a structural model of this core, the CS-Rosetta package was used (Shen et al., 2008; Shen et al., 2009). The input chemical shift information required by CS-Rosetta was taken from a recent solid state NMR study on fibrils of humPrP<sub>23-144</sub> (Helmus et al., 2008). Helmus and coworkers report that in measurements above -20°C only signals from residues 112-140 are observable which is line with our findings and justifies the use of chemical shift information provided by the authors.

#### 3.2.4.1. MFR mode

The CS-Rosetta run was performed as described in 2.4.6 to generate 200 candidates for 3-residue and 9-residue fragments using the molecular fragment replacement (MFR) search protocol. The so-called “flight maps” showing the  $\Phi / \Psi$  angles of the 10 best 9-residue fragment candidates (**Figure 3-20**) were generated using the scrollRama.tcl script of the NMRPipe system (Delaglio et al., 1995).

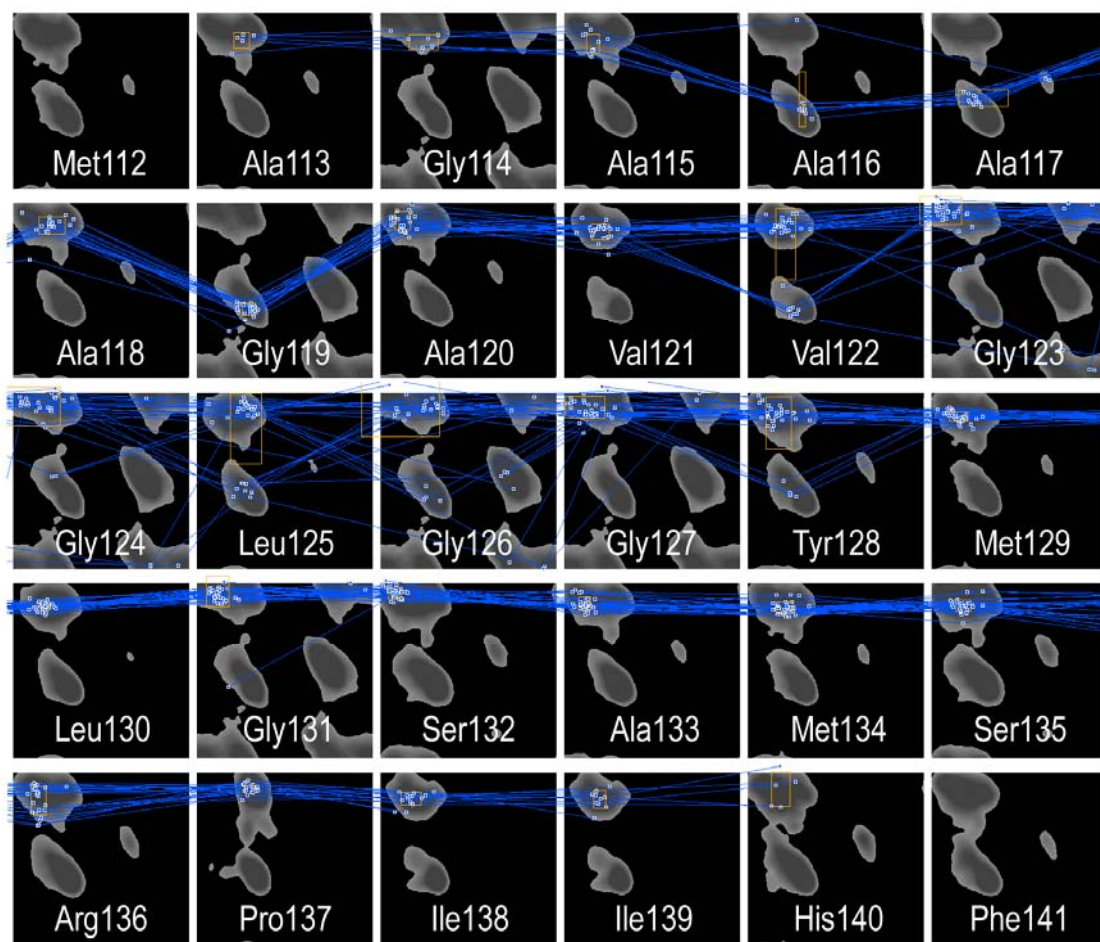
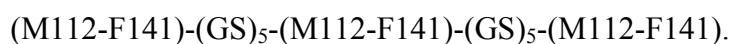


**Figure 3-20.** Flight maps for the 10 best 9-residue fragment candidates.

$\Phi$  /  $\Psi$  trajectories are plotted onto Ramachandran maps with possible conformations of the polypeptide chain marked in grey; orange boxes indicate the average  $\Phi$  /  $\Psi$  value  $\pm$  one standard deviation.

For residues 129–140, the  $\Phi$  /  $\Psi$  angles of all 10 fragments fall into the  $\beta$ -strand region of the Ramachandran plot. Higher structural diversity is observed for the glycine rich region 123–127, however also here a general tendency for  $\beta$ -strand is clearly visible. Interestingly, an evident turn is predicted around Gly119 and Ala120, which is in very good agreement with the H/D exchange data. Considering that the input chemical shifts were obtained for fibrils of humPrP<sub>23-144</sub>, this finding further supports the idea that fibrils of different stop mutants of the human prion protein share common structural features.

To prevent occurrence of end effects, a “triplicate” fragment was generated in which the three monomeric segments comprising residues 113-140 are connected by a 20-residue flexible linker consisting of Gly-Ser repeats, with the final sequence:



For the linker region random coil chemical shift values of Gly and Ser (Wishart et al., 1995) were used to complete the CS-Rosetta input table. **Figure 3-21** shows the flight maps of the

central monomer together with the preceding 3 and proceeding 2 residues of the linker. As expected, no significant changes are seen in the core region with respect to the previous prediction (see **Figure 3-20**). The N-terminal extension by as little as two additional residues of the linker, more clearly shows the formation of a  $\beta$ -strand including residues 112-115 and the Ser-Gly pair of the linker. This suggests the first strand of the humPrP<sub>23-159</sub> fibril core to encompass residues 111-115. On the other hand, no such effect is observed for the C-terminal linker extension, where the predicted core ends clearly at His140.

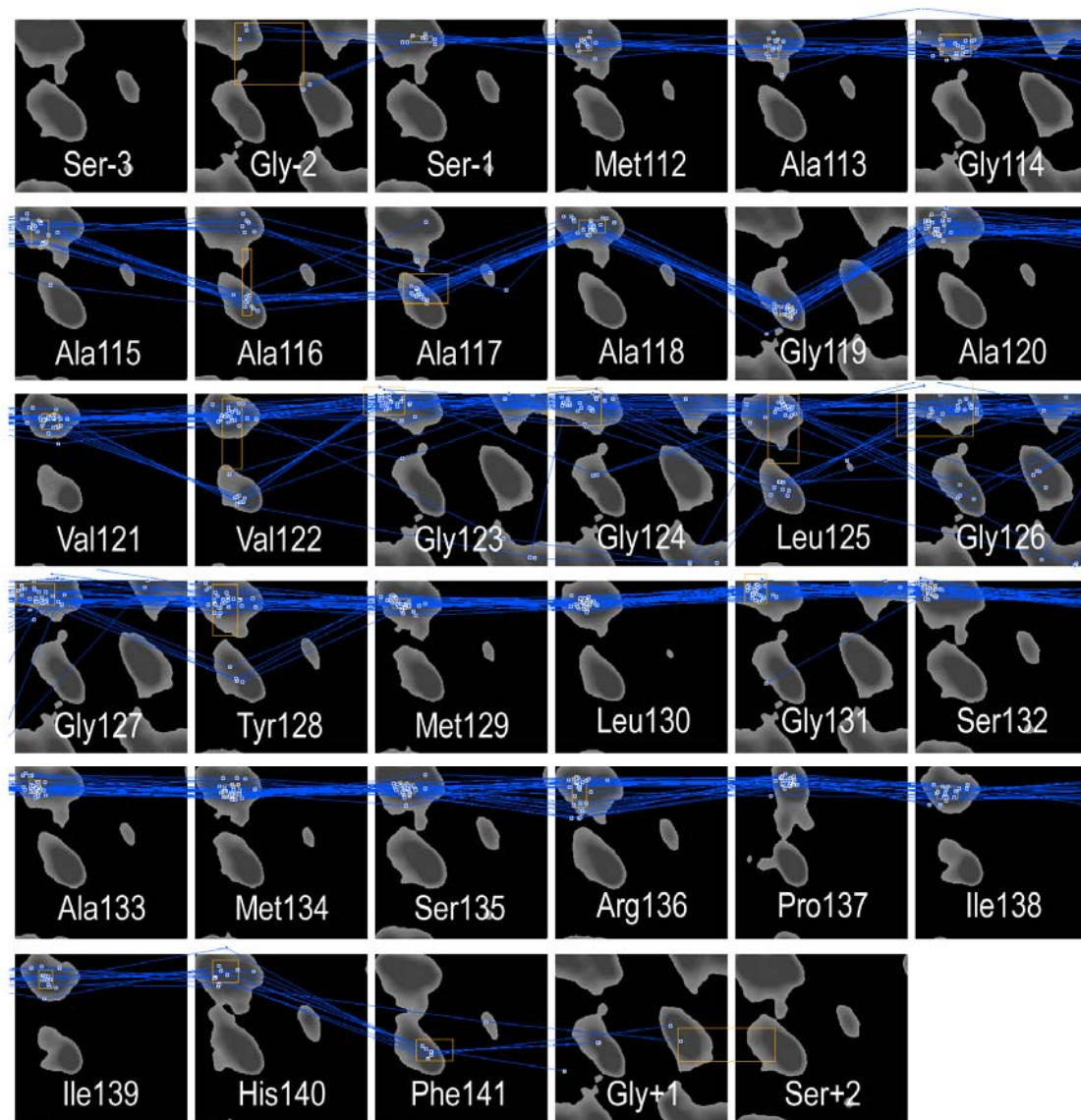


**Figure 3-21.** Flight map of the 10 best 9-residue fragments for the “triplicated” peptide.

### 3.2.4.2. Hybrid mode

The hybrid mode of CS-Rosetta is an alternative approach to the MFR fragment search, and is recommended in case of incomplete/imperfect input chemical shift assignments

(Shen et al., 2009). For the “hybrid” fragment search the same input chemical shift table was used as in the MFR fragment selection. After the fragment selection was completed, the resulting fragments were sorted according to the CS-Rosetta scores and fragments with a CS-score larger than 2.5 were discarded. The flight maps for the remaining best scoring fragments are shown in **Figure 3-22**.



**Figure 3-22.** Flight maps of the best 9-residue fragments selected with the hybrid approach.

An overall agreement is found between the flight maps of the best fragments selected with the MFR (**Figure 3-20**) and hybrid (**Figure 3-22**) modes, however the trajectories obtained with the hybrid approach tend to vary more and cover a larger area of the Ramachandran space. This is the case for residues 116-119, 123-127, and 130-135.

Inspection of the 9-residue fragments containing the Gly-rich region 123-127 identified two of the best 10 fragments centered around Leu125 to have both low chemical shift score and very high sequence similarity to the target sequence (VVGGLGGYM). Both fragments were found to contain the GGXGG motif, and one of the fragments contained

additionally a hydrophobic and an aromatic residue at positions 125 and 128, respectively. These two fragments originated from pdb files 1xez and 2hah (**Figure 3-23a,b**). In both of the corresponding proteins the Gly-rich motifs are forming loops within  $\beta$ -sheets (**Figure 3-23c,d**), which further supports the hypothesis that residues 123-127 form a loop between two  $\beta$ -strands in the core of humPrP fibrils.

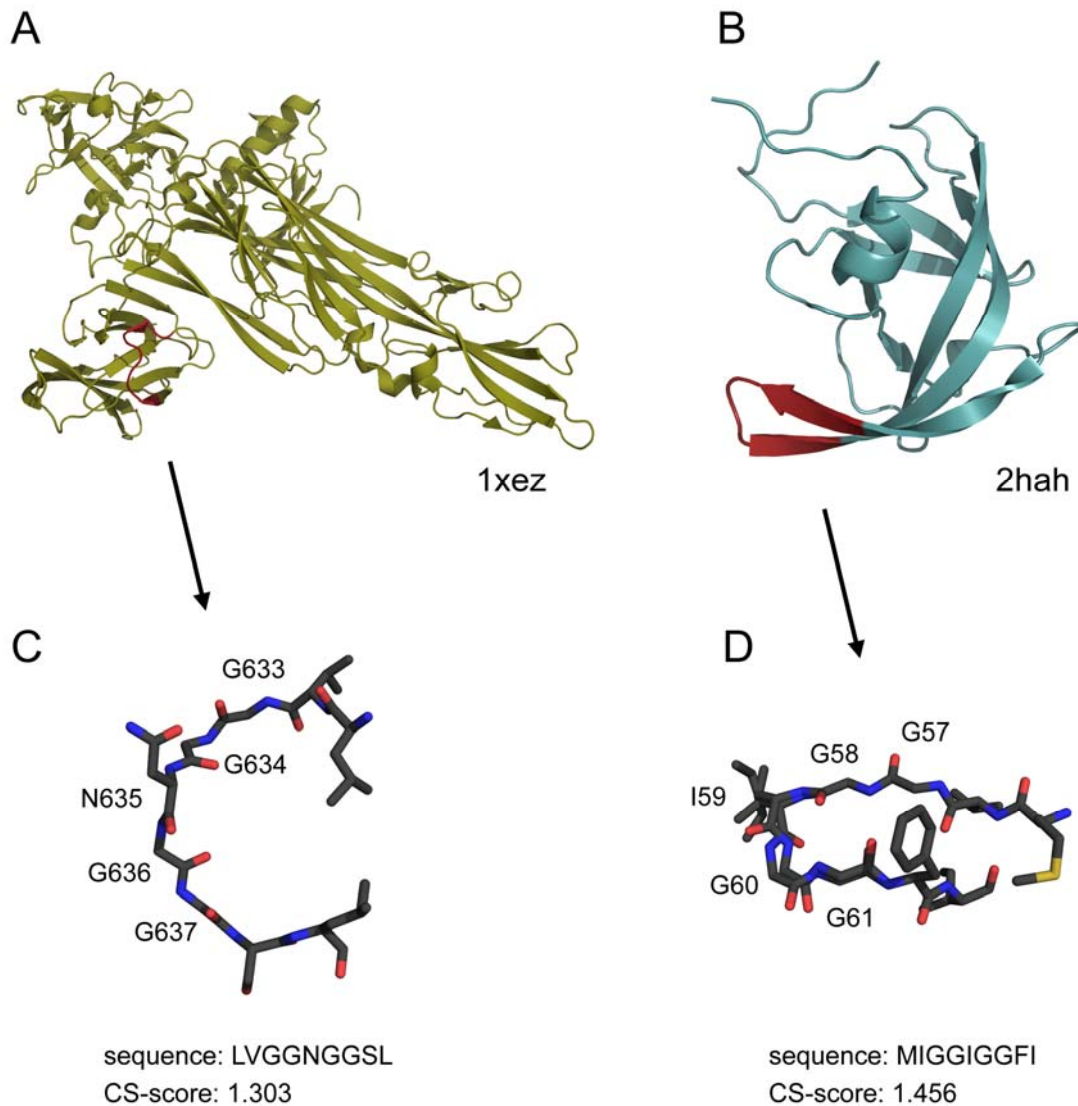


**Figure 3-23.** Structures of Gly-rich regions in fragments selected by CS-Rosetta. **(a)** Structure of the *Vibrio Cholerae* Cytolysin pro-toxin (pdb entry 1xez) and **(c)** the 9-residue fragment between residues 631-639 selected by CS-Rosetta. **(b)** Structure of the FIV 12S protease (pdb entry 2hah) and **(d)** the 9-residue fragment between residues 55-63 selected by CS-Rosetta. **(a,c)** The selected 9-residue fragments are highlighted in red; **(b,d)** atom colors are: C (black), N (blue), O (red), S (yellow), H atoms are not shown.



### 3.3. Discussion

Transmissible spongiform encephalopathies are a group of diseases in humans and animals, caused by conversion of the cellular prion protein to its pathogenic “scrapie” form and aggregation thereof. In this work the aggregation properties and fibrillar structure of the human prion protein was studied based on two stop mutants - humPrP<sub>23-144</sub> and humPrP<sub>23-159</sub>. Importantly, both of these constructs are disease related causing a Gerstmann-Sträussler-Scheinker-like phenotype (Ghetti et al., 1996; Finckh et al., 2000) and were found to aggregate *in vitro* under non-denaturing conditions (Kundu et al., 2003; Watzlawik et al., 2006).

The following paragraphs discuss the novel experimental data and their importance for understanding the mechanism of the prion diseases. Implications for prion protein polymorphism and the species barrier are presented, and finally the recently proposed structural models of PrP<sup>SC</sup> are discussed in the light of our findings.

#### 3.3.1. The role of helix 1 in the aggregation of human prion protein

Conversion of PrP<sup>C</sup> to its pathogenic form PrP<sup>SC</sup> results in significantly increased  $\beta$ -sheet content in the latter (see 3.1.5). As helices 2 and 3 are stabilized by a disulfide bridge, it was postulated that conversion of the charged and structurally isolated helix 1 into  $\beta$ -strand is the starting point in formation of PrP<sup>SC</sup> (Huang et al., 1995). Here, by using two naturally occurring stop mutants of the human prion protein – humPrP<sub>23-144</sub> and humPrP<sub>23-159</sub> – it was shown that helix 1 is not resistant to digestion with proteinase K in the fibrillar form of humPrP<sub>23-159</sub> (**Figure 3-12**). Supported by the solvent accessibility of this region in the fibrillar form of PrP (**Figure 3-16**), this provides strong evidence that the helix 1 region is not converted to  $\beta$ -strand upon aggregation of the prion protein.

Furthermore, humPrP<sub>23-159</sub> was found to aggregate faster than humPrP<sub>23-144</sub> in a concentration independent fashion (**Figure 3-11**). This is rather surprising as helix 1 contains charged residues, which would normally be expected to increase the solubility and hinder aggregation. The faster fibril formation of humPrP<sub>23-159</sub> strongly suggests involvement of helix 1 in the aggregation mechanism, however the nature of this aggregation-promoting effect is unknown. One possible explanation is formation of intermolecular salt bridges (Morrissey and Shakhnovich, 1999) by aspartates and arginines within the helix 1 region. An alternative mechanism would involve an interaction between the N-terminus and the helix 1 region, resulting in stabilization of the aggregates. Such an interaction could be concluded

from the NMR-data presented in **Figure 3-10** and was previously suggested by Watanabe and coworkers based on results of a cysteine-scanning spin-labeling experiment (Watanabe et al., 2006).

Interestingly, faster aggregation of humPrP<sub>23-159</sub> with respect to humPrP<sub>23-144</sub> correlates with a clinical report of a patient carrying the Q160stop mutation (Finckh et al., 2000), who developed symptoms six years earlier than patients carrying the Y145stop mutation (Ghetti et al., 1996).

### 3.3.2. Evaluation of structural models of PrP<sup>SC</sup>

The experimental data presented in this work have several consequences for the possible architecture of fibrils of human prion protein, and by providing structural restraints can be used to evaluate the existing structural models of PrP<sup>SC</sup>.

Firstly, using two independent approaches we have provided strong evidence that helix 1 region is not converted to  $\beta$ -strand upon aggregation of humPrP. The biochemical assay utilizing limited proteolysis showed that helix 1 does not contribute to the proteinase K resistant region in the humPrP<sub>23-159</sub> fragment. This was confirmed by hydrogen/deuterium exchange measurement revealing solvent exposure of helix 1 region in amyloid fibrils of stop mutants of humPrP. Furthermore, the region corresponding to  $\beta$ -strand 2 in the monomeric protein was also found to be solvent accessible as evidenced by the exchange pattern of humPrP<sub>23-173</sub>. Even though helix 1 does not contribute to the  $\beta$ -sheet core of the fibrils, it was found to have a promoting effect on aggregation of humPrP.

Secondly, a combination of H/D exchange data and the CS-Rosetta predictions leads to the conclusion that the rigid core of amyloid fibrils of human prion protein stop mutants consists of four  $\beta$ -strands (residues 111-115, 120-122(-123), (127-)128-135 and 137-140) with the first strand being the least- and the last being the most-solvent protected.

Even though the GSS-related prion protein constructs used in this study did not contain the C-terminal helices 2 and 3, evidence exists that these segments are buried in the fibrils (Lu et al., 2007), however are not converted to  $\beta$ -strands during the aggregation process (Wille et al., 2002; Govaerts et al., 2004). A conversion of these regions to  $\beta$ -strands would be unlikely due to the presence of the disulfide bridge stabilizing the two helices and it was shown that no formation of intermolecular disulfide bonds occurs in multimeric assemblies of the prion protein (Welker et al., 2002). Furthermore, the involvement of helices 2 and 3 in formation of PrP<sup>SC</sup> was suggested in neuroblastoma cells, where truncated variants of the

prion protein lacking helices 2 or 3 were much less resistant to digestion with proteinase K than full length PrP<sup>SC</sup> (Muramoto et al., 1996).

Taken together, none of the PrP<sup>SC</sup> models shown in section 3.1.5 fully accounts for all the experimental data:

(i) The model assuming a four stranded  $\beta$ -sheet covered with helices 2 and 3 (Huang et al., 1995), assumes conversion of helix 1 into a  $\beta$ -strand (see **Figure 3-5a**) and therefore does not comply to our experimental findings,

(ii) The model of Govaerts and coworkers (see **Figure 3-5b**) suggests a  $\beta$ -helical arrangement in the region between residues 89-175 (Govaerts et al., 2004). Even though the positions of individual  $\beta$ -strands do not fit the data presented here, this model cannot be excluded as it has been suggested based on 2D crystals of the prion protein, which might be morphologically distinct from amyloid fibrils but are found in preparations of PrP<sub>23-30</sub> together with amyloid fibrils (Wille et al., 2002),

(iii) The MD simulation by DeMarco and Daggett of humPrP<sub>90-230</sub> at acidic pH (**Figure 3-5c**) leads to six  $\beta$ -strands in the region 90-166 (E1: 90-95, E2: 99-102, E3: 119-121, E4: 126-134, E5: 137-139 and E6: 160-165). Although the positions of strands E4 and E5 fit very well to our experimental data, no evidence was found for the formation of strands in regions E1, E2 and E6 of the MD simulation. Furthermore, the position of strand E3 is in disagreement with the turn observed at Gly119,

(iv) Another MD-based model was proposed based on a simulation of conversion of Syrian hamster PrP(109-219) with D147N mutation at low pH (DeMarco and Daggett, 2004). Similarly to the other model suggested by the same authors, helix 1 is not converted into a  $\beta$ -strand and is considered to exist in PrP<sup>SC</sup>, which is in agreement with the proteinase K digestion experiment, however the H/D exchange data strongly suggest that helix 1 region is unstructured in the fibrils of humPrP. Helices 2 and 3 are significantly shortened, matching the decreased  $\alpha$ -helical content in PrP<sup>SC</sup> with respect to PrP<sup>C</sup> (see **Table 3-3**). Presence of four  $\beta$ -strands is predicted in the core of the fibrils at positions 116-119, 129-131, 135-140 and 161-163. While the first three strands match relatively well the CS-Rosetta prediction, no evidence is found for the formation of a  $\beta$ -strand encompassing residues 161-163, similarly to the other MD-based model.

### 3.3.3. Core of amyloid fibrils of human prion protein stop mutants

A recent study by Lu and coworkers (Lu et al., 2007) utilized hydrogen / deuterium exchange and detection by mass spectrometry to map the fibrillar core of the 90-230 fragment of the human prion protein. The authors report the highly protected fibrillar core to be located in the C-terminal part in regions corresponding to  $\alpha$ -helix 2, major part of helix 3, and the loop between these two helices. No significant protection was detected in the N-terminal part of the used construct (residues 90-130), however this conclusion was drawn based only on two peptic fragments of 32 and 40 residues. The analysis of such strikingly long fragments is prone to oversimplification and presence of short, highly protected regions cannot be excluded. It is also unexpected that the proteinase K resistant region situated between residues 98 and 144 would be solvent exposed in the fibrils.

Another investigation of mass spectrometry-detected hydrogen / deuterium exchange in fibrils of full length mouse PrP concluded presence of two highly protected regions comprising residues 24-98 and 182-212, while residues 99-181 were found to be more solvent exposed, but less than in the monomeric protein (Nazabal et al., 2009). The high protection of the N-terminal region and lower protection of residues 99-181 is not only contradicting our data but also basic biochemical proteinase K digestion assays, which show that the N-terminal residues 23-90 are highly susceptible to proteolytic cleavage in PrP<sup>Sc</sup> (Kocisko et al., 1996).

To examine in detail the solvent protection of humPrP fibrils we have used H/D exchange in combination with detection by NMR, which (in contrast to mass spectroscopy) offers single residue resolution. Our data indicate clearly that the rigid, and highly solvent protected core of humPrP<sub>23-159</sub> fibrils comprises residues 111-139 (**Figure 3-16**). A detailed analysis of protection maps obtained after varying the exchange time suggests presence of three regions with different solvent protection levels – 111-118, 121-127, and 129-139 (**Figure 3-17**).

An NMR-detected H/D exchange study of mature fibrils formed by mouse PrP fragment 106-126 (corresponding to residues 107-127 of the human prion protein) reports high protection for residues 110-119 (111-120 in humPrP), confirmed by a MD simulation predicting  $\beta$ -sheet conformation in this region (Kuwata et al., 2003). Comparison with our data reveals that fibrils of the 106-126 fragment and of humPrP<sub>23-159</sub> have different cores, and indicates that the region investigated in the two peptide studies comprises only a part of the core of PrP fibrils. Furthermore, the aggregation of mouse PrP(106-126) was performed under non-physiological conditions in presence of 50 % acetonitrile.

A very recent publication by Walsh and coworkers explores the structure of amyloid fibrils formed by a peptide encompassing residues 106-126 of the human prion protein (Walsh et al., 2009). The authors report an extended  $\beta$ -strand conformation between residues 113 and 126. As a proof of principle, we have performed a CS-Rosetta fragment search using the chemical shift data reported by the authors (**Figure 3-24**). Indeed, in agreement with the published data, a fully extended structure is predicted for region 113-126.

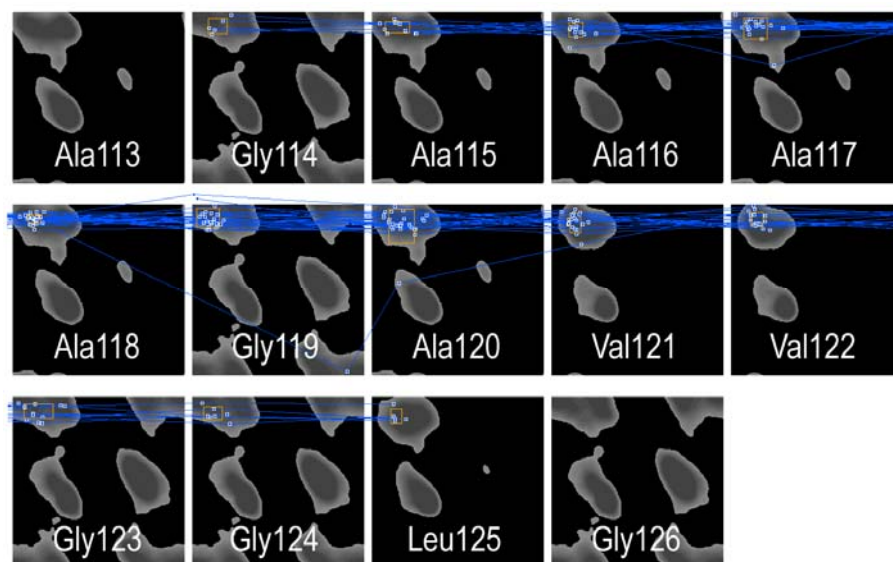


**Figure 3-24.** Flight map of the best 10 fragments assembled for residues 113-126 of the amyloid forming peptide 106-126. CS-Rosetta prediction was run only on residues 113-126, as the chemical shifts for residues 106-112 were not reported (Walsh et al., 2009).

Our observation that the fibrillar core of humPrP<sub>23-159</sub> and humPrP<sub>23-173</sub> is located around residues 111-139 is in agreement with a solid-state NMR study on humPrP<sub>23-144</sub> by Helmus and coworkers (Helmus et al., 2008). The authors report that in measurements above -20 °C only signals from residues 112-140 are observable, and based on a simplified chemical shift-based structure prediction conclude the presence of 3 strands in the core of the fibrils (residues 112-115, 118-122 and 130-139). However, the PSSI algorithm used by Helmus and coworkers tends to be unreliable for Gly residues, and the results of the PSSI prediction are in disagreement with our H/D exchange data. The chemical shift information provided by the authors was therefore used in an attempt to predict the structure of the fibrillar core using the CS-Rosetta package (Shen et al., 2008; Shen et al., 2009). The results of the CS-Rosetta runs (**Figures 3-20 to 3-22**) suggest a presence of four  $\beta$ -strands within the core of the fibrils. These are located in regions 111-115, 120-122(-123), (127-)-128-135 and 137-140.

Furthermore, in agreement with results of the H/D exchange experiment, a turn was found at Gly119.

The experimental data presented here and the expected structure in the C-terminal region of the human prion protein (see 3.3.2) are summarized in **Figure 3-25**.

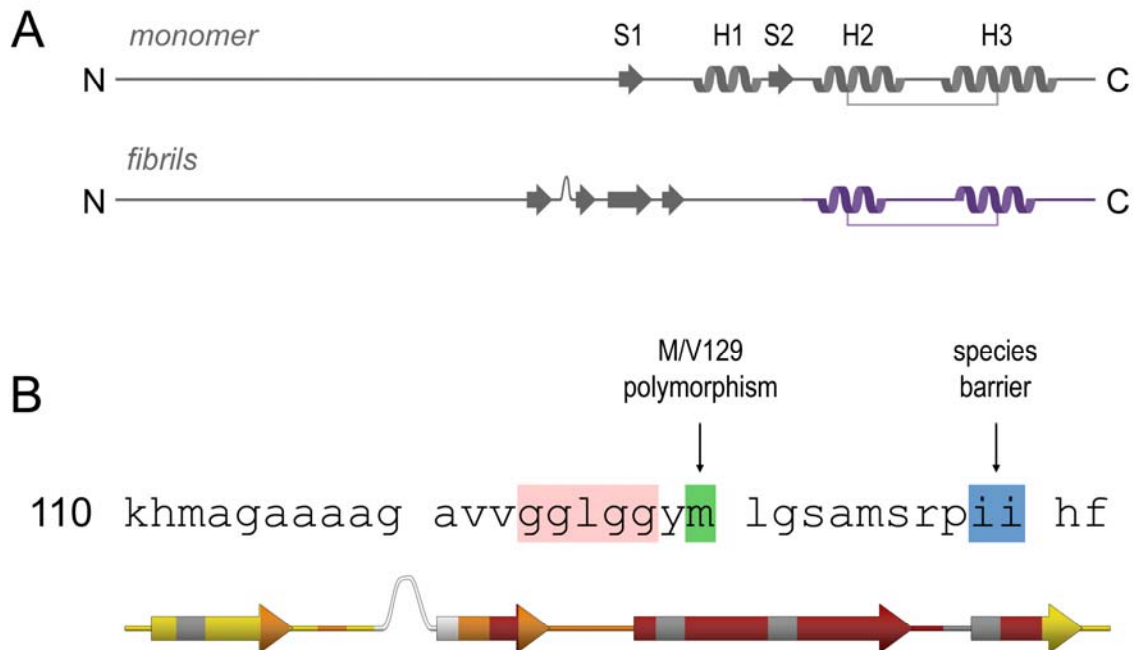


**Figure 3-25.** Structural architecture of humPrP fibrils.

(a) Schematic representation of structural differences between PrP<sup>C</sup> and PrP<sup>SC</sup>; H1,H2,H3 – helices 1, 2 and 3; S1,S2 –  $\beta$ -strands 1 and 2; the expected structure of the C-terminal region of the fibrillar form (magenta) was concluded from data available in literature (see 3.3.2). (b) The core of amyloid fibrils of humPrP stop mutants. NMR-detected H/D exchange reveals presence of three regions with protection levels increasing towards the C-terminus ( $I_{24h}/I_0$  values are: 0.5-0.75 (red), 0.75-1.0 (orange), 1.0-1.25 (yellow), >1.25 (white), unknown (grey)) and a turn at Gly119-Ala120. Presence of four  $\beta$ -strands is predicted by CS-Rosetta based on chemical shift data from a solid-state NMR study on fibrils of humPrP<sub>23-144</sub> (Helmus et al 2008); a turn at Gly119 is also found in the chemical shift prediction. Regions of importance for pathology of the disease are indicated in green and blue; the Gly-rich region is marked in pink.

#### 3.3.4. Implications for prion protein polymorphism and the species barrier

The most prominent hallmarks of transmissible spongiform encephalopathy pathology are the existence of prion strains and the so-called “species barrier” (see 3.1.3.).

The highest sequence homology to human prion protein is found in the hamster, with only 18 residues differing between the two proteins and one insertion at position 206 in the hamster PrP. Interestingly, only two amino acid substitutions are found in the region 111-139 forming the core of the humPrP<sub>23-159</sub> fibrils. These are Ile138 and Ile139, which are both replaced by methionines in the hamster variant of the protein. In NMR spectra, the signal of Ile138 is overlapping with another resonance, while Ile139 is very well separated and can be reliably studied. According to both the H/D exchange data and CS-Rosetta predictions, both isoleucines are found in a  $\beta$ -strand in the most protected region in the amyloid fibril core (see **Figure 3-25**). Strikingly, Ile139 also showed the highest solvent protection over the entire length of the studied fragment (**Figure 3-16**). It was also shown that especially the amino acid alterations I138M and I139M are responsible for the sequence-based barrier preventing cross-seeding of human and hamster prion proteins (Vanik et al., 2004). These observations highlight the importance of positions 138 and 139 for the species barrier and indicate that replacement of isoleucines with methionines could change the fibrillar core and that the species barrier might be therefore related to the fibril architecture. In fact, evidence exists that differences in fibril morphology are a result of changes in the excited states of the proteins (Kremer et al., 2007).

The second factor determining the pathology of prion diseases is the polymorphism at position 129. The human *Prnp* gene exists as two alleles encoding either methionine or valine at codon 129 (Owen et al., 1990). The frequency of the evolutionary primitive (found in other mammals) Met129 allele is  $\sim 0.7$ , resulting in more than 40 % frequency of heterozygotes (reviewed in Mitrova et al., 2005). The polymorphism affects both susceptibility to disease and the onset of clinical symptoms (Collinge et al., 1991; Palmer et al., 1991; Brown et al., 1994; MacDonald et al., 1996; Kovacs et al., 2000). In fact, the course of the disease can be altered to such extent that it leads to a different phenotype. The D178N mutation causes fatal familial insomnia when codon 129 encodes Met, however if a Val residue is present at position 129 the D178N mutation leads to dementia and classifies as familial Creutzfeldt-Jakob disease (Goldfarb et al., 1992). Interestingly, an effect of M/V129 polymorphism was reported also for the humPrP<sub>23-159</sub> fragment causing a GSS-like phenotype. A case study of two brothers carrying the Q160stop mutation revealed an earlier onset and a severe and rapidly progressing course in the patient homozygous for M129, while the other one was heterozygous and his disease had a mild course (Finckh et al., 2000). In our study of humPrP<sub>23-159</sub>, Met129 (similarly to Ile138 and Ile139) was found to be highly protected from solvent exchange (**Figure 3-16**). The presence of Met129 in a  $\beta$ -strand at the edge of the

deeply buried region in the core of the fibrils suggests that replacement of this residue with a valine might cause changes in the kinetics of aggregation as well as in the structure of the core.

The deuterium incorporation curves of residues 129 and 139 are in agreement with the logical expectation that sites responsible for different aggregation behavior and resulting disease pathology should occur in regions strategic for fibril architecture.

### 3.3.5. Conclusions and outlook

Summarizing the data presented here (**Figures 3-12** and **3-25**) and reported in the literature (see 3.3.2), we propose the following model for amyloid fibrils of the human prion protein. The core of the fibrils contains four hydrogen-bonded  $\beta$ -strands (111-115, 120-123, 127-135 and 137-140) with possible turns around Gly119 and the GGXGG motif (123-127), and two disulfide-bridged helices originating from helix 2 and helix 3 segments. Considering lack of structure in the helix 1 region and the decreased  $\alpha$ -helical content in PrP<sup>SC</sup> with respect to PrP<sup>C</sup>, both helices would need to be shorter than in the monomeric protein, however not converted into  $\beta$ -strands. High solvent protection of these two regions could be explained by intra-helical hydrogen bonding or packing on the interface of the  $\beta$ -sheet core. The N-terminal residues 23-98, as well as regions corresponding to helix 1 and  $\beta$ -strand 2 are proposed to be largely unstructured and solvent accessible on the outer surface of the fibrils.

Useful information for determination of the structure of humPrP fibrils can be obtained from subsequent solid-state NMR studies.

Further research plans include a combined study on amyloid fibrils of the full length human prion protein utilizing the NMR-detected H/D exchange experiment and the high-resolution magic angle spinning (HR-MAS) technique, in order to investigate the presence of helices 2 and 3 in the fibrils of humPrP, and solvent protection of the C-terminal region. Furthermore, the structural differences underlying the species barrier will be explored by comparing solvent protection maps of human and Syrian hamster PrP.



## 4. Human beta-2-microglobulin

### 4.1. Introduction

#### 4.1.1. $\beta$ -2-microglobulin and dialysis-related amyloidosis

The rising incidence of protein misfolding diseases in recent times may be associated with increasing life expectancy in many parts of the world and several other risk factors such as obesity, which often reaches a scale unrecorded in the human history (Csermely, 2001). In that sense, these diseases may be thought of as lifestyle related or even human-caused. A particular example of a disease related to human activity is dialysis-related amyloidosis, which is caused by long-term hemodialysis used to treat kidney failure. In this unfortunate case, a medical procedure meant to improve the status of people with chronic renal failure leads to an inevitable onset of another disorder. DRA is characterized by pain and decreasing mobility resulting from deposition of amyloid aggregates in skeletal tissue (Casey et al., 1986). These deposits (**Figure 4-1**) contain fibrils of  $\beta$ -2-microglobulin (h $\beta$ 2m) (Gejyo et al., 1985), which is the light chain of the major histocompatibility complex I (MHC-I) and as such it is presented on the surface of every cell in the body displaying MHC-I.

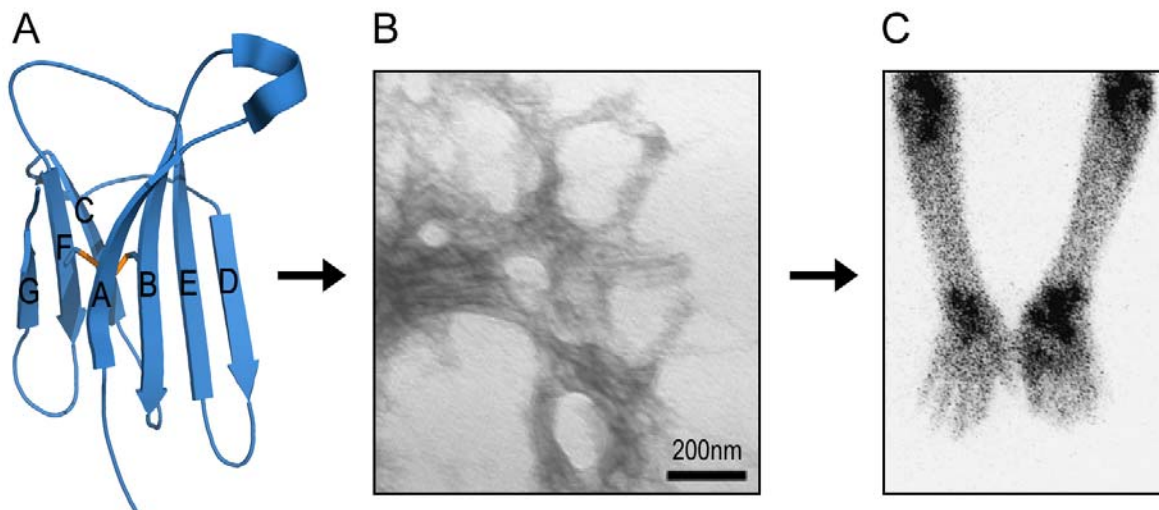


**Figure 4-1.** Aggregation of  $\beta$ -2-microglobulin causes dialysis-related amyloidosis. (a) Structure of native h $\beta$ 2m (pdb entry 1LDS); the disulfide bridge between C25 and C80 is marked in orange. (b) A negatively stained TEM image of *ex-vivo* fibrils of h $\beta$ 2m (adapted from Jahn et al., 2008). (c) Scintigraphy image of amyloid deposits in DRA patients (adapted from Linke et al., 2000).

The protein is regularly released in a process of turnover (Floege and Ehlerding, 1996) and degraded in the kidney. In healthy individuals, h $\beta$ 2m reaches a plasma concentration of 1-3 mg/L, however in case of kidney failure and subsequent long term treatment by dialysis the concentration rises more than 10-fold as the current procedures are not able to properly remove  $\beta$ -2-microglobulin from the organism (Ohashi, 2001). Accumulation of the protein leads to self-association presumably as a result of spontaneous population of less folded states or interaction with copper ions originating from the dialysis membrane.

$\beta$ -2-microglobulin is 99 residues long (MW of 11.8kDa) and natively has a seven-stranded  $\beta$ -sandwich fold with strands A, B, D and E forming one  $\beta$ -sheet, and strands C, F and G forming the other (**Figure 4-1a**). The two sheets are stabilized by a disulfide bridge between Cys25 and Cys80 in strands B and F, respectively (Becker and Reeke, 1985; Madden et al., 1993).

#### 4.1.2. Folding, unfolding and aggregation of h $\beta$ 2m

Folding of  $\beta$ -2-microglobulin is a two stage process, in which the second very slow kinetic phase involves a *trans-cis* isomerization of the highly conserved Pro32 (Jahn et al., 2006). Refolding experiments on a P32G mutant of h $\beta$ 2m showed that this variant folds without the slow phase. A crystallographic study of a closely related P32A mutant revealed that the proline isomerization step imposes further structural rearrangements leading to removal of a  $\beta$ -bulge in edge strand D and dimerization of the mutant protein (Eakin et al., 2006). The  $\beta$ -bulge is present when h $\beta$ 2m is bound to the MHC-I complex (Trinh et al., 2002) and it is postulated to prevent the protein from edge-to-edge aggregation (Richardson and Richardson, 2002).

It has been shown that high concentration of h $\beta$ 2m alone are insufficient to cause aggregation and that the amyloid fibril formation requires a partial unfolding of the protein (**Figure 4-2**) (Chiti et al., 2001). This can be achieved *in vitro* by copper binding (Morgan et al., 2001), addition of non-esterified fatty acids (Hasegawa et al., 2008) or acid denaturation. In the latter case, the highest population of the partially unfolded intermediate occurs at pH 3.6, where also the rate of fibril formation reaches a maximum (McParland et al., 2000). Conformational heterogeneity leads to only 28 signals being observable under these conditions. A denaturant titration experiment allowed for identification of 4 groups of residues depending on their denaturation profile (McParland et al., 2002). The study reports that residues in the N-terminal region including  $\beta$ -strand A unfold already at low

concentrations of urea, followed by the C-terminal strand G. Strands C and D become denatured at 1.5 M urea. At an urea concentration of 3 M only parts of strands B and F and strand E remain structured and further denaturation leads to 63 resonances observable in presence of 9 M urea. This suggests that dissociation of the N- and C-terminal strands may be sufficient to initiate aggregation of the protein, however the applicability of these findings to elucidation of the disease mechanism is questionable, as the aggregates formed at pH 3.6 have a form of thin and flexible filaments (McParland et al., 2000) and are therefore morphologically distinct from *in vivo* amyloid fibrils. The optimal conditions for *in vitro* formation of h $\beta$ 2m fibrils were found at pH 2.5, where the protein is largely unstructured (Naiki et al., 1997; Yamaguchi et al., 2001). Interestingly, the presence of the disulfide bridge is required for formation of long and straight fibrils and reduction of the disulfide bond leads to an assembly of fibrils morphologically similar to those formed at pH 3.6 (Katou et al., 2002). Interestingly, in low pH molecular dynamics simulations disappearance of the  $\beta$ -bulge is observed (Park and Saven, 2006), which suggests that its removal, whether by acid denaturation or as an effect of Pro32 isomerization, promotes amyloid fibril formation of h $\beta$ 2m.

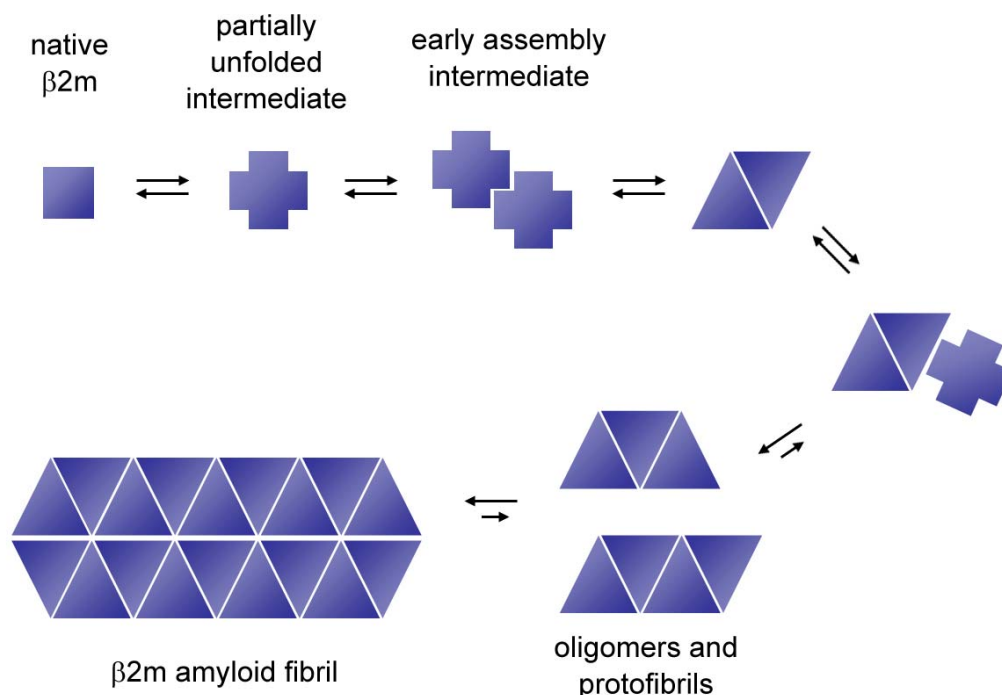


**Figure 4-2.** Schematic representation of amyloid fibril formation by h $\beta$ 2m (adapted from Kelly, 2000).

Structural characterization of the partially unfolded intermediate ensembles and determination of the relation between these species and the morphology of the fully matured fibrils are the key challenges in understanding the mechanism of amyloid fibril formation by h $\beta$ 2m.

#### 4.1.3. Variants of h $\beta$ 2m

Numerous mutagenesis studies have been performed to gain insight into stabilization / destabilization of  $\beta$ -2-microglobulin. It has been generally observed that single residue mutations to proline within any of the seven native  $\beta$ -strands hinder aggregation (Chiba et al., 2003), while side-chain truncations of buried hydrophobic residues led to significant destabilization of the protein, yet no spontaneous aggregation occurred at physiological pH (Smith et al., 2003). A naturally occurring asparagine deamidation at residue 17 (Odani et al., 1990) was also shown to significantly destabilize the protein although, as in other destabilized mutants, acidification was still necessary for the N17D-h $\beta$ 2m to aggregate *in vitro* (Kad et al., 2001).

Another variant found *in vivo* is a result of removal of the N-terminal hexapeptide, which accounts for 30 % of h $\beta$ 2m amyloid deposits in hemodialyzed patients (Linke et al., 1987). From the structural point of view, only part of the  $\beta$ -sheet pairing is retained in the  $\Delta$ N6 mutant by the stabilizing effect of the disulfide bond (Esposito et al., 2000). Perturbations of the tertiary structure resulting from the N-terminal truncation have such a pronounced effect on the stability of the protein that in contrast to other variants and the wild type protein, the  $\Delta$ N6 mutant is able to form amyloid fibrils at pH 7.0. Addition of  $\Delta$ N6-h $\beta$ 2m was also shown to greatly accelerate the aggregation of full length h $\beta$ 2m at physiological pH (Piazza et al., 2006). The high self-association tendency of  $\Delta$ N6-h $\beta$ 2m explains *in vivo* observations that this mutant was neither found in plasma nor in the insoluble non-fibrillar deposits in the heart and spleen (Stoppini et al., 2005).

Proteolysis of h $\beta$ 2m by the lysine-specific *Achromobacter* protease I results in release of nine peptides, one of which (Ser20-Lys48, termed K3) spontaneously fibrillizes at low pH (Kozhukh et al., 2002). Recently, the structure of protofilament-like K3 fibrils was solved by solid-state NMR (Iwata et al., 2006). The fibrils were found to consist of in parallel, head-to-head stacked K3 monomers in a  $\beta$ -strand-loop- $\beta$ -strand conformation (**Figure 4-3**).

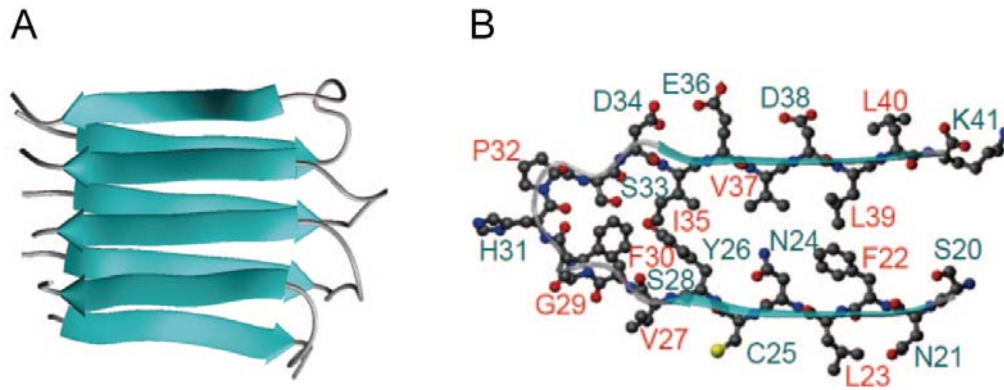


**Figure 4-3.** 3D structure of K3 fibrils.

(a) Ribbon model of a K3 tetramer in parallel head-to-head arrangement with a +1 register shift. (b) Conformation of a K3 monomer in fibrillar state (adapted from Iwata et al., 2006).

Although the K3 peptide is not the only h $\beta$ 2m fragment able to form fibrils (Ivanova et al., 2003; Jones et al., 2003), the authors provide invaluable information on the K3 fibrils and conclude that fibril formation of full length h $\beta$ 2m might require tight packing of side chains on the intermolecular surface. Still, the structure of the wild type h $\beta$ 2m fibrils remains unknown.

## 4.2. Results

### 4.2.1. Acid denaturation of h $\beta$ 2m

Aggregation of human  $\beta$ -2-microglobulin in dialysis related amyloidosis requires partial unfolding of the protein, which can be achieved *in vitro* by acid denaturation. Structural rearrangements occurring upon unfolding are clearly reflected in the NMR spectra of h $\beta$ 2m recorded under different conditions (**Figure 4-4**).

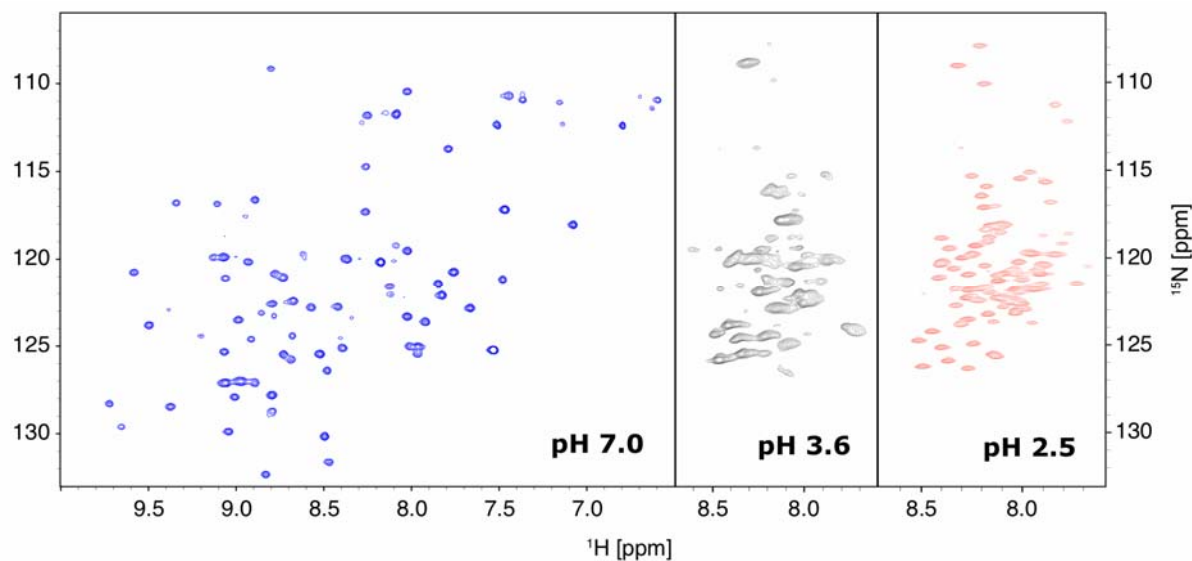


**Figure 4-4.** Unfolding of human  $\beta$ -2-microglobulin followed by NMR.  $^1\text{H}$ ,  $^{15}\text{N}$ -HSQC spectra were acquired for h $\beta$ 2m in 50 mM phosphate buffer at pH 7.0 (blue), and in pure water at pH 3.6 (black) and pH 2.5 (red).

At pH 7.0 the protein adopts the native immunoglobulin fold, which gives rise to a well-dispersed spectrum characteristic for a protein rich in  $\beta$ -strands. At a pH value of 3.6 the partially unfolded state is populated to a high degree and conformational heterogeneity of the unstructured states leads to disappearance of many signals. A decrease of pH to 2.5 further denatures the protein and the signals not observable at pH 3.6 reappear in the spectrum. Due to the loss of  $\beta$ -sheet structure, the signals cover a very narrow ppm range and significant spectral overlap is observed.

Unfolding of a protein changes its compaction and size, therefore the process of acid denaturation of h $\beta$ 2m can be followed by a measurement of the protein's diffusion properties. A diffusion ordered spectroscopy (DOSY) NMR experiment allows reflecting the hydrodynamic properties of a molecule as a decay of signal under pulsed field gradients. **Figure 4-5** shows the signal decay curves of h $\beta$ 2m at pH 7.0, 5.6, 3.6, and 2.5.

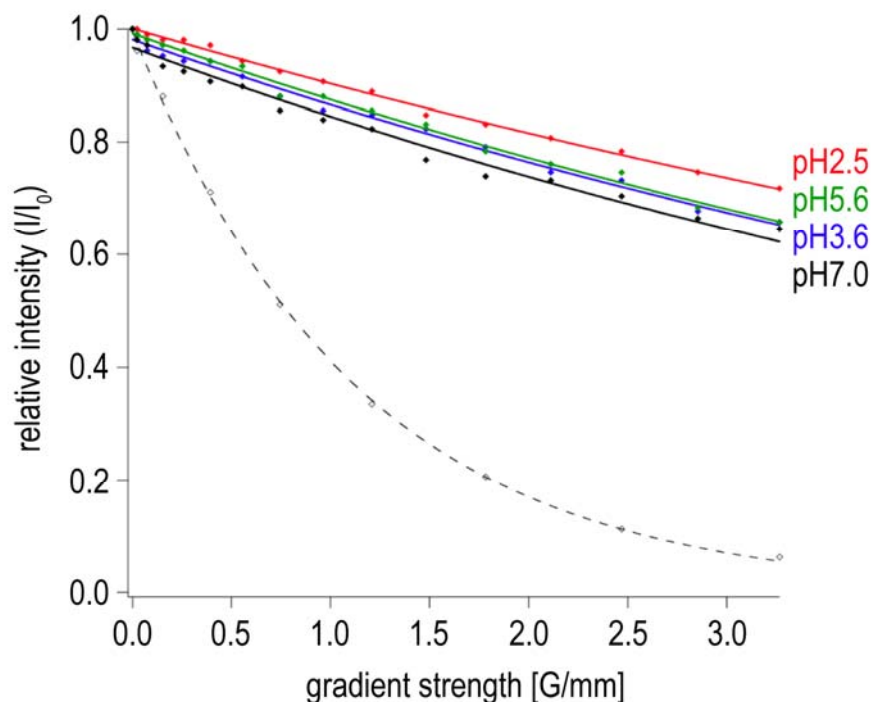


**Figure 4-5.** Changes in hydrodynamic radius of h $\beta$ 2m upon acid denaturation. The changes in size were followed by a measurement of diffusion coefficients at pH 7.0 (black), 5.6 (green), 3.6 (blue), and 2.5 (red). Upon acid denaturation the diffusion coefficient of h $\beta$ 2m decreases reflecting unfolding of the protein.

Under physiological pH, the signal decay is faster as compared to the other conditions, which reports a smaller size. The well-defined fold increases the compactness of the polypeptide chain and therefore the molecule diffuses faster and a higher decrease of the signal is observed. In partially denatured states (pH 5.6 and 3.6), the signal decays slower evidencing an increase in the protein's size. At pH 2.5, an even slower decay is observed due to further unfolding of the protein. Fitting of the decays to an exponential function and calculation of hydrodynamic radii using 1,4-dioxane as internal reference led to  $r_H$  values of: 1.8 nm at pH 7.0, 2.0 nm at pH 5.6 and pH 3.6, and 2.3 nm at pH 2.5.

#### 4.2.2. Structural analysis of the unfolded states

##### 4.2.2.1. pH 3.6

The highest population of partially unfolded states by  $\beta$ -2-microglobulin occurs at pH 3.6 (McParland et al., 2000). However, as shown above in **Figure 4-4**, under these conditions only about 30 signals are observable. Due to severe line broadening caused by chemical exchange it is not possible to obtain assignment of these signals using standard NMR experiments. Recently, direct  $^{13}\text{C}$  detection emerged as a very useful technique to overcome

fast relaxation of  $^1\text{H}$  nuclei (Bertini et al., 2004; Bermel et al., 2005). The so-called protonless NMR experiments have not only proven useful in studies of proteins binding paramagnetic ions (Banci et al., 2006; Caillet-Saguy et al., 2006; Bertini et al., 2008) but also in case of intrinsically unstructured proteins (Bermel et al., 2006; Csizmok et al., 2008). We have applied the direct carbon detected CON and CACO experiments in order to detect the exchange-broadened resonances of the unfolding intermediate of human  $\beta$ -2-microglobulin (Figure 4-6).

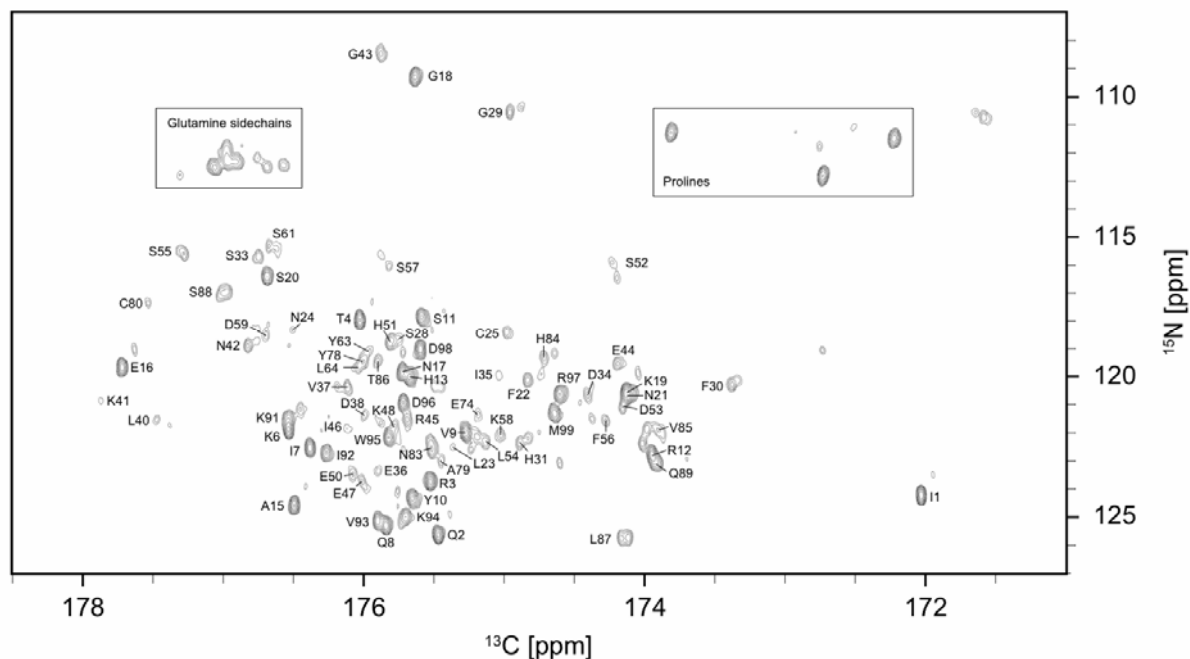


**Figure 4-6.** Direct carbon detection allows for observation of highly dynamic regions of h $\beta$ 2m at pH 3.6. The  $^{13}\text{C}$ -CON spectrum allows for observation of resonances, which cannot be detected with standard  $^1\text{H}$ -detected experiments due to severe line broadening. The spectrum was recorded at 298 K on a 800 MHz Bruker Avance spectrometer equipped with a TCI cryo probehead using the pulse sequence depicted in Figure 2-5.

Indeed, about 90 peaks were observable in the  $^{13}\text{C}$ -CON spectrum, however the spectrum was clearly showing two subpopulations of peaks with different intensity. The intense peaks corresponded to those residues, which were observable in standard proton-based NMR experiments, while the exchange-broadened peaks undetectable in  $^1\text{H}$ -detected experiments yielded signals with low intensity in the  $^{13}\text{C}$ -detected spectra. As a result, the three dimensional COCON experiment used for assignment of protonless NMR spectra failed to provide the sequential connectivity information necessary to attain the assignment. Instead, an approach combining  $^1\text{H}$ - and  $^{13}\text{C}$ -detected experiments was used. The backbone



assignment of h $\beta$ 2m obtained with traditional experiments at pH 2.5 was first transferred to the  $^{13}\text{C}$ -CON spectrum. This resulted in assignment of 76 residues under these conditions. Then, a titration experiment was performed in which the pH was changed stepwise from 2.5 to 3.6. Following this approach, a large number of resonances of the unfolding intermediate of h $\beta$ 2m at pH 3.6 could be assigned (**Figure 4-7a**).

Out of 94 possible assignments, 23 were missing at pH 3.6, out of which 18 residues were unassigned already at pH 2.5. For Leu23, Ile35, Glu36, and Val39 the changes in chemical shifts could be followed only in the first few steps of the pH titration experiment. Interestingly, the signals originating from these four residues disappeared around pH 3.1 and a general decrease in signal intensity was seen under these conditions, suggesting that the structural transition takes place at pH  $\sim$  3.1 (**Figure 4-7e**). In addition, peak doubling was observed for a number of residues at pH 3.6 (G29, F30, H31, S52, S57, S61, L87 – see **Figure 4-6**) indicative of conformational heterogeneity of the partially unfolded intermediate ensembles of h $\beta$ 2m.

The analysis of signal intensities in the  $^{13}\text{C}$ -detected CON experiment (**Figure 4-7b**) reveals that residues in the central part of the protein (22-82) give rise to low intensity signals indicative of increased chemical exchange in this region. Furthermore, a comparison between  $^{13}\text{C}'$  chemical shift at pH 2.5 and 3.6 (**Figure 4-7c**) identifies residues 35-41, 46-49, 54-64, and 80-88 to have increased  $\alpha$ -helical propensities at pH 3.6 with respect to pH 2.5, while in the C-terminal region the opposite effect is observed for residues 91-97, which display higher propensity for extended structure at pH 3.6. The largest downfield shifts (more  $\alpha$ -helical or turn propensity) are seen for residues 64 and 80 lying at the edges of the exchange-broadened region 65-78.

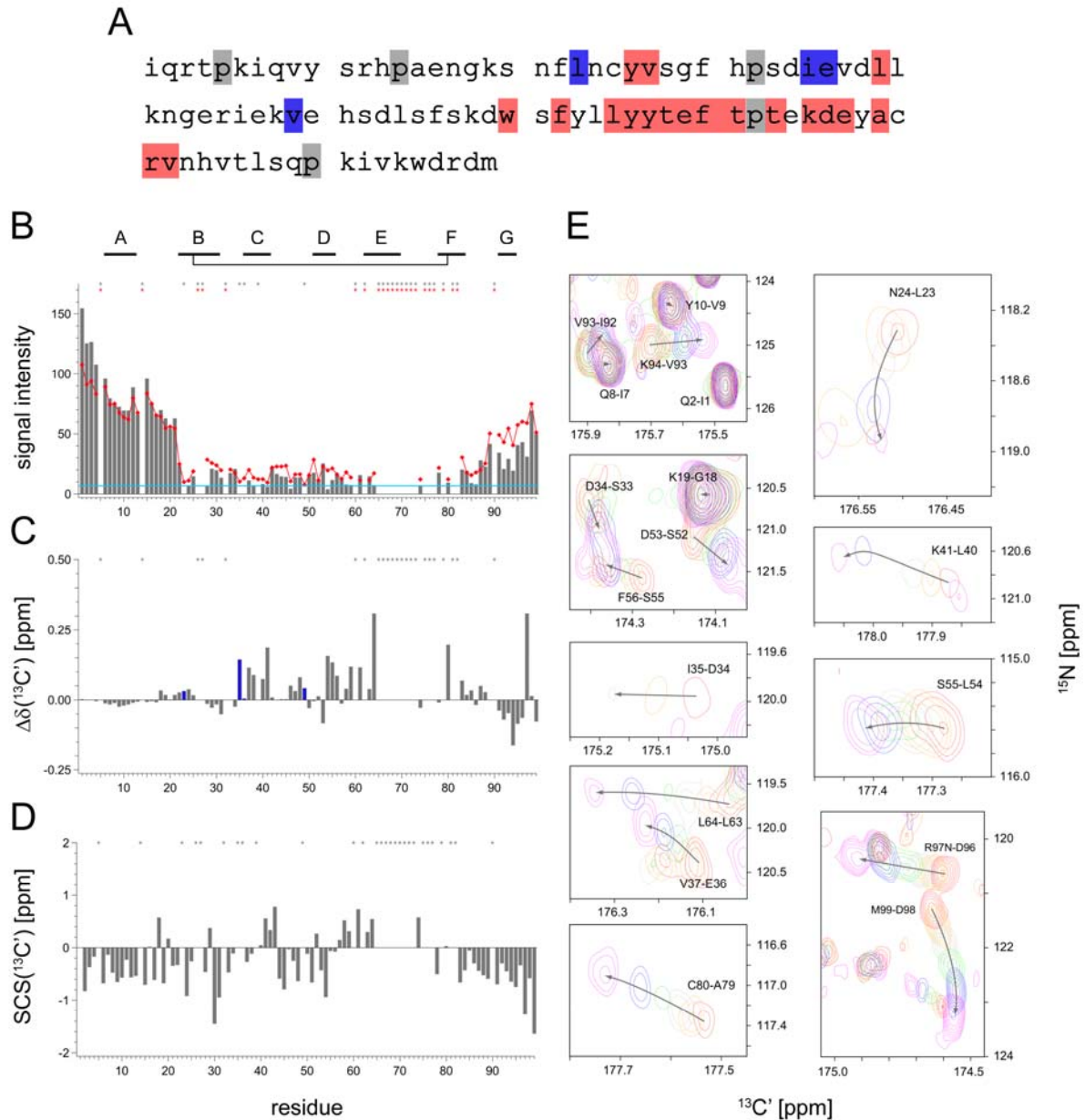


**Figure 4-7.** Structural properties of h $\beta$ 2m at pH 3.6.

(a) Schematic representation of completeness of assignment; unassigned residues and prolines are highlighted in red and grey, respectively; blue color indicates residues for which signals could be observed only in the first few steps of the titration. (b) Signal intensities in the  $^{13}\text{C}$ -CON experiment at pH 2.5 (red) and pH 3.6 (grey); noise level in the spectra is marked in cyan; missing assignments are indicated by asterisks for both conditions; structural elements found under native conditions and the position of the disulfide bridge are indicated above the plot. (c) Changes in  $^{13}\text{C}'$  chemical shift upon pH change from 2.5 to 3.6; blue bars indicate residues for which the assignment at pH 3.6 was missing, and the value from pH 3.1 was used for the calculation. (d) Secondary chemical shifts of h $\beta$ 2m at pH 3.6 calculated using the  $^{13}\text{C}'$  chemical shift. (e) Excerpts from the  $^{13}\text{C}$ -CON spectra showing residues with the largest changes; pH values are: 2.5 (red), 2.7 (orange), 2.9 (light grey), 3.1 (green), 3.3 (blue), and 3.6 (magenta).

In the CON experiment, the nitrogen chemical shift of residue  $i$  is correlated with the C' chemical shift of residue  $i-1$ . Therefore, the values reported for residues 35, 54, 97, and 99 might be influenced by sidechain protonation of the preceding aspartates, which occurs around pH 3.6.

By applying carbon detected experiments, assignment of more than 80 % residues of the unfolded intermediate of h $\beta$ 2m at pH 3.6 could be obtained. The assigned C' chemical shifts were then used to calculate the secondary chemical shifts shown in **Figure 4-7d**. Stretches of negative secondary chemical shifts are found at pH 3.6 for residues 1-33, 45-55, and 83-99, indicating a propensity for extended structure in these regions. Due to chemical exchange, no clear indication of secondary structure preferences is observed in the central part of the protein (residues 65-82).

#### 4.2.2.2. pH 2.5

Although the partially unfolded intermediate of h $\beta$ 2m is highly populated at pH 3.6, the most optimal aggregation conditions were found to be at an even lower pH. Amyloid fibrils formed by h $\beta$ 2m at pH 2.5 are long and straight and closely resemble those extracted from patients, in contrast to short, worm-like aggregates obtained at pH 3.6. Therefore, it seems more disease relevant to investigate the structure of h $\beta$ 2m intermediate and the amyloid fibrils formed at pH 2.5. To prevent spontaneous aggregation of the protein under the aggregation promoting conditions it is required that the ionic strength of the solution is kept at minimum. Therefore, the sample for investigation of secondary structure of monomeric  $\beta$ -2-microglobulin at pH 2.5 was prepared by dissolving the protein in pure water without presence of any salt or buffer. Residue specific assignment was obtained using standard 3D (HA)CANNH and HNCO, and secondary chemical shifts (**Figure 4-8**) were calculated as described in 2.4.2.

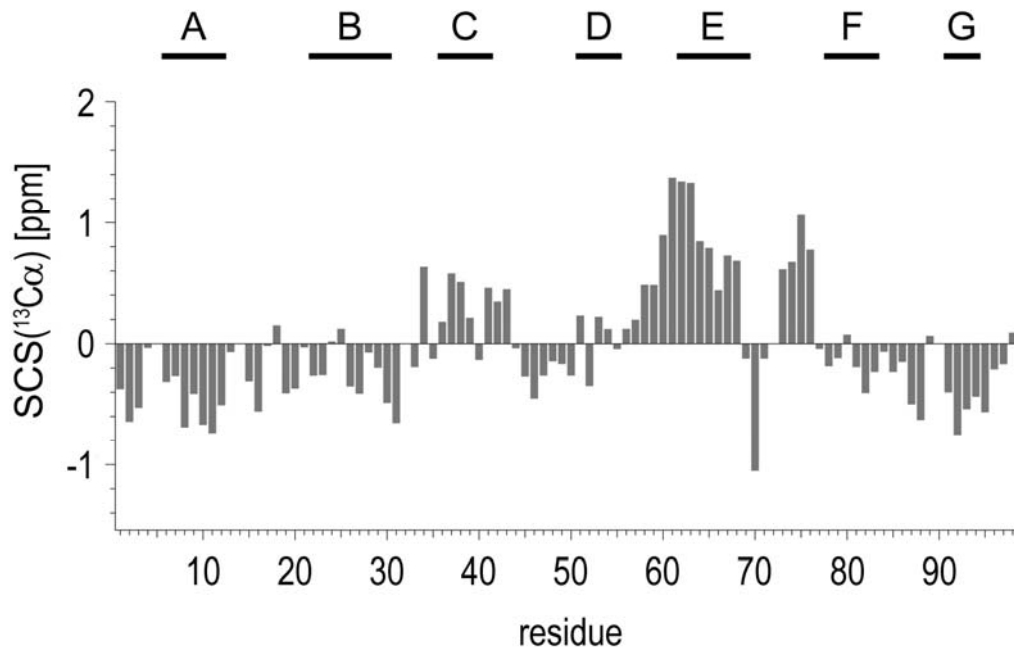


**Figure 4-8.** Secondary chemical shifts of h $\beta$ 2m at pH 2.5. Secondary structure elements present at pH 7.0 are indicated by black bars.

Interestingly, even though the protein is largely unstructured under the studied conditions, a propensity for  $\alpha$ -helical structure is found in regions corresponding to strands C and E, and the DE and EF loops. This is surprising as the native fold is formed only by  $\beta$ -strands, which implies that major structural rearrangements occur upon acid denaturation of h $\beta$ 2m.

#### 4.2.3. Observation of flexible regions in h $\beta$ 2m fibrils

Aggregation of h $\beta$ 2m was performed at 37 °C with agitation at 500 rpm, in a mixed buffer consisting of 25 mM sodium acetate and 25 mM sodium phosphate at pH 2.5. Even though fibril formation occurred already a few hours after the initiation of aggregation, it was necessary to continue the reaction for 7 days to fully convert all the monomer into fibrils (**Figure 4-9**).

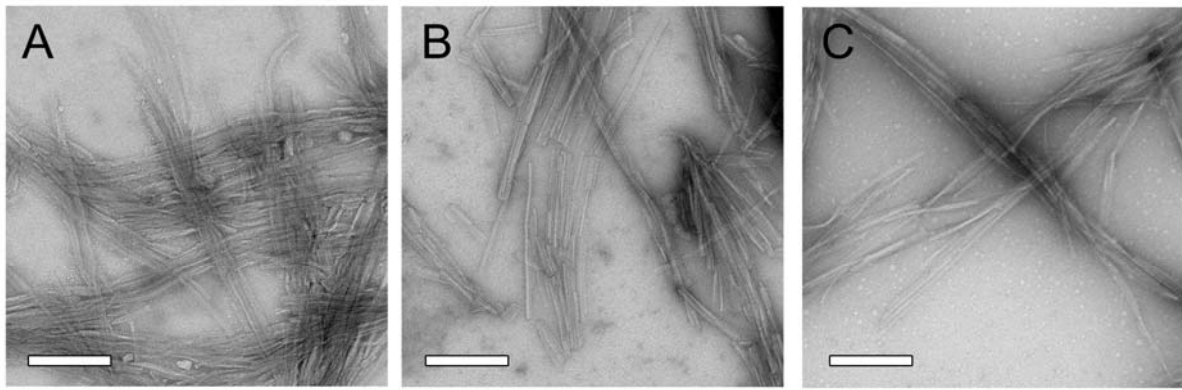


**Figure 4-9.** Amyloid fibril formation by h $\beta$ 2m. Negatively stained EM images were taken after (a) 1, (b) 3, and (c) 7 days of incubation at 37 °C. The white bar indicates a size of 200 nm.

Mature fibrils were washed to remove residual monomer and filled into a 5 mm HR-MAS rotor. Under magic angle spinning at 7.2 kHz, nitrogen and carbon HSQCs (**Figure 4-10**), as well as  $^1\text{H}$ ,  $^1\text{H}$ - and HCCH-TOCSY spectra were acquired. Based on these experiments residue-type assignment was performed revealing the absence of signals from aspartates, cysteines, and phenylalanines. Furthermore, histidines (4 occurrences in the sequence), leucines (7 occurrences) and tyrosines (6 occurrences) yielded low intensity signals, suggesting that not all residues of each type are observable in the spectrum.

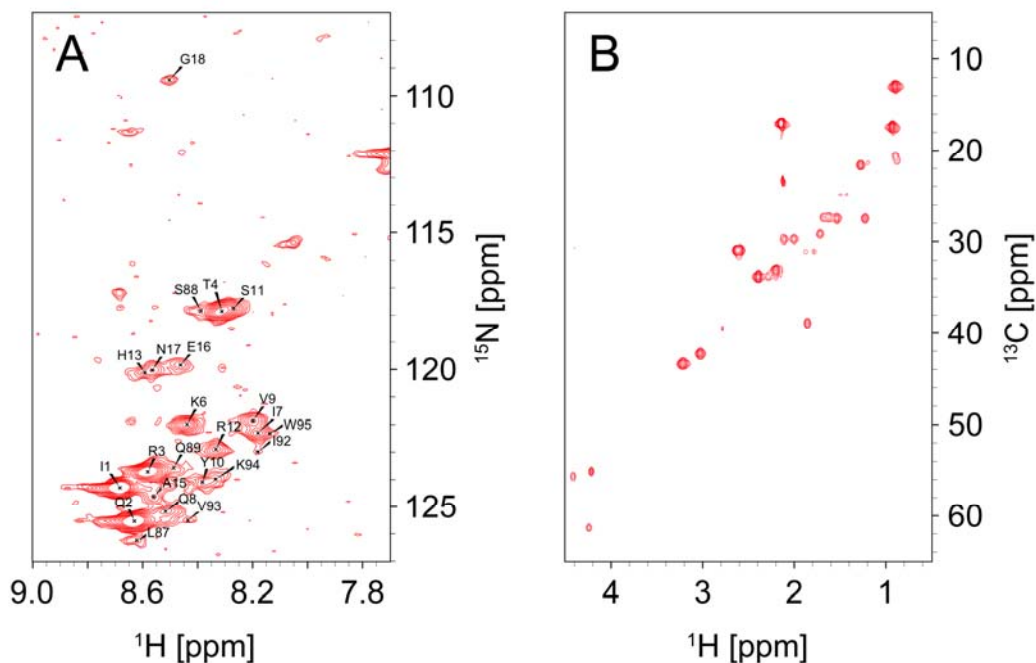


**Figure 4-10.** NMR spectra of h $\beta$ 2m fibrils under high-resolution magic angle spinning. (a)  $^1\text{H}$ ,  $^{15}\text{N}$ -HSQC, (b)  $^1\text{H}$ ,  $^{13}\text{C}$ -HSQC. Both spectra were recorded at 310 K with MAS at 7.2 kHz.

A sequence specific assignment could be obtained for majority of the observable peaks, based only on two-dimensional projections of HNCA and HNCOC experiments (**Figure 4-11a**).

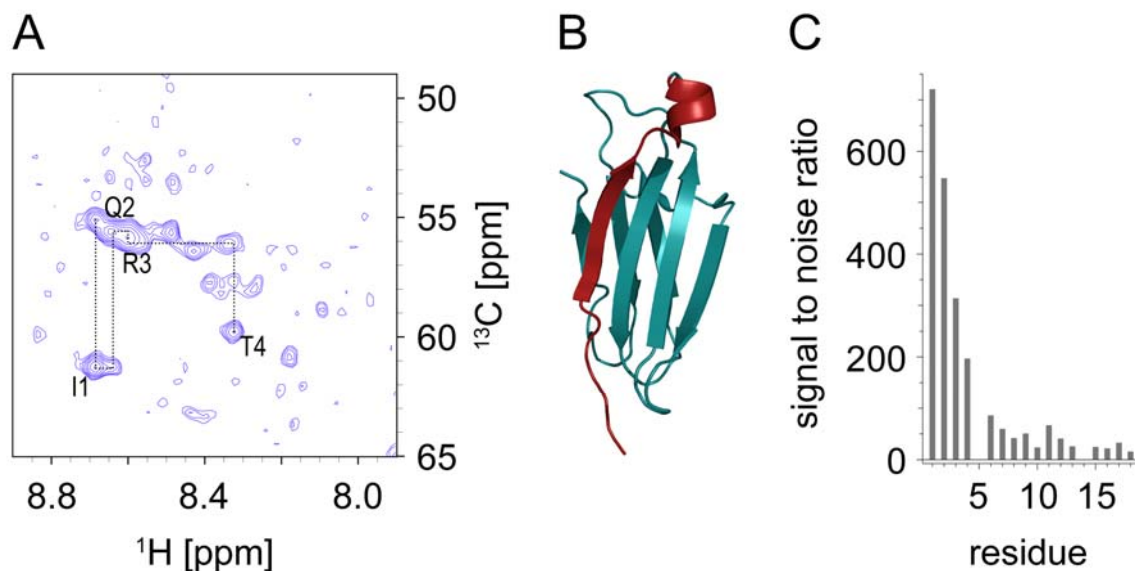


**Figure 4-11.** Identification of flexible regions in amyloid fibrils of hβ2m. (a) 2D projection of an HNCA spectrum used for assignment of signals from the flexible region. (b) Mapping of assigned HR-MAS peaks (red) onto the native fold. (c) Analysis of signal intensities in the flexible region reveals rapidly increasing rigidity when moving away from the N-terminus.

Seventeen of a total of 22 signals in the  $^1\text{H}$ ,  $^{15}\text{N}$ -HSQC were sequentially assigned to the N-terminal residues reporting that the region corresponding to β-strand A in the native fold is flexible in the fibrillar form of β-2-microglobulin (**Figure 4-11b**). Furthermore, the analysis of signal intensity for residues 1-20 (**Figure 4-11c**) shows an exponential decay indicating a rapidly increasing rigidity while moving away from the N-terminus along the polypeptide chain.

#### 4.2.4. Mapping the core of hβ2m fibrils by H/D exchange

As described in section 1.2.1, NMR-detected proton / deuterium exchange experiment provides valuable information about the structure of amyloid fibrils. Using the 50 %  $\text{H}_2\text{O}$  / 50 %  $\text{D}_2\text{O}$  buffer system for dissolution of the fibrils, the H/D exchange profile was studied for hβ2m fibrils. As a results of the experimental conditions used (see 3.2.3.2. for details), in the protection map depicted in **Figure 4-12**, residues that are solvent accessible in more than 50 % in the fibrils will give rise to  $I/I_0$  values greater than 1 at the end of the back-exchange

process. Residues that are buried in the core will not be subject to significant H/D exchange, and for those residues the normalized intensity at the end of the back-exchange process will lay between 0.5 and 1.0, where 0.5 indicates full protection and 1.0 corresponds to 50 % protection in the fibril.

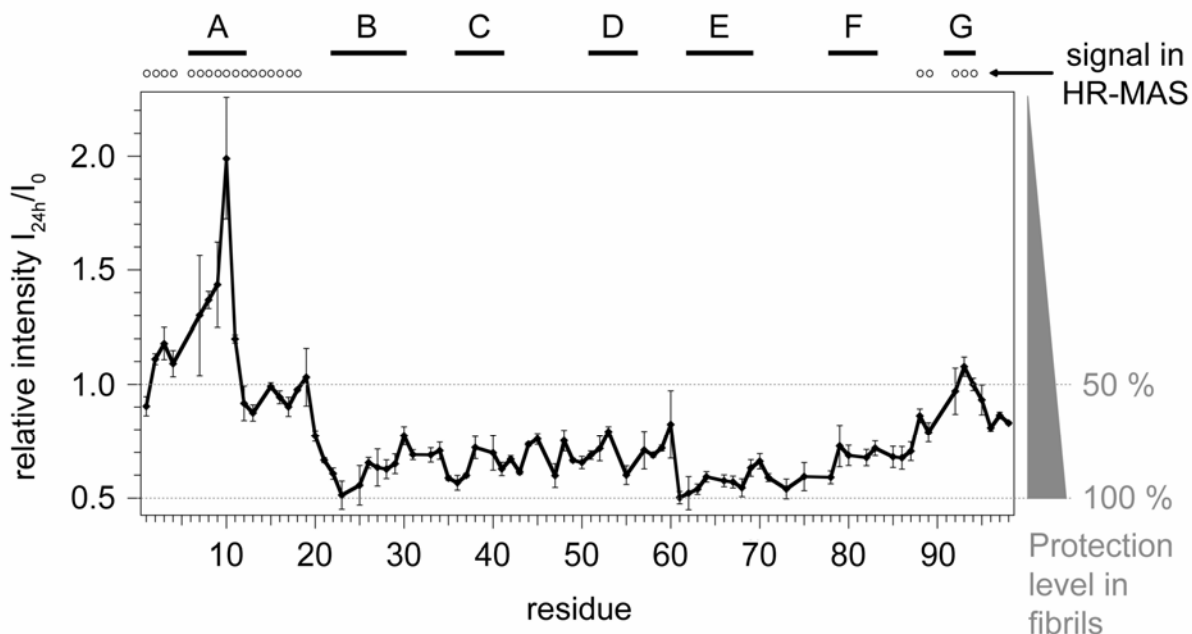


**Figure 4-12.** H/D exchange map for fibrils of human  $\beta$ -2-microglobulin.

The protection map was recorded after 7 days of exchange with  $D_2O$ . Structural elements found in the native fold at physiological pH are indicated by black bars. Open circles indicate residues observable in HR-MAS spectra.

As evidenced by the H/D exchange experiment, the N- and C-terminal regions of the protein show increased solvent exposure, while residues 20-90 are generally buried in the fibril core. The highest protection levels are seen in regions 21-29, 35-38 and 61-78, corresponding to strands B, C and E, and the EF loop. Since NMR-detection of exchange rates provides single residue resolution, further important observations can be made revealing details of the h $\beta$ 2m fibril architecture. In regions corresponding to  $\beta$ -strands B and E, a slope in the  $I/I_0$  values is detected. In both these regions (23-30 and 61-70), the solvent protection decreases along the sequence. Since in the native fold strands B and E are arranged antiparallely, this finding suggests that a rearrangement of the strands occurs upon aggregation of the protein.

Interestingly, even though solvent exchange and observability of signal in HR-MAS fall into different time regimes, a correlation between those two properties is seen for fibrils of human  $\beta$ -2-microglobulin. The solvent accessible residues from N- and C-termini are also

giving rise to peaks in HR-MAS spectra (indicated by open circles in **Figure 4-12**), therefore hinting that local flexibility of those regions occurs on a range of timescales.

Taken together, our data provides strong evidence that the N- and C-termini are flexible in the amyloid fibrils of human  $\beta$ -2-microglobulin as evidenced by both high-resolution magic angle spinning experiments and NMR-detected proton / deuterium exchange.

### 4.3. Discussion

Dialysis-related amyloidosis is caused by increased serum levels and spontaneous aggregation of human  $\beta$ -2-microglobulin in patients undergoing long-term hemodialysis. To cure and/or prevent the disease, the mechanism of amyloid fibril formation by h $\beta$ 2m needs to be revealed and understood. Here, we have concentrated on two aspects of the fibrillization pathway.

Firstly, using NMR secondary chemical shifts we have studied the structural properties of unfolding intermediates of h $\beta$ 2m under aggregation prone conditions. At a pH value of 2.5, the protein forms amyloid fibrils *in vitro* which share a common architecture with the *in vivo* ones, as evidenced by a Fourier transform infrared spectroscopy (FTIR) study by Jahn and coworkers (Jahn et al., 2008). The secondary chemical shifts (**Figure 4-13a**) reveal that the protein displays a propensity to adopt  $\alpha$ -helical conformation in regions 34-44, 58-68 and 73-76. Our data are in general agreement with previously published observation of Katou and coworkers (**Figure 4-13b**), who reported  $\alpha$ -helical propensities in regions corresponding to  $\beta$ -strands C, D and E in the native fold (Katou et al., 2002). It should be noted however that an offset of  $\sim 0.5$  ppm is present between the two datasets, which might be due to different random coil chemical shifts used in the calculation.

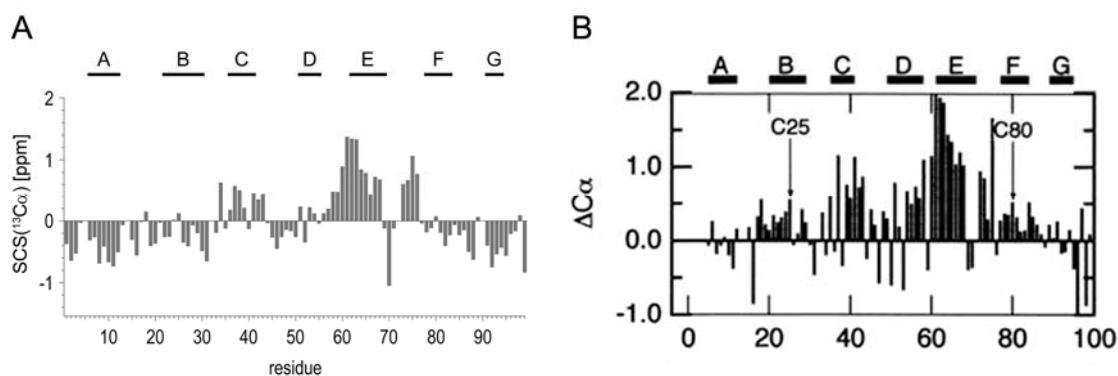


**Figure 4-13.** Secondary chemical shifts report  $\alpha$ -helical propensities in h $\beta$ 2m at pH 2.5. A comparison between SCS (**a**) obtained in this study and (**b**) previously reported by Katou and coworkers (adapted from Katou et al., 2002).



Based on this information we have investigated the differences between the intermediate states at pH 2.5 and 3.6. In the latter case, the highest population of unfolded states has been reported (McParland et al., 2000). Previous attempts to obtain information about the structure of the unfolding intermediate at pH 3.6 were unsuccessful as increased conformational heterogeneity led to disappearance of many signals in the NMR spectrum (McParland et al., 2002). By applying direct  $^{13}\text{C}$ -detected experiments we were able to obtain more than 80 % assignment of h $\beta$ 2m at pH 3.6 which allowed to identify regions undergoing severe conformational exchange, that are located around residues 35-41, 46-49, 54-64, and 80-88 as evidenced by loss of signal in these regions and significant changes in secondary structure propensities (towards  $\alpha$ -helical conformation) upon pH change from 2.5 to 3.6 (**Figure 4-7b,c**). Furthermore, an increase in the propensity for extended structure was found in the C-terminal residues 82-99 (**Figure 4-7d**). Taken together our data suggest that the structural variations between the two partially unfolded states at pH 2.5 and 3.6, presented by different aggregation kinetics and fibril morphology, are located between residue ~22 and the C-terminus.

Our findings also demonstrate that a significant amount of local structure is present in the acid-denatured intermediate ensembles of h $\beta$ 2m, which is in agreement with a recent NMR study on dynamics of the unfolded intermediate of h $\beta$ 2m at pH 2.5 (Platt et al., 2005). The authors report that although the N- and C-termini are predominantly unfolded in the acid-denatured state, the experimental  $^{15}\text{N}$  transverse relaxation rates for residues 26-84 are much higher than the values predicted using a random polymer model containing a single disulfide bond between residues 25 and 80 (**Figure 4-14**). This correlates well with the lower signal intensities observed for those residues in the  $^{13}\text{C}$ -CON spectra (see **Figure 4-7b**).

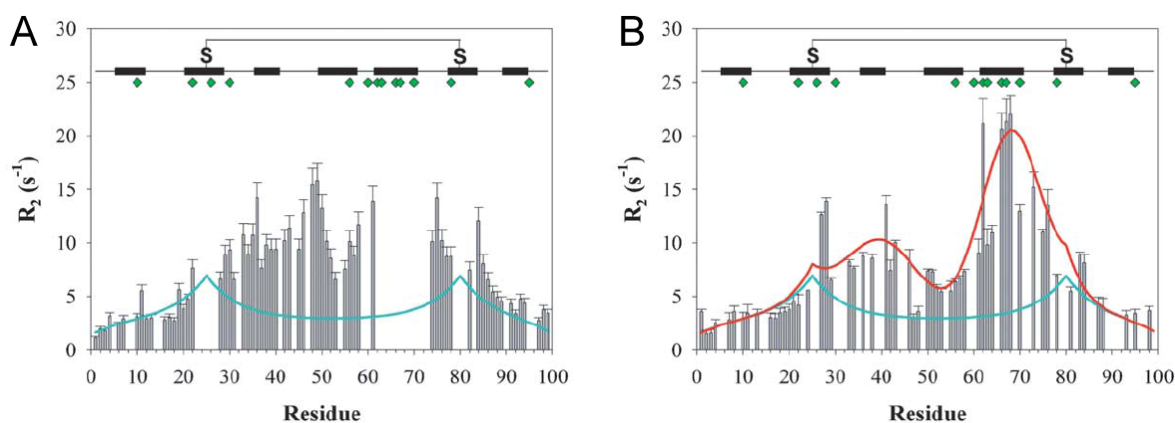


**Figure 4-14.** Residue-specific  $R_2$  relaxation rates for h $\beta$ 2m at pH 2.5.

$R_2$  rates were measured in (a) water and (b) 1.3 M urea. Position of  $\beta$ -strands in the native state is indicated by black bars, aromatic residues are marked by green diamonds. The predicted random coil  $R_2$  rates are shown in cyan. Red line represents fitting of the experimental data to a random coil model that contains two regions of non-random structure located around the hydrophobic clusters 29-51 and 59-78 (adapted from Platt et al., 2005).

Importantly, the residues with highest  $^{15}\text{N}$   $R_2$  relaxation rates became observable only in presence of 1.3 M urea (**Figure 4-14b**), and similarly to our data assignment of this region could not be obtained in a non-denaturing environment (**Figure 4-14a**). The significance of the predominantly hydrophobic residues 62-70 for the aggregation of h $\beta$ 2m is further supported by subsequent mutagenesis experiments from the same research group. The study shows that mutations of residues in this region (in particular F62, Y63, L65, Y67 and F70) designed to decrease hydrophobicity, change the kinetics of aggregation and lead to an increase in the lag phase. The authors conclude that non-native hydrophobic clustering might be the mechanism of initiation of h $\beta$ 2m aggregation (Platt et al., 2008; Routledge et al., 2009).

The second part of our study focused on the structure of mature h $\beta$ 2m fibrils obtained *in vitro* at pH 2.5. Using high-resolution magic angle spinning, we reported observation of flexible regions in the fibrillar form of h $\beta$ 2m located at the N- and C-termini of the polypeptide chain (see **Figure 4-12**). This finding is in line with a previous urea-denaturation study (McParland et al., 2002), which concluded that unfolding of strands A and G might be sufficient to initiate the aggregation of human  $\beta$ -2-microglobulin, however these data were obtained at pH 3.6, where the fibrils are known to have a different morphology.

The results of the HR-MAS experiments were further confirmed by amide proton exchange rates investigated by NMR-detected H/D exchange. The experimental data (**Figures 4-12** and **4-15a**) report on increased deuterium incorporation in the N- and C-terminal regions of the protein while the amide protons of residues 20-85 are protected from exchange with the solvent. The lower protection of the N-terminus with respect to the C-terminus could explain the results of a limited pepsin proteolysis study of h $\beta$ 2m fibrils formed at pH 2.5, where a single cleavage site at Val9 was found (Myers et al., 2006).

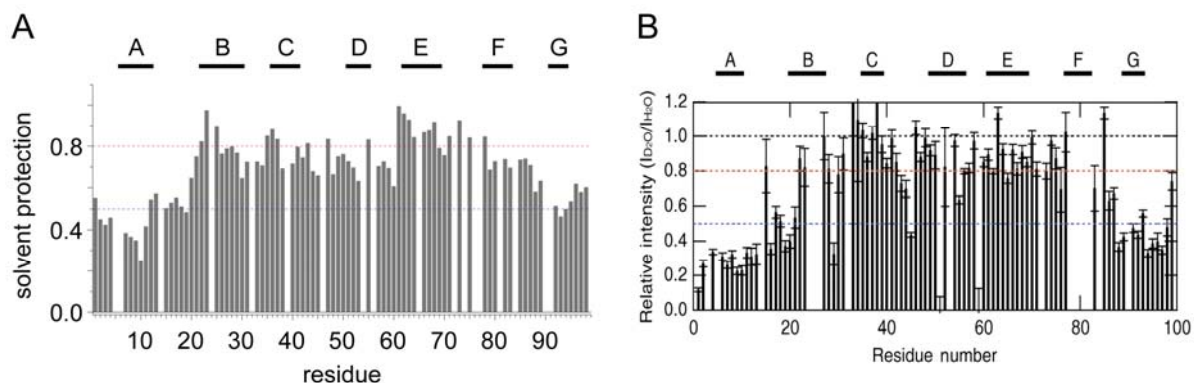


**Figure 4-15.** Deuterium incorporation into amyloid fibrils of h $\beta$ 2m.

(a) The levels of deuterium incorporation were calculated by normalizing the inversed  $I_{24h}/I_0$  values depicted in Figure 4-12. (b) H/D exchange of h $\beta$ 2m fibrils as reported by Hoshino and coworkers (Hoshino et al., 2002).

While our data are in overall agreement with published H/D exchange data (**Figure 4-15b**) (Hoshino et al., 2002), we provide new information on amide proton exchange rates in regions corresponding to the disulfide-bridged  $\beta$ -strands B and F, which were previously not detected due to the use of a different buffer system for dissolution of amyloid fibrils. Here we showed that the above-mentioned regions stay protected from solvent exchange. This finding is of high importance considering that reduction of the disulfide bridge between cysteins 25 and 80 leads to amyloid fibrils of different morphology (Katou et al., 2002).

The H/D exchange experiment also shows that the highest protection from exchange occurs in regions corresponding to strands B, C and E, and the EF loop. This matches the positions of the aromatic residues and regions with the highest  $R_2$  relaxation rates shown in **Figure 4-14b** (Platt et al., 2005). Strikingly, a very good agreement is found between the signal intensities in the spectra of the partially unfolded intermediates of h $\beta$ 2m and the solvent protection pattern in the fibril (**Figure 4-16**). Regions with the lowest deuterium incorporation in the fibrils located around residues 22-25 and 61-78 correspond to the residues

giving lowest signal in the  $^{13}\text{C}$ -CON experiment. Moreover, a slight increase of solvent exposure of residues 29-60 correlates well with the increase of signal intensities in the spectra of the partially unfolded state, thereby proving a close relationship between the dynamics of the precursor ensembles with morphology of the mature fibrils. This region includes the  $\beta$ -strand D, which was shown to adopt different conformations under native conditions when studied with different techniques. In the crystal structure of h $\beta$ 2m bound to the major histocompatibility complex-I (MHC-I) the strand is broken by a  $\beta$ -bulge (Khan et al., 2000), while in crystals of isolated h $\beta$ 2m  $\beta$ -strand D is long and continuous (Trinh et al., 2002). In the NMR structure in solution strand D exists as two short strands D1 (50-52) and D2 (55-57) (Okon et al., 1992) and displays conformational dynamics (Verdone et al., 2002).

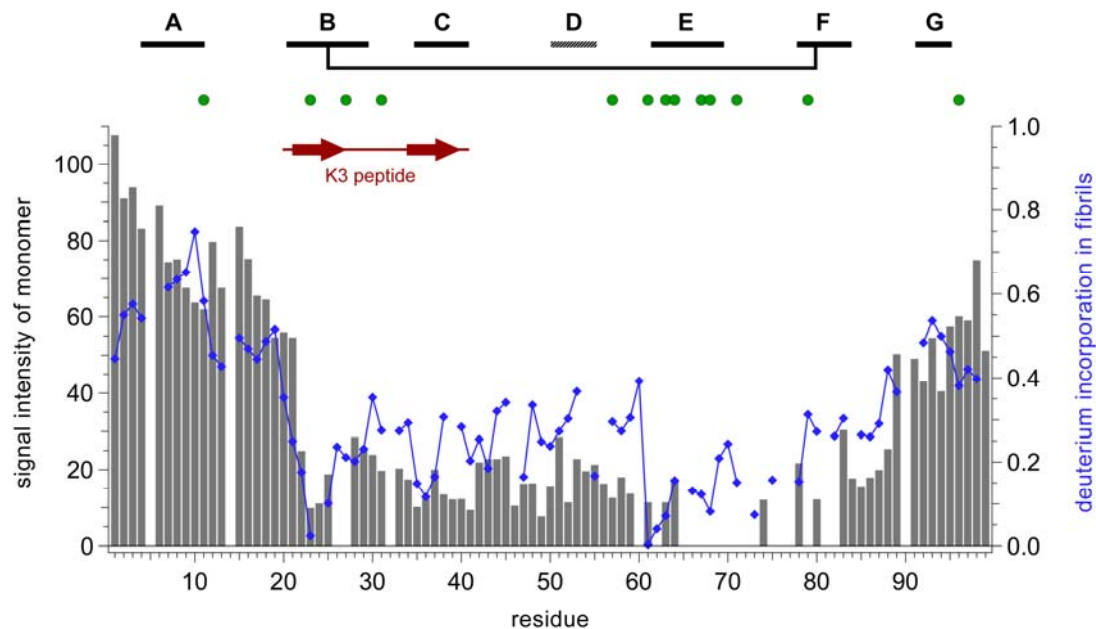


**Figure 4-16.** Relationship between the dynamics of the h $\beta$ 2m intermediate and structural architecture of the fibrils. Grey bars represent signal intensities in the  $^{13}\text{C}$ -CON experiment at pH 2.5, relative deuterium incorporation into amyloid fibrils is shown in blue. Structural elements of native h $\beta$ 2m are indicated above the plot, with the conformationally heterogeneous strand D indicated with a hashed bar; green circles mark positions of aromatic residues in the sequence; residues encompassed by the K3 peptide and structure of K3 fibrils are shown in red (based on Kozhukh et al., 2001).

Furthermore, two peptides related to the highly protected regions around strands B and E were reported to self-associate *in vitro* forming amyloid fibrils. The first region is encompassed by the K3 peptide (residues 20-41) released from h $\beta$ 2m as a product of proteolytic cleavage of h $\beta$ 2m with *Achromobacter* protease I (Kozhukh et al., 2002). Interestingly, the positions of  $\beta$ -strands in the amyloid fibrils of the K3 peptide match the dips around residues 23 and 36 in H/D exchange pattern of the full-length h $\beta$ 2m fibrils (**Figure 4-16**). The second aggregation-prone peptide (residues 59-71) includes the hydrophobic region of strand E (Jones et al., 2003).

The H/D exchange data is additionally summarized in **Figure 4-17** by mapping the levels of deuterium incorporation into the amyloid fibrils onto the native fold of h $\beta$ 2m.

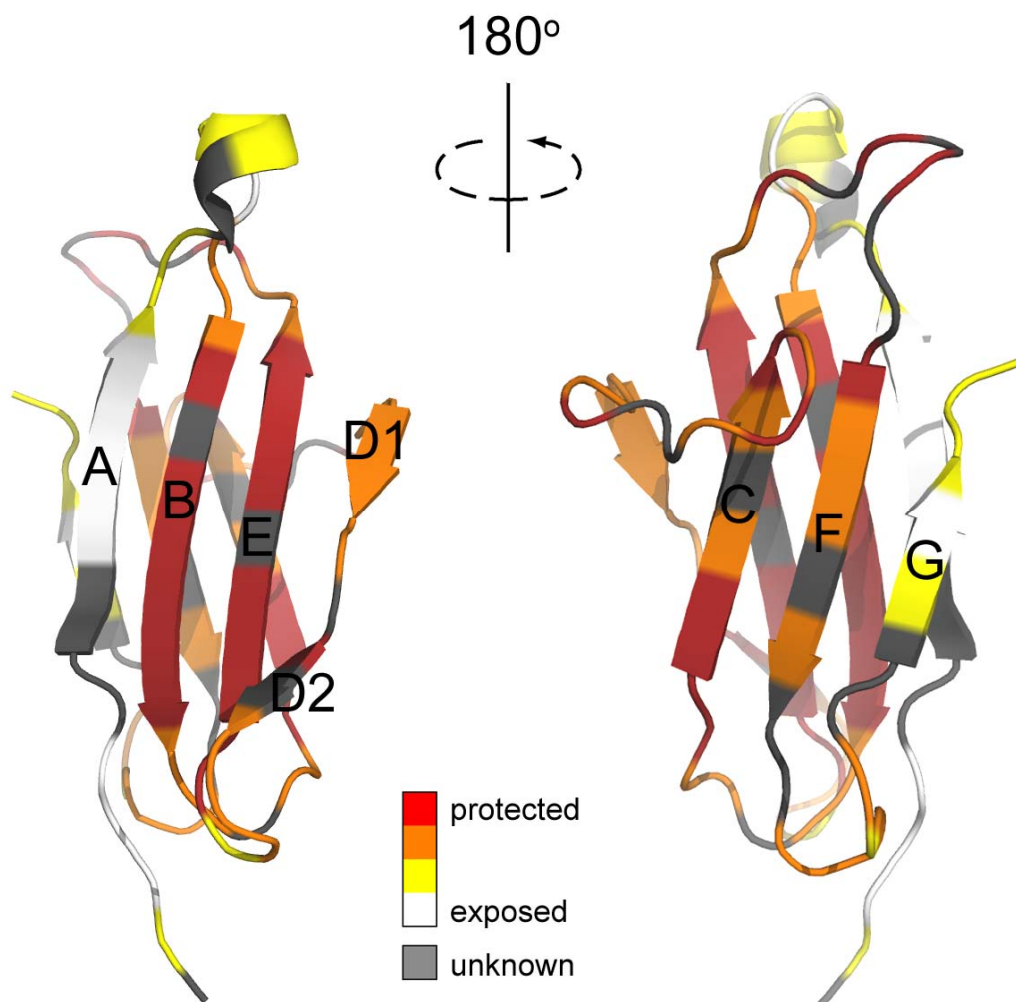


**Figure 4-17.** Mapping of h $\beta$ 2m amyloid fibril solvent protection levels onto the native fold. The  $I_{24h}/I_0$  values were color-coded using the thresholds: 0.5-0.65 (red), 0.65-0.8 (orange), 0.8-1.0 (yellow), >1.0 (white).

In summary, we report that:

- (i) signals of the partially unfolded intermediate ensembles broadened due to conformational exchange can be observed and assigned using direct carbon detected NMR experiments,
- (ii) signal intensities in the  $^{13}\text{C}$ -detected spectra correlate with previously published  $^{15}\text{N}$  transverse relaxation rates,
- (iii) structural differences between the partially unfolded states at pH 2.5 and 3.6 resulting in different fibril morphology are located in the region between residue 22 and the C-terminus; with respect to pH 2.5, the unfolding intermediate at pH 3.6 has increased  $\alpha$ -helical propensities in regions 35-41, 46-49, 54-64 and 80-88, while an increase in propensity for extended structure is found in the C-terminal residues 91-97,
- (iv) flexible regions in amyloid fibrils of h $\beta$ 2m are present at the N- and C-termini and can be observed and sequentially assigned using high-resolution magic angle spinning technique,
- (v) the HR-MAS data correlate well with increased solvent exposure of the N- and C-terminal regions in the H/D exchange experiment,
- (vi) highest protection rates in fibrils of h $\beta$ 2m are found for residues 21-29, 35-38 and 61-78, which reflects the position of aromatic residues in the sequence and provides evidence that hydrophobic clustering might be the mechanism of initiation of h $\beta$ 2m aggregation,
- (vii) a close relationship is seen between the dynamic properties of the partially unfolded intermediate species and the morphology of mature amyloid fibrils of h $\beta$ 2m.

A subsequent solid-state NMR investigation would be helpful to determine the exact number and positions of  $\beta$ -strands within the core of h $\beta$ 2m fibrils and suggest a structural model for these aggregates.

## Literature

- Alexeeva, I., Elliott E. J., Rollins S., Gasparich G. E., Lazar J., Rohwer R. G. (2006). Absence of Spiroplasma or other bacterial 16s rRNA genes in brain tissue of hamsters with scrapie. *J. Clin. Microbiol.* **44**, 91-97.
- Andronesi, O. C., Becker S., Seidel K., Heise H., Young H. S., Baldus M. (2005). Determination of membrane protein structure and dynamics by magic-angle-spinning solid-state NMR spectroscopy. *J. Am. Chem. Soc.* **127**, 12965-12974.
- Anfinsen, C. B. (1973). Principles that govern the folding of protein chains. *Science* **181**, 223-230.
- Baldwin, A. J., Christodoulou J., Barker P. D., Dobson C. M., Lippens G. (2007). Contribution of rotational diffusion to pulsed field gradient diffusion measurements. *J. Chem. Phys.* **127**, 114505.
- Banci, L., Bertini I., Cantini F., Felli I. C., Gonnelli L., Hadjiliadis N., Pierattelli R., Rosato A., Voulgaris P. (2006). The Atx1-Ccc2 complex is a metal-mediated protein-protein interaction. *Nat Chem Biol* **2**, 367-368.
- Bastian, F. O. (2005). Spiroplasma as a candidate agent for the transmissible spongiform encephalopathies. *J. Neuropathol. Exp. Neurol.* **64**, 833-838.
- Bastian, F. O., Sanders D. E., Forbes W. A., Hagius S. D., Walker J. V., Henk W. G., Enright F. M., Elzer P. H. (2007). Spiroplasma spp. from transmissible spongiform encephalopathy brains or ticks induce spongiform encephalopathy in ruminants. *J. Med. Microbiol.* **56**, 1235-1242.
- Becker, J. W., Reeke G. N., Jr. (1985). Three-dimensional structure of beta 2-microglobulin. *Proc. Natl. Acad. Sci. U. S. A.* **82**, 4225-4229.
- Beringue, V., Vilotte J. L., Laude H. (2008). Prion agent diversity and species barrier. *Vet. Res.* **39**, 47.
- Bermel, W., Bertini I., Felli I. C., Lee Y. M., Luchinat C., Pierattelli R. (2006). Protonless NMR experiments for sequence-specific assignment of backbone nuclei in unfolded proteins. *J. Am. Chem. Soc.* **128**, 3918-3919.
- Bermel, W., Bertini I., Duma L., Felli I. C., Emsley L., Pierattelli R., Vasos P. R. (2005). Complete assignment of heteronuclear protein resonances by protonless NMR spectroscopy. *Angew. Chem. Int. Ed. Engl.* **44**, 3089-3092.
- Bernoulli, C., Siegfried J., Baumgartner G., Regli F., Rabinowicz T., Gajdusek D. C., Gibbs C. J., Jr. (1977). Danger of accidental person-to-person transmission of Creutzfeldt-Jakob disease by surgery. *Lancet* **1**, 478-479.
- Bertini, I., Jimenez B., Pierattelli R., Wedd A. G., Xiao Z. (2008). Protonless <sup>13</sup>C direct detection NMR: characterization of the 37 kDa trimeric protein CutA1. *Proteins* **70**, 1196-1205.
- Bertini, I., Duma L., Felli I. C., Fey M., Luchinat C., Pierattelli R., Vasos P. R. (2004). A Heteronuclear Direct-Detection NMR Spectroscopy Experiment for Protein-Backbone Assignment. *Angew. Chem. Int. Ed. Engl.* **43**.
- Billette de Villemeur, T., Deslys J. P., Pradel A., Soubrie C., Alperovitch A., Tardieu M., Chaussain J. L., Hauw J. J., Dormont D., Ruberg M., Agid Y. (1996). Creutzfeldt-Jakob disease from contaminated growth hormone extracts in France. *Neurology* **47**, 690-695.
- Blaise, B. J., Giacomotto J., Elena B., Dumas M. E., Toulhoat P., Segalat L., Emsley L. (2007). Metabotyping of Caenorhabditis elegans reveals latent phenotypes. *Proc. Natl. Acad. Sci. U. S. A.* **104**, 19808-19812.

- Bolton, D. C., McKinley M. P., Prusiner S. B. (1982). Identification of a protein that purifies with the scrapie prion. *Science* **218**, 1309-1311.
- Brockwell, D. J., Radford S. E. (2007). Intermediates: ubiquitous species on folding energy landscapes? *Curr. Opin. Struct. Biol.* **17**, 30-37.
- Brown, P., Gajdusek D. C. (1991). The human spongiform encephalopathies: kuru, Creutzfeldt-Jakob disease, and the Gerstmann-Straussler-Scheinker syndrome. *Curr. Top. Microbiol. Immunol.* **172**, 1-20.
- Brown, P., Preece M. A., Will R. G. (1992). "Friendly fire" in medicine: hormones, homografts, and Creutzfeldt-Jakob disease. *Lancet* **340**, 24-27.
- Brown, P., Cervenakova L., Goldfarb L. G., McCombie W. R., Rubenstein R., Will R. G., Pocchiari M., Martinez-Lage J. F., Scalici C., Masullo C., et al. (1994). Iatrogenic Creutzfeldt-Jakob disease: an example of the interplay between ancient genes and modern medicine. *Neurology* **44**, 291-293.
- Browning, S. R., Mason G. L., Seward T., Green M., Eliason G. A., Mathiason C., Miller M. W., Williams E. S., Hoover E., Telling G. C. (2004). Transmission of prions from mule deer and elk with chronic wasting disease to transgenic mice expressing cervid PrP. *J. Virol.* **78**, 13345-13350.
- Bucciantini, M., Giannoni E., Chiti F., Baroni F., Formigli L., Zurdo J., Taddei N., Ramponi G., Dobson C. M., Stefani M. (2002). Inherent toxicity of aggregates implies a common mechanism for protein misfolding diseases. *Nature* **416**, 507-511.
- Bueler, H., Aguzzi A., Sailer A., Greiner R. A., Autenried P., Aguet M., Weissmann C. (1993). Mice devoid of PrP are resistant to scrapie. *Cell* **73**, 1339-1347.
- Caillet-Saguy, C., Delepierre M., Lecroisey A., Bertini I., Piccioli M., Turano P. (2006). Direct-detected <sup>13</sup>C NMR to investigate the iron(III) hemophore HasA. *J. Am. Chem. Soc.* **128**, 150-158.
- Casey, T. T., Stone W. J., DiRaimondo C. R., Brantley B. D., DiRaimondo C. V., Gorevic P. D., Page D. L. (1986). Tumoral amyloidosis of bone of beta 2-microglobulin origin in association with long-term hemodialysis: a new type of amyloid disease. *Hum. Pathol.* **17**, 731-738.
- Caughey, B., Chesebro B. (1997). Prion protein and the transmissible spongiform encephalopathies. *Trends Cell Biol.* **7**, 56-62.
- Caughey, B., Kocisko D. A., Raymond G. J., Lansbury P. T., Jr. (1995). Aggregates of scrapie-associated prion protein induce the cell-free conversion of protease-sensitive prion protein to the protease-resistant state. *Chem. Biol.* **2**, 807-817.
- Caughey, B. W., Dong A., Bhat K. S., Ernst D., Hayes S. F., Caughey W. S. (1991). Secondary structure analysis of the scrapie-associated protein PrP 27-30 in water by infrared spectroscopy. *Biochemistry (Mosc).* **30**, 7672-7680.
- Chapman, J., Brown P., Goldfarb L. G., Arlazoroff A., Gajdusek D. C., Korczyn A. D. (1993). Clinical heterogeneity and unusual presentations of Creutzfeldt-Jakob disease in Jewish patients with the PRNP codon 200 mutation. *J. Neurol. Neurosurg. Psychiatry* **56**, 1109-1112.
- Chesebro, B. (2003). Introduction to the transmissible spongiform encephalopathies or prion diseases. *Br. Med. Bull.* **66**, 1-20.
- Chiba, T., Hagihara Y., Higurashi T., Hasegawa K., Naiki H., Goto Y. (2003). Amyloid fibril formation in the context of full-length protein: effects of proline mutations on the amyloid fibril formation of beta2-microglobulin. *J. Biol. Chem.* **278**, 47016-47024.
- Chiti, F., Webster P., Taddei N., Clark A., Stefani M., Ramponi G., Dobson C. M. (1999). Designing conditions for in vitro formation of amyloid protofilaments and fibrils. *Proc. Natl. Acad. Sci. U. S. A.* **96**, 3590-3594.



- Chiti, F., De Lorenzi E., Grossi S., Mangione P., Giorgetti S., Caccialanza G., Dobson C. M., Merlini G., Ramponi G., Bellotti V. (2001). A partially structured species of beta 2-microglobulin is significantly populated under physiological conditions and involved in fibrillogenesis. *J. Biol. Chem.* **276**, 46714-46721.
- Collinge, J., Palmer M. S., Dryden A. J. (1991). Genetic predisposition to iatrogenic Creutzfeldt-Jakob disease. *Lancet* **337**, 1441-1442.
- Creutzfeldt, H. G. (1920). Über eine eigenartige herdförmige Erkrankung des Zentralnervensystems. *Z. Ges. Neurol. Psychiatr.* **57**, 1-18.
- Crick, F. (1970). Central dogma of molecular biology. *Nature* **227**, 561-563.
- Csermely, P. (2001). Chaperone overload is a possible contributor to 'civilization diseases'. *Trends Genet.* **17**, 701-704.
- Csizmok, V., Felli I. C., Tompa P., Banci L., Bertini I. (2008). Structural and dynamic characterization of intrinsically disordered human securin by NMR spectroscopy. *J. Am. Chem. Soc.* **130**, 16873-16879.
- Delaglio, F., Grzesiek S., Vuister G. W., Zhu G., Pfeifer J., Bax A. (1995). NMRPipe: a multidimensional spectral processing system based on UNIX pipes. *J. Biomol. NMR* **6**, 277-293.
- DeMarco, M. L., Daggett V. (2004). From conversion to aggregation: protofibril formation of the prion protein. *Proc. Natl. Acad. Sci. U. S. A.* **101**, 2293-2298.
- DeMarco, M. L., Daggett V. (2007). Molecular mechanism for low pH triggered misfolding of the human prion protein. *Biochemistry (Mosc.)* **46**, 3045-3054.
- Dill, K. A., Chan H. S. (1997). From Levinthal to pathways to funnels. *Nat. Struct. Biol.* **4**, 10-19.
- Dobson, C. M. (1999). Protein misfolding, evolution and disease. *Trends Biochem. Sci.* **24**, 329-332.
- Dobson, C. M. (2001). The structural basis of protein folding and its links with human disease. *Philos. Trans. R. Soc. Lond. B. Biol. Sci.* **356**, 133-145.
- Dobson, C. M. (2003). Protein folding and misfolding. *Nature* **426**, 884-890.
- Duffy, P., Wolf J., Collins G., DeVoe A. G., Streeten B., Cowen D. (1974). Letter: Possible person-to-person transmission of Creutzfeldt-Jakob disease. *N. Engl. J. Med.* **290**, 692-693.
- Dyson, H. J., Wright P. E. (1998). Equilibrium NMR studies of unfolded and partially folded proteins. *Nat. Struct. Biol.* **5 Suppl**, 499-503.
- Eakin, C. M., Berman A. J., Miranker A. D. (2006). A native to amyloidogenic transition regulated by a backbone trigger. *Nat Struct Mol Biol* **13**, 202-208.
- Elghetany, M. T., Saleem A. (1988). Methods for staining amyloid in tissues: a review. *Stain Technol.* **63**, 201-212.
- Esposito, G., Michelutti R., Verdone G., Viglino P., Hernandez H., Robinson C. V., Amoresano A., Dal Piaz F., Monti M., Pucci P., Mangione P., Stoppini M., Merlini G., Ferri G., Bellotti V. (2000). Removal of the N-terminal hexapeptide from human beta2-microglobulin facilitates protein aggregation and fibril formation. *Protein Sci.* **9**, 831-845.
- Finckh, U., Muller-Thomsen T., Mann U., Eggers C., Marksteiner J., Meins W., Binetti G., Alberici A., Hock C., Nitsch R. M., Gal A. (2000). High prevalence of pathogenic mutations in patients with early-onset dementia detected by sequence analyses of four different genes. *Am. J. Hum. Genet.* **66**, 110-117.
- Floege, J., Ehlerding G. (1996). Beta-2-microglobulin-associated amyloidosis. *Nephron* **72**, 9-26.
- Fradkin, J. E., Schonberger L. B., Mills J. L., Gunn W. J., Piper J. M., Wysowski D. K., Thomson R., Durako S., Brown P. (1991). Creutzfeldt-Jakob disease in pituitary growth hormone recipients in the United States. *JAMA* **265**, 880-884.

- Gajdusek, D. C. (1977). Unconventional viruses and the origin and disappearance of kuru. *Science* **197**, 943-960.
- Gajdusek, D. C., Zigas V. (1957). Degenerative disease of the central nervous system in New Guinea; the endemic occurrence of kuru in the native population. *N. Engl. J. Med.* **257**, 974-978.
- Gajdusek, D. C., Gibbs C. J., Alpers M. (1966). Experimental transmission of a Kuru-like syndrome to chimpanzees. *Nature* **209**, 794-796.
- Gasset, M., Baldwin M. A., Fletterick R. J., Prusiner S. B. (1993). Perturbation of the secondary structure of the scrapie prion protein under conditions that alter infectivity. *Proc. Natl. Acad. Sci. U. S. A.* **90**, 1-5.
- Gejyo, F., Yamada T., Odani S., Nakagawa Y., Arakawa M., Kunitomo T., Kataoka H., Suzuki M., Hirasawa Y., Shirahama T., et al. (1985). A new form of amyloid protein associated with chronic hemodialysis was identified as beta 2-microglobulin. *Biochem. Biophys. Res. Commun.* **129**, 701-706.
- Gerstmann, J., Sträussler E., Scheinker I. (1936). Über eine eigenartige hereditär-familiäre Erkrankung des Zentralnervensystems. Zugleich ein Beitrag zur Frage des vorzeitigen lokalen Alterns. *Z. Ges. Neurol. Psychiatr.* **154**, 736-762.
- Ghetti, B., Piccardo P., Spillantini M. G., Ichimiya Y., Porro M., Perini F., Kitamoto T., Tateishi J., Seiler C., Frangione B., Bugiani O., Giaccone G., Prelli F., Goedert M., Dlouhy S. R., Tagliavini F. (1996). Vascular variant of prion protein cerebral amyloidosis with tau-positive neurofibrillary tangles: the phenotype of the stop codon 145 mutation in PRNP. *Proc. Natl. Acad. Sci. U. S. A.* **93**, 744-748.
- Gibbs, C. J., Jr., Gajdusek D. C. (1973). Experimental subacute spongiform virus encephalopathies in primates and other laboratory animals. *Science* **182**, 67-68.
- Goddard, T. D., Kneller D. G. SPARKY 3, University of California, San Francisco.
- Goldfarb, L. G., Petersen R. B., Tabaton M., Brown P., LeBlanc A. C., Montagna P., Cortelli P., Julien J., Vital C., Pendelbury W. W., et al. (1992). Fatal familial insomnia and familial Creutzfeldt-Jakob disease: disease phenotype determined by a DNA polymorphism. *Science* **258**, 806-808.
- Govaerts, C., Wille H., Prusiner S. B., Cohen F. E. (2004). Evidence for assembly of prions with left-handed beta-helices into trimers. *Proc. Natl. Acad. Sci. U. S. A.* **101**, 8342-8347.
- Griffith, J. S. (1967). Self-replication and scrapie. *Nature* **215**, 1043-1044.
- Guijarro, J. I., Sunde M., Jones J. A., Campbell I. D., Dobson C. M. (1998). Amyloid fibril formation by an SH3 domain. *Proc. Natl. Acad. Sci. U. S. A.* **95**, 4224-4228.
- Hadlow, W. J. (1959). Scrapie and kuru. *Lancet* **2**, 289-290.
- Harper, J. D., Wong S. S., Lieber C. M., Lansbury P. T. (1997). Observation of metastable Abeta amyloid protofibrils by atomic force microscopy. *Chem. Biol.* **4**, 119-125.
- Harries-Jones, R., Knight R., Will R. G., Cousens S., Smith P. G., Matthews W. B. (1988). Creutzfeldt-Jakob disease in England and Wales, 1980-1984: a case-control study of potential risk factors. *J. Neurol. Neurosurg. Psychiatry* **51**, 1113-1119.
- Hasegawa, K., Tsutsumi-Yasuhara S., Ookoshi T., Ohhashi Y., Kimura H., Takahashi N., Yoshida H., Miyazaki R., Goto Y., Naiki H. (2008). Growth of beta(2)-microglobulin-related amyloid fibrils by non-esterified fatty acids at a neutral pH. *Biochem. J.* **416**, 307-315.
- Hegde, R. S., Rane N. S. (2003). Prion protein trafficking and the development of neurodegeneration. *Trends Neurosci.* **26**, 337-339.
- Hegde, R. S., Mastrianni J. A., Scott M. R., DeFea K. A., Tremblay P., Torchia M., DeArmond S. J., Prusiner S. B., Lingappa V. R. (1998). A transmembrane form of the prion protein in neurodegenerative disease. *Science* **279**, 827-834.

- Heise, H. (2008). Solid-state NMR spectroscopy of amyloid proteins. *ChemBiochem* **9**, 179-189.
- Helmus, J. J., Surewicz K., Nadaud P. S., Surewicz W. K., Jaroniec C. P. (2008). Molecular conformation and dynamics of the Y145Stop variant of human prion protein in amyloid fibrils. *Proc. Natl. Acad. Sci. U. S. A.* **105**, 6284-6289.
- Hill, A. F., Antoniou M., Collinge J. (1999). Protease-resistant prion protein produced in vitro lacks detectable infectivity. *J. Gen. Virol.* **80 ( Pt 1)**, 11-14.
- Hill, A. F., Desbruslais M., Joiner S., Sidle K. C., Gowland I., Collinge J., Doey L. J., Lantos P. (1997). The same prion strain causes vCJD and BSE. *Nature* **389**, 448-450, 526.
- Holmes, E., Tsang T. M., Tabrizi S. J. (2006). The application of NMR-based metabonomics in neurological disorders. *NeuroRx* **3**, 358-372.
- Holscher, C., Bach U. C., Dobberstein B. (2001). Prion protein contains a second endoplasmic reticulum targeting signal sequence located at its C terminus. *J. Biol. Chem.* **276**, 13388-13394.
- Horwich, A. (2002). Protein aggregation in disease: a role for folding intermediates forming specific multimeric interactions. *J. Clin. Invest.* **110**, 1221-1232.
- Hoshino, M., Katou H., Yamaguchi K., Goto Y. (2007). Dimethylsulfoxide-quenched hydrogen/deuterium exchange method to study amyloid fibril structure. *Biochim. Biophys. Acta* **1768**, 1886-1899.
- Hoshino, M., Katou H., Hagihara Y., Hasegawa K., Naiki H., Goto Y. (2002). Mapping the core of the beta(2)-microglobulin amyloid fibril by H/D exchange. *Nat. Struct. Biol.* **9**, 332-336.
- Huang, Z., Prusiner S. B., Cohen F. E. (1995). Scrapie prions: a three-dimensional model of an infectious fragment. *Fold. Des.* **1**, 13-19.
- Ippel, J. H., Olofsson A., Schleucher J., Lundgren E., Wijmenga S. S. (2002). Probing solvent accessibility of amyloid fibrils by solution NMR spectroscopy. *Proc. Natl. Acad. Sci. U. S. A.* **99**, 8648-8653.
- Ivanova, M. I., Gingery M., Whitson L. J., Eisenberg D. (2003). Role of the C-terminal 28 residues of beta2-microglobulin in amyloid fibril formation. *Biochemistry (Mosc).* **42**, 13536-13540.
- Iwata, K., Fujiwara T., Matsuki Y., Akutsu H., Takahashi S., Naiki H., Goto Y. (2006). 3D structure of amyloid protofilaments of beta2-microglobulin fragment probed by solid-state NMR. *Proc. Natl. Acad. Sci. U. S. A.* **103**, 18119-18124.
- Jack, E., Newsome M., Stockley P. G., Radford S. E., Middleton D. A. (2006). The organization of aromatic side groups in an amyloid fibril probed by solid-state <sup>2</sup>H and <sup>19</sup>F NMR spectroscopy. *J. Am. Chem. Soc.* **128**, 8098-8099.
- Jacobson, D. R., Buxbaum J. N. (1991). Genetic aspects of amyloidosis. *Adv. Hum. Genet.* **20**, 69-123, 309-111.
- Jahn, T. R., Radford S. E. (2005). The Yin and Yang of protein folding. *Febs J* **272**, 5962-5970.
- Jahn, T. R., Tennent G. A., Radford S. E. (2008). A common beta-sheet architecture underlies in vitro and in vivo beta2-microglobulin amyloid fibrils. *J. Biol. Chem.* **283**, 17279-17286.
- Jahn, T. R., Parker M. J., Homans S. W., Radford S. E. (2006). Amyloid formation under physiological conditions proceeds via a native-like folding intermediate. *Nat Struct Mol Biol* **13**, 195-201.
- Jakob, A. M. (1921). Über eigenartige Erkrankungen des Zentralnervensystems mit bemerkenswertem anatomischen Befunde (spastische Pseudosklerose-Encephalomyelopathie mit disseminierten Degenerationsherden). *Z. Ges. Neurol. Psychiatr.* **64**, 147-228.

- Jaroniec, C. P., MacPhee C. E., Bajaj V. S., McMahon M. T., Dobson C. M., Griffin R. G. (2004). High-resolution molecular structure of a peptide in an amyloid fibril determined by magic angle spinning NMR spectroscopy. *Proc. Natl. Acad. Sci. U. S. A.* **101**, 711-716.
- Jones, E. M., Surewicz W. K. (2005). Fibril conformation as the basis of species- and strain-dependent seeding specificity of mammalian prion amyloids. *Cell* **121**, 63-72.
- Jones, S., Manning J., Kad N. M., Radford S. E. (2003). Amyloid-forming peptides from beta2-microglobulin-Insights into the mechanism of fibril formation in vitro. *J. Mol. Biol.* **325**, 249-257.
- Kad, N. M., Thomson N. H., Smith D. P., Smith D. A., Radford S. E. (2001). Beta(2)-microglobulin and its deamidated variant, N17D form amyloid fibrils with a range of morphologies in vitro. *J. Mol. Biol.* **313**, 559-571.
- Kaneko, K., Vey M., Scott M., Pilkuhn S., Cohen F. E., Prusiner S. B. (1997). COOH-terminal sequence of the cellular prion protein directs subcellular trafficking and controls conversion into the scrapie isoform. *Proc. Natl. Acad. Sci. U. S. A.* **94**, 2333-2338.
- Katou, H., Kanno T., Hoshino M., Hagihara Y., Tanaka H., Kawai T., Hasegawa K., Naiki H., Goto Y. (2002). The role of disulfide bond in the amyloidogenic state of beta(2)-microglobulin studied by heteronuclear NMR. *Protein Sci.* **11**, 2218-2229.
- Kelly, J. W. (2000). Mechanisms of amyloidogenesis. *Nat. Struct. Biol.* **7**, 824-826.
- Kelly, J. W., Lansbury P. T. (1994). A chemical approach to elucidate the mechanism of transthyretin and beta-protein amyloid fibril formation. *Amyloid Int. J. Exp. Clin. Invest.* **1**, 186-205.
- Khan, A. R., Baker B. M., Ghosh P., Biddison W. E., Wiley D. C. (2000). The structure and stability of an HLA-A\*0201/octameric tax peptide complex with an empty conserved peptide-N-terminal binding site. *J. Immunol.* **164**, 6398-6405.
- Kheterpal, I., Zhou S., Cook K. D., Wetzel R. (2000). Abeta amyloid fibrils possess a core structure highly resistant to hydrogen exchange. *Proc. Natl. Acad. Sci. U. S. A.* **97**, 13597-13601.
- Kisilevsky, R. (1983). Amyloidosis: a familiar problem in the light of current pathogenetic developments. *Lab. Invest.* **49**, 381-390.
- Kisilevsky, R. (2000). Amyloids: tombstones or triggers? *Nat. Med.* **6**, 633-634.
- Klatzo, I., Gajdusek D. C., Zigas V. (1959). Pathology of Kuru. *Lab. Invest.* **8**, 799-847.
- Klein, W. L., Krafft G. A., Finch C. E. (2001). Targeting small Abeta oligomers: the solution to an Alzheimer's disease conundrum? *Trends Neurosci.* **24**, 219-224.
- Kocisko, D. A., Lansbury P. T., Jr., Caughey B. (1996). Partial unfolding and refolding of scrapie-associated prion protein: evidence for a critical 16-kDa C-terminal domain. *Biochemistry (Mosc).* **35**, 13434-13442.
- Kovacs, G. G., Head M. W., Bunn T., Laszlo L., Will R. G., Ironside J. W. (2000). Clinicopathological phenotype of codon 129 valine homozygote sporadic Creutzfeldt-Jakob disease. *Neuropathol. Appl. Neurobiol.* **26**, 463-472.
- Kozhukh, G. V., Hagihara Y., Kawakami T., Hasegawa K., Naiki H., Goto Y. (2002). Investigation of a peptide responsible for amyloid fibril formation of beta 2-microglobulin by achromobacter protease I. *J. Biol. Chem.* **277**, 1310-1315.
- Kremer, W., Kachel N., Kuwata K., Akasaka K., Kalbitzer H. R. (2007). Species-specific differences in the intermediate states of human and Syrian hamster prion protein detected by high pressure NMR spectroscopy. *J. Biol. Chem.* **282**, 22689-22698.
- Kretzschmar, H. A., Prusiner S. B., Stowring L. E., DeArmond S. J. (1986). Scrapie prion proteins are synthesized in neurons. *Am. J. Pathol.* **122**, 1-5.
- Kundu, B., Maiti N. R., Jones E. M., Surewicz K. A., Vanik D. L., Surewicz W. K. (2003). Nucleation-dependent conformational conversion of the Y145Stop variant of human prion

- protein: structural clues for prion propagation. *Proc. Natl. Acad. Sci. U. S. A.* **100**, 12069-12074.
- Kuwata, K., Matumoto T., Cheng H., Nagayama K., James T. L., Roder H. (2003). NMR-detected hydrogen exchange and molecular dynamics simulations provide structural insight into fibril formation of prion protein fragment 106-126. *Proc. Natl. Acad. Sci. U. S. A.* **100**, 14790-14795.
- LaFauci, G., Carp R. I., Meeker H. C., Ye X., Kim J. I., Natelli M., Cedeno M., Petersen R. B., Kascsak R., Rubenstein R. (2006). Passage of chronic wasting disease prion into transgenic mice expressing Rocky Mountain elk (*Cervus elaphus nelsoni*) PrPC. *J. Gen. Virol.* **87**, 3773-3780.
- Lambert, M. P., Barlow A. K., Chromy B. A., Edwards C., Freed R., Liosatos M., Morgan T. E., Rozovsky I., Trommer B., Viola K. L., Wals P., Zhang C., Finch C. E., Krafft G. A., Klein W. L. (1998). Diffusible, nonfibrillar ligands derived from A $\beta$ 1-42 are potent central nervous system neurotoxins. *Proc. Natl. Acad. Sci. U. S. A.* **95**, 6448-6453.
- Lazo, N. D., Downing D. T. (1997). Beta-helical fibrils from a model peptide. *Biochem. Biophys. Res. Commun.* **235**, 675-679.
- Legname, G., Baskakov I. V., Nguyen H. O., Riesner D., Cohen F. E., DeArmond S. J., Prusiner S. B. (2004). Synthetic mammalian prions. *Science* **305**, 673-676.
- Linke, R. P., Hampl H., Bartel-Schwarze S., Eulitz M. (1987). Beta 2-microglobulin, different fragments and polymers thereof in synovial amyloid in long-term hemodialysis. *Biol. Chem. Hoppe. Seyler* **368**, 137-144.
- Linke, R. P., Schaeffer J., Gielow P., Lindner P., Lottspeich F., Pluckthun A., Weiss E. H. (2000). Production of recombinant human beta2-microglobulin for scintigraphic diagnosis of amyloidosis in uremia and hemodialysis. *Eur. J. Biochem.* **267**, 627-633.
- Lu, X., Wintrode P. L., Surewicz W. K. (2007). Beta-sheet core of human prion protein amyloid fibrils as determined by hydrogen/deuterium exchange. *Proc. Natl. Acad. Sci. U. S. A.* **104**, 1510-1515.
- MacDonald, S. T., Sutherland K., Ironside J. W. (1996). Prion protein genotype and pathological phenotype studies in sporadic Creutzfeldt-Jakob disease. *Neuropathol. Appl. Neurobiol.* **22**, 285-292.
- Madden, D. R., Garboczi D. N., Wiley D. C. (1993). The antigenic identity of peptide-MHC complexes: a comparison of the conformations of five viral peptides presented by HLA-A2. *Cell* **75**, 693-708.
- Makarava, N., Lee C. I., Ostapchenko V. G., Baskakov I. V. (2007). Highly promiscuous nature of prion polymerization. *J. Biol. Chem.* **282**, 36704-36713.
- Makin, O. S., Serpell L. C. (2005). Structures for amyloid fibrils. *Febs J* **272**, 5950-5961.
- Masters, C. L., Richardson E. P., Jr. (1978). Subacute spongiform encephalopathy (Creutzfeldt-Jakob disease). The nature and progression of spongiform change. *Brain* **101**, 333-344.
- Masters, C. L., Gajdusek D. C., Gibbs C. J., Jr. (1981). The familial occurrence of Creutzfeldt-Jakob disease and Alzheimer's disease. *Brain* **104**, 535-558.
- McParland, V. J., Kalverda A. P., Homans S. W., Radford S. E. (2002). Structural properties of an amyloid precursor of beta(2)-microglobulin. *Nat. Struct. Biol.* **9**, 326-331.
- McParland, V. J., Kad N. M., Kalverda A. P., Brown A., Kirwin-Jones P., Hunter M. G., Sunde M., Radford S. E. (2000). Partially unfolded states of beta(2)-microglobulin and amyloid formation in vitro. *Biochemistry (Mosc.)* **39**, 8735-8746.
- Merz, P. A., Somerville R. A., Wisniewski H. M., Iqbal K. (1981). Abnormal fibrils from scrapie-infected brain. *Acta Neuropathol* **54**, 63-74.

- Mitrova, E., Mayer V., Jovankovicova V., Slivarichova D., Wsolova L. (2005). Creutzfeldt-Jakob disease risk and PRNP codon 129 polymorphism: necessity to revalue current data. *Eur. J. Neurol.* **12**, 998-1001.
- Moka, D., Vorreuther R., Schicha H., Spraul M., Humpfer E., Lipinski M., Foxall P. J., Nicholson J. K., Lindon J. C. (1998). Biochemical classification of kidney carcinoma biopsy samples using magic-angle-spinning 1H nuclear magnetic resonance spectroscopy. *J. Pharm. Biomed. Anal.* **17**, 125-132.
- Morgan, C. J., Gelfand M., Atreya C., Miranker A. D. (2001). Kidney dialysis-associated amyloidosis: a molecular role for copper in fiber formation. *J. Mol. Biol.* **309**, 339-345.
- Morrissey, M. P., Shakhnovich E. I. (1999). Evidence for the role of PrP(C) helix 1 in the hydrophilic seeding of prion aggregates. *Proc. Natl. Acad. Sci. U. S. A.* **96**, 11293-11298.
- Muramoto, T., Scott M., Cohen F. E., Prusiner S. B. (1996). Recombinant scrapie-like prion protein of 106 amino acids is soluble. *Proc. Natl. Acad. Sci. U. S. A.* **93**, 15457-15462.
- Myers, S. L., Thomson N. H., Radford S. E., Ashcroft A. E. (2006). Investigating the structural properties of amyloid-like fibrils formed in vitro from beta2-microglobulin using limited proteolysis and electrospray ionisation mass spectrometry. *Rapid Commun. Mass Spectrom.* **20**, 1628-1636.
- Naiki, H., Hashimoto N., Suzuki S., Kimura H., Nakakuki K., Gejyo F. (1997). Establishment of a kinetic model of dialysis-related amyloid fibril extension in vitro. *Amyloid Int. J. Exp. Clin. Invest.* **4**, 223-232.
- Nazabal, A., Hornemann S., Aguzzi A., Zenobi R. (2009). Hydrogen/deuterium exchange mass spectrometry identifies two highly protected regions in recombinant full-length prion protein amyloid fibrils. *J. Mass Spectrom.*
- Odani, H., Oyama R., Titani K., Ogawa H., Saito A. (1990). Purification and complete amino acid sequence of novel beta 2-microglobulin. *Biochem. Biophys. Res. Commun.* **168**, 1223-1229.
- Ohashi, K. (2001). Pathogenesis of beta2-microglobulin amyloidosis. *Pathol. Int.* **51**, 1-10.
- Okon, M., Bray P., Vucelic D. (1992). 1H NMR assignments and secondary structure of human beta 2-microglobulin in solution. *Biochemistry (Mosc).* **31**, 8906-8915.
- Olofsson, A., Sauer-Eriksson A. E., Ohman A. (2006). The solvent protection of alzheimer amyloid-beta-(1-42) fibrils as determined by solution NMR spectroscopy. *J. Biol. Chem.* **281**, 477-483.
- Olofsson, A., Ippel J. H., Wijmenga S. S., Lundgren E., Ohman A. (2004). Probing solvent accessibility of transthyretin amyloid by solution NMR spectroscopy. *J. Biol. Chem.* **279**, 5699-5707.
- Ottiger, M., Delaglio F., Bax A. (1998). Measurement of J and dipolar couplings from simplified two-dimensional NMR spectra. *J. Magn. Reson.* **131**, 373-378.
- Owen, F., Poulter M., Collinge J., Crow T. J. (1990). Codon 129 changes in the prion protein gene in Caucasians. *Am. J. Hum. Genet.* **46**, 1215-1216.
- Palmer, M. S., Dryden A. J., Hughes J. T., Collinge J. (1991). Homozygous prion protein genotype predisposes to sporadic Creutzfeldt-Jakob disease. *Nature* **352**, 340-342.
- Pan, K. M., Baldwin M., Nguyen J., Gasset M., Serban A., Groth D., Mehlhorn I., Huang Z., Fletterick R. J., Cohen F. E., et al. (1993). Conversion of alpha-helices into beta-sheets features in the formation of the scrapie prion proteins. *Proc. Natl. Acad. Sci. U. S. A.* **90**, 10962-10966.
- Panchal, S. C., Bhavesh N. S., Hosur R. V. (2001). Improved 3D triple resonance experiments, HNN and HN(C)N, for HN and 15N sequential correlations in (13C, 15N) labeled proteins: application to unfolded proteins. *J. Biomol. NMR* **20**, 135-147.
- Park, S., Saven J. G. (2006). Simulation of pH-dependent edge strand rearrangement in human beta-2 microglobulin. *Protein Sci.* **15**, 200-207.

- Pepys, M. B. (1988) Amyloidosis. In: Immunological diseases (4th ed) (Samter M, Talmage, D. W., Frank, M. M., Austen, K. F., Claman, H. N., ed), pp 631-674. Boston: Little Brown and Co.
- Peretz, D., Williamson R. A., Matsunaga Y., Serban H., Pinilla C., Bastidas R. B., Rozenshteyn R., James T. L., Houghten R. A., Cohen F. E., Prusiner S. B., Burton D. R. (1997). A conformational transition at the N terminus of the prion protein features in formation of the scrapie isoform. *J. Mol. Biol.* **273**, 614-622.
- Perrin, F. (1934). Mouvement brownien d'un ellipsoïde - I. Dispersion diélectrique pour des molécules ellipsoïdales. *J. Phys. Radium* **5**, 497-511.
- Perutz, M. F., Finch J. T., Berriman J., Lesk A. (2002). Amyloid fibers are water-filled nanotubes. *Proc. Natl. Acad. Sci. U. S. A.* **99**, 5591-5595.
- Piazza, R., Pierno M., Iacopini S., Mangione P., Esposito G., Bellotti V. (2006). Microheterogeneity and aggregation in beta2-microglobulin solutions: effects of temperature, pH, and conformational variant addition. *Eur. Biophys. J.* **35**, 439-445.
- Platt, G. W., Routledge K. E., Homans S. W., Radford S. E. (2008). Fibril growth kinetics reveal a region of beta2-microglobulin important for nucleation and elongation of aggregation. *J. Mol. Biol.* **378**, 251-263.
- Platt, G. W., McParland V. J., Kalverda A. P., Homans S. W., Radford S. E. (2005). Dynamics in the unfolded state of beta2-microglobulin studied by NMR. *J. Mol. Biol.* **346**, 279-294.
- Prusiner, S. B. (1982). Novel proteinaceous infectious particles cause scrapie. *Science* **216**, 136-144.
- Prusiner, S. B. (1991). Molecular biology of prion diseases. *Science* **252**, 1515-1522.
- Prusiner, S. B. (1996). Transgenetics of prion diseases. *Curr. Top. Microbiol. Immunol.* **206**, 275-304.
- Prusiner, S. B., McKinley M. P., Bowman K. A., Bolton D. C., Bendheim P. E., Groth D. F., Glenner G. G. (1983). Scrapie prions aggregate to form amyloid-like birefringent rods. *Cell* **35**, 349-358.
- Richardson, J. S., Richardson D. C. (2002). Natural beta-sheet proteins use negative design to avoid edge-to-edge aggregation. *Proc. Natl. Acad. Sci. U. S. A.* **99**, 2754-2759.
- Riek, R., Hornemann S., Wider G., Billeter M., Glockshuber R., Wuthrich K. (1996). NMR structure of the mouse prion protein domain PrP(121-321). *Nature* **382**, 180-182.
- Routledge, K. E., Tartaglia G. G., Platt G. W., Vendruscolo M., Radford S. E. (2009). Competition between Intramolecular and Intermolecular Interactions in an Amyloid-Forming Protein. *J. Mol. Biol.* **389**, 776-786.
- Ruckert, M., Otting G. (2000). Alignment of biological macromolecules in novel nonionic liquid crystalline media for NMR experiments. *J. Am. Chem. Soc.* **122**, 7793-7797.
- Salmona, M., Morbin M., Massignan T., Colombo L., Mazzoleni G., Capobianco R., Diomede L., Thaler F., Mollica L., Musco G., Kourie J. J., Bugiani O., Sharma D., Inouye H., Kirschner D. A., Forloni G., Tagliavini F. (2003). Structural properties of Gerstmann-Straussler-Scheinker disease amyloid protein. *J. Biol. Chem.* **278**, 48146-48153.
- Sarradin, P. (2007) Transgenic models to study human and animal diseases: prion diseases. In: 2nd International Meeting on Rabbit Biotechnology.
- Schwarzinger, S., Kroon G. J., Foss T. R., Chung J., Wright P. E., Dyson H. J. (2001). Sequence-dependent correction of random coil NMR chemical shifts. *J. Am. Chem. Soc.* **123**, 2970-2978.
- Selkoe, D. J. (1997). Alzheimer's disease: genotypes, phenotypes, and treatments. *Science* **275**, 630-631.
- Shen, Y., Vernon R., Baker D., Bax A. (2009). De novo protein structure generation from incomplete chemical shift assignments. *J. Biomol. NMR* **43**, 63-78.

- Shen, Y., Lange O., Delaglio F., Rossi P., Aramini J. M., Liu G., Eletsky A., Wu Y., Singarapu K. K., Lemak A., Ignatchenko A., Arrowsmith C. H., Szyperski T., Montelione G. T., Baker D., Bax A. (2008). Consistent blind protein structure generation from NMR chemical shift data. *Proc. Natl. Acad. Sci. U. S. A.* **105**, 4685-4690.
- Siemer, A. B., Arnold A. A., Ritter C., Westfeld T., Ernst M., Riek R., Meier B. H. (2006). Observation of highly flexible residues in amyloid fibrils of the HET-s prion. *J. Am. Chem. Soc.* **128**, 13224-13228.
- Sigurdsson, B. (1954). Observations on three slow infections of sheep. *Br. Vet. J.* **110**, 341-354.
- Skora, L., Cho M. K., Kim H. Y., Becker S., Fernandez C. O., Blackledge M., Zweckstetter M. (2006). Charge-induced molecular alignment of intrinsically disordered proteins. *Angew. Chem. Int. Ed. Engl.* **45**, 7012-7015.
- Smith, D. P., Jones S., Serpell L. C., Sunde M., Radford S. E. (2003). A systematic investigation into the effect of protein destabilisation on beta 2-microglobulin amyloid formation. *J. Mol. Biol.* **330**, 943-954.
- Snyder, S. W., Ladrer U. S., Wade W. S., Wang G. T., Barrett L. W., Matayoshi E. D., Huffaker H. J., Krafft G. A., Holzman T. F. (1994). Amyloid-beta aggregation: selective inhibition of aggregation in mixtures of amyloid with different chain lengths. *Biophys. J.* **67**, 1216-1228.
- Speare, J. O., Rush T. S., 3rd, Bloom M. E., Caughey B. (2003). The role of helix 1 aspartates and salt bridges in the stability and conversion of prion protein. *J. Biol. Chem.* **278**, 12522-12529.
- Stejskal, E. O., Tanner J. E. (1965). Spin Diffusion Measurements: Spin Echoes in the Presence of a Time-Dependent Field Gradient. *J. Chem. Phys.* **42**, 288-292.
- Stoppini, M., Mangione P., Monti M., Giorgetti S., Marchese L., Arcidiaco P., Verga L., Segagni S., Pucci P., Merlini G., Bellotti V. (2005). Proteomics of beta2-microglobulin amyloid fibrils. *Biochim. Biophys. Acta* **1753**, 23-33.
- Swietnicki, W., Morillas M., Chen S. G., Gambetti P., Surewicz W. K. (2000). Aggregation and fibrillization of the recombinant human prion protein huPrP90-231. *Biochemistry (Mosc)*. **39**, 424-431.
- Tan, S. Y., Pepys M. B. (1994). Amyloidosis. *Histopathology* **25**, 403-414.
- Tanford, C., Kawahara K., Lapanje S. (1966). Proteins in 6-M guanidine hydrochloride. Demonstration of random coil behavior. *J. Biol. Chem.* **241**, 1921-1923.
- Tate, A. R., Foxall P. J., Holmes E., Moka D., Spraul M., Nicholson J. K., Lindon J. C. (2000). Distinction between normal and renal cell carcinoma kidney cortical biopsy samples using pattern recognition of (1)H magic angle spinning (MAS) NMR spectra. *NMR Biomed.* **13**, 64-71.
- Thomas, P. J., Qu B. H., Pedersen P. L. (1995). Defective protein folding as a basis of human disease. *Trends Biochem. Sci.* **20**, 456-459.
- Trinh, C. H., Smith D. P., Kalverda A. P., Phillips S. E., Radford S. E. (2002). Crystal structure of monomeric human beta-2-microglobulin reveals clues to its amyloidogenic properties. *Proc. Natl. Acad. Sci. U. S. A.* **99**, 9771-9776.
- Vanik, D. L., Surewicz K. A., Surewicz W. K. (2004). Molecular basis of barriers for interspecies transmissibility of mammalian prions. *Mol. Cell* **14**, 139-145.
- Verdone, G., Corazza A., Viglino P., Pettirossi F., Giorgetti S., Mangione P., Andreola A., Stoppini M., Bellotti V., Esposito G. (2002). The solution structure of human beta2-microglobulin reveals the prodromes of its amyloid transition. *Protein Sci.* **11**, 487-499.
- Vey, M., Pilkuhn S., Wille H., Nixon R., DeArmond S. J., Smart E. J., Anderson R. G., Taraboulos A., Prusiner S. B. (1996). Subcellular colocalization of the cellular and scrapie



- prion proteins in caveolae-like membranous domains. *Proc. Natl. Acad. Sci. U. S. A.* **93**, 14945-14949.
- Walsh, D. M., Klyubin I., Fadeeva J. V., Cullen W. K., Anwyl R., Wolfe M. S., Rowan M. J., Selkoe D. J. (2002). Naturally secreted oligomers of amyloid beta protein potently inhibit hippocampal long-term potentiation in vivo. *Nature* **416**, 535-539.
- Walsh, P., Simonetti K., Sharpe S. (2009). Core structure of amyloid fibrils formed by residues 106-126 of the human prion protein. *Structure* **17**, 417-426.
- Watanabe, Y., Inanami O., Horiuchi M., Hiraoka W., Shimoyama Y., Inagaki F., Kuwabara M. (2006). Identification of pH-sensitive regions in the mouse prion by the cysteine-scanning spin-labeling ESR technique. *Biochem. Biophys. Res. Commun.* **350**, 549-556.
- Watzlawik, J., Skora L., Frense D., Griesinger C., Zweckstetter M., Schulz-Schaeffer W. J., Kramer M. L. (2006). Prion protein helix1 promotes aggregation but is not converted into beta-sheet. *J. Biol. Chem.* **281**, 30242-30250.
- Weissmann, C., Fischer M., Raeber A., Bueler H., Sailer A., Shmerling D., Rulicke T., Brandner S., Aguzzi A. (1996). The use of transgenic mice in the investigation of transmissible spongiform encephalopathies. *Int. J. Exp. Pathol.* **77**, 283-293.
- Welker, E., Raymond L. D., Scheraga H. A., Caughey B. (2002). Intramolecular versus intermolecular disulfide bonds in prion proteins. *J. Biol. Chem.* **277**, 33477-33481.
- Westaway, D., DeArmond S. J., Cayetano-Canlas J., Groth D., Foster D., Yang S. L., Torchia M., Carlson G. A., Prusiner S. B. (1994). Degeneration of skeletal muscle, peripheral nerves, and the central nervous system in transgenic mice overexpressing wild-type prion proteins. *Cell* **76**, 117-129.
- Will, R. G. (1993). Epidemiology of Creutzfeldt-Jakob disease. *Br. Med. Bull.* **49**, 960-970.
- Will, R. G., Ironside J. W., Zeidler M., Cousens S. N., Estibeiro K., Alperovitch A., Poser S., Pocchiari M., Hofman A., Smith P. G. (1996). A new variant of Creutzfeldt-Jakob disease in the UK. *Lancet* **347**, 921-925.
- Wille, H., Michelitsch M. D., Guenebaut V., Supattapone S., Serban A., Cohen F. E., Agard D. A., Prusiner S. B. (2002). Structural studies of the scrapie prion protein by electron crystallography. *Proc. Natl. Acad. Sci. U. S. A.* **99**, 3563-3568.
- Williams, A. D., Portelius E., Kheterpal I., Guo J. T., Cook K. D., Xu Y., Wetzel R. (2004). Mapping abeta amyloid fibril secondary structure using scanning proline mutagenesis. *J. Mol. Biol.* **335**, 833-842.
- Wiltfang, J., Esselmann H., Cupers P., Neumann M., Kretzschmar H., Beyermann M., Schleuder D., Jahn H., Ruther E., Kornhuber J., Annaert W., De Strooper B., Saftig P. (2001). Elevation of beta-amyloid peptide 2-42 in sporadic and familial Alzheimer's disease and its generation in PS1 knockout cells. *J. Biol. Chem.* **276**, 42645-42657.
- Windl, O., Buchholz M., Neubauer A., Schulz-Schaeffer W., Groschup M., Walter S., Arendt S., Neumann M., Voss A. K., Kretzschmar H. A. (2005). Breaking an absolute species barrier: transgenic mice expressing the mink PrP gene are susceptible to transmissible mink encephalopathy. *J. Virol.* **79**, 14971-14975.
- Wishart, D. S., Sykes B. D. (1994). Chemical shifts as a tool for structure determination. *Methods Enzymol.* **239**, 363-392.
- Wishart, D. S., Bigam C. G., Holm A., Hodges R. S., Sykes B. D. (1995). <sup>1</sup>H, <sup>13</sup>C and <sup>15</sup>N random coil NMR chemical shifts of the common amino acids. I. Investigations of nearest-neighbor effects. *J. Biomol. NMR* **5**, 67-81.
- Wolynes, P. G., Onuchic J. N., Thirumalai D. (1995). Navigating the folding routes. *Science* **267**, 1619-1620.
- Wu, D., Chen A., Johnson C. S. (1995). An improved diffusion-ordered spectroscopy experiment incorporating bipolar gradient pulses. *J. Magn. Reson. A* **115**, 260-264.

- Yamaguchi, I., Hasegawa K., Naiki H., Mitsu T., Matuo Y., Gejyo F. (2001). Extension of A beta2M amyloid fibrils with recombinant human beta2-microglobulin. *Amyloid* **8**, 30-40.
- Yong, W., Lomakin A., Kirkitadze M. D., Teplow D. B., Chen S. H., Benedek G. B. (2002). Structure determination of micelle-like intermediates in amyloid beta -protein fibril assembly by using small angle neutron scattering. *Proc. Natl. Acad. Sci. U. S. A.* **99**, 150-154.
- Zahn, R., Liu A., Luhrs T., Riek R., von Schroetter C., Lopez Garcia F., Billeter M., Calzolari L., Wider G., Wuthrich K. (2000). NMR solution structure of the human prion protein. *Proc. Natl. Acad. Sci. U. S. A.* **97**, 145-150.

## Appendix A. Charge-induced molecular alignment of intrinsically disordered proteins

In form of a reprint, a study concerning the effects of electrostatic interactions on molecular alignment of intrinsically disordered proteins, is presented here.

Intrinsically disordered or unstructured proteins (IUPs) play key roles in normal and pathological biochemical processes. Despite their importance for function, this category of proteins remains beyond the reach of classical structural biology because of their inherent conformational heterogeneity. Recently, it was shown that the local conformational behavior of IUPs can be described using a simple model based on residue-specific Phi/Psi propensities and that residual dipolar couplings (RDCs) observed in IUPs can be predicted from this model assuming a steric interaction between the protein and the alignment medium (1, 2). In addition, we recently showed that RDCs are also sensitive detectors of transient long-range interactions in IUPs (3).

It is demonstrated here, that the assumption of a steric-like interaction (4) between intrinsically disordered proteins and the alignment medium is only valid in case of uncharged alignment media. Alignment of intrinsically disordered proteins in charged media depends critically on electrostatic interactions, especially in charged regions of the protein, scales with ionic strength of the solution and can be predicted using a simplified electrostatic model (5). This has important consequences for the RDC-based interpretation of the structure and dynamics of the unstructured state.

1. Bernado P, Blanchard L, Timmins P, Marion D, Ruigrok RW, Blackledge M. *Proc. Natl. Acad. Sci. USA*. **2005**, *102*, 17002-17007
2. Jha AK, Colubri A, Freed KF, Sosnick TR. *Proc. Natl. Acad. Sci. USA*. **2005**, *102*, 13099-13104
3. Bernado P, Bertoncini CW, Griesinger C, Zweckstetter M, Blackledge M. *J. Am. Chem. Soc.* **2005**, *127*, 17968-17969
4. Zweckstetter M, Bax A. *J. Am. Chem. Soc.* **2000**, *122*, 3791-3792
5. Zweckstetter M, Hummer G, Bax A. *Biophys. J.* **2004**, *86*, 3444-3460

DOI: 10.1002/anie.200602317

**Charge-Induced Molecular Alignment of Intrinsically Disordered Proteins\*\****Lukasz Skora, Min-Kyu Cho, Hai-Young Kim, Stefan Becker, Claudio O. Fernandez, Martin Blackledge, and Markus Zweckstetter\**


Intrinsically disordered or unstructured proteins (IUPs) play a key role in normal and pathological biochemical processes. Despite their importance for function, this category of proteins remains beyond the reach of classical structural biology because of their inherent conformational heterogeneity. Measurements of global dimensions strongly suggested a random coil-like behavior of IUPs.<sup>[1]</sup> In contrast to these findings, NMR spectroscopy detected significant amounts of local structure in denatured and unfolded states. Recently, these two apparently contradicting behaviors were reconciled when it was shown that the local conformational behavior of IUPs can be described by a simple model based on residue-specific  $\phi/\psi$  propensities.<sup>[2,3]</sup> In particular, residual dipolar couplings (RDCs), which can be measured for proteins that are weakly aligned in dilute liquid-crystalline media, could be predicted from this model by assuming a steric interaction between the protein and the alignment medium. Furthermore, we showed that RDCs are also sensitive detectors of transient long-range interactions in IUPs.<sup>[4,5]</sup>

[\*] L. Skora, M.-K. Cho, H.-Y. Kim, S. Becker, Dr. M. Zweckstetter  
Department of NMR-based Structural Biology  
Max Planck Institute for Biophysical Chemistry  
Am Fassberg 11, 37077 Göttingen (Germany)  
Fax: (+49) 551-201-2202  
E-mail: mzwecs@gwdg.de  
Homepage:  
<http://www.mpibpc.gwdg.de/abteilungen/030/zweckstetter>

Dr. C. O. Fernandez  
Instituto de Biología Molecular y Celular de Rosario  
Consejo Nacional de Investigaciones Científicas y Técnicas  
Universidad Nacional de Rosario  
Suipacha 531, S2002LRK Rosario (Argentina)

Dr. M. Blackledge  
Institute de Biologie Structurale Jean-Pierre Ebel  
CNRS-CEA-UJF, UMR 5085  
41 rue Jules Horowitz  
38027 Grenoble Cedex (France)

[\*\*] L.S. acknowledges a Marie Curie fellowship (MEST-CT-2004-504193), M.-K.C. a DFG-Graduiertenkolleg (GRK782) scholarship, C.F. an institutional partnership supported by the Alexander von Humboldt Foundation, and M.Z. a DFG Emmy Noether grant (ZW 71/1-5). This work was supported by the CMPB Göttingen and by the European Union through UPMAN. We thank Christophe Fares for help with the CPCL medium and Prof. Dr. Christian Griesinger for stimulating discussions.

 Supporting information for this article is available on the WWW under <http://www.angewandte.org> or from the author.

Herein, we demonstrate that the assumption of a steric interaction between intrinsically disordered proteins and the alignment medium is only valid in the case of uncharged alignment media. Alignment of IUPs in charged media depends critically on electrostatic interactions, especially in charged regions of the protein, and is scaled with the ionic strength of the solution. In this case the RDCs can be predicted using a simplified electrostatic model.<sup>[6]</sup>

In our approach we investigated the molecular alignment of  $\alpha$ -synuclein ( $\alpha$ S), a natively unstructured protein of 140 amino acid residues that is implicated in the onset of Parkinson's disease, in two charged alignment media with different electrostatic properties: filamentous phage Pf1<sup>[7]</sup> and quaternary surfactant cetylpyridinium chloride/hexanol/NaCl (CPCI).<sup>[8]</sup>

RDCs in  $\alpha$ S that was weakly aligned in filamentous phage Pf1 are shown in Figure 1. At 300 and 500 mM NaCl the RDC profile resembles the one that was previously observed in an

uncharged alignment medium.<sup>[4]</sup> All RDCs were positive, and regions with sizeable RDCs were separated by residues with RDC values close to zero. The C-terminal domain displayed the largest RDCs. At 100 mM NaCl, the RDCs of residues 23, 46, 50, 59, 86, and 103–104 turned from near-zero values to negative. Furthermore, the magnitude of RDCs for residues 15–21 increased, and for residues 124–131 it was nearly doubled. At even lower salt concentration, the RDCs in the N-terminal domain were further increased, thereby making several residues undetectable owing to strong  $^1\text{H}, ^1\text{H}$  dipolar couplings, and in the central part of  $\alpha$ S nearly all RDCs became negative. This behavior is in agreement with the electrostatics of the system. The Pf1 alignment medium bears an overall negative charge on the outer, protein-accessible side<sup>[9]</sup> and therefore, at low salt concentrations, strongly attracts the positively charged N-terminal domain of  $\alpha$ S (Figure 1 a). At the same time, the negatively charged C-terminal domain of  $\alpha$ S is repelled from the Pf1 surface.

Experimental RDCs were compared to values that were predicted from an ensemble of structures by using the software PALES. An ensemble comprising 50000 structures was generated using the flexible-meccano algorithm,<sup>[3]</sup> which sequentially builds peptide chains by random selection of  $\phi/\psi$  angles from a database of amino acid specific conformations found in loop regions of high-resolution X-ray structures. From these 50000 structures (30000–50000 structures were needed for convergence) RDCs were predicted on the basis of a highly simplified alignment model that approximates the electrostatic interaction between a solute and an ordered liquid-crystal particle as that between the solute side-chain charge and the electric field of the phage.<sup>[6]</sup> For Pf1 bacteriophage the following parameters were used: average surface charge density  $-0.47 \text{ e nm}^{-2}$ , order parameter 0.9, concentration  $15 \text{ mg mL}^{-1}$ . CPCI was modelled as a  $26.8\text{-\AA}$  thick, uniformly charged wall with a surface charge density of  $+0.08 \text{ e nm}^{-2}$ , order parameter of 0.8, and a concentration of 5% (w/v).<sup>[10]</sup>

Reasonably close agreement between experimental and charge-shape-predicted RDC patterns was found under all investigated conditions for Pf1 alignment medium (Figure 1 c,d and the Supporting Information). The prediction of the magnitude of alignment is better at intermediate ionic strengths whereas at higher salt concentrations the RDC magnitude tends to be underestimated by PALES.<sup>[6]</sup>

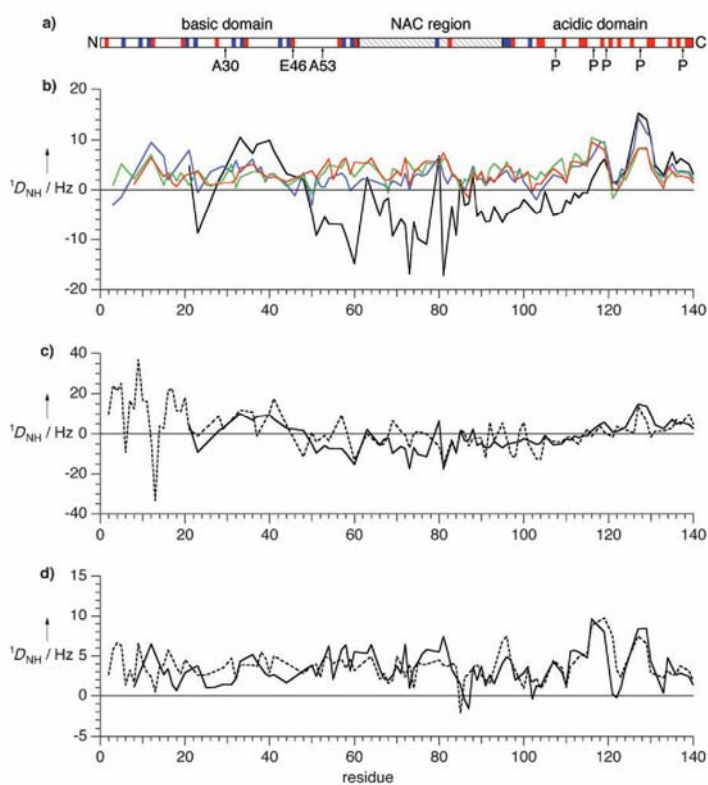


**Figure 1.** a) Surface charge distribution in  $\alpha$ S. Positively and negatively charged residues are marked blue and red, respectively. Sites of mutations associated with Parkinson's disease and proline residues are indicated by arrows. b)  $^1\text{H}, ^{15}\text{N}$  RDCs in Pf1 phage at 50 mM (black), 100 mM (blue), 300 mM (green), and 500 mM (red) NaCl, scaled with respect to the splitting of the  $^2\text{H}$  signal at 50 mM NaCl. All spectra were acquired on a Bruker DRX600 spectrometer with 0.2 mM  $\alpha$ S in 20 mM Tris-HCl, pH 7.4, at 288 K. c, d) Comparison of experimental (solid line) and predicted (dashed line)  $^1\text{H}, ^{15}\text{N}$  RDCs in  $15 \text{ mg mL}^{-1}$  Pf1 bacteriophage at 50 mM NaCl (c) and 500 mM NaCl (d). Below 200 mM NaCl the predicted and experimental RDC magnitude strongly depend on the exact ionic-strength value and the Pf1 batch used.

Therefore, average RDC values predicted at 100 mM and 500 mM NaCl were scaled up by factors of 2.5 and 4, respectively, to maximize agreement with experimental values. At 50 mM NaCl no scaling was required.

CPCI is positively charged and interacts strongly with the acidic C-terminal region of  $\alpha$ S, such that severe line broadening and disappearance of the corresponding signals was observed (Supporting Information). In agreement with the disappearance of signals, PALES predicted an up to eightfold increase in the RDC magnitude of residues 110–140. However, RDCs for residues 10–90 remained small, thus suggesting that the different domains of  $\alpha$ S align independently. Experimental RDCs in this region fit reasonably well to predicted values. Moreover, a strong influence of the electrostatic interaction on the alignment properties of CPCI was observed. At 150 mM NaCl, the liquid-crystalline phase showed a  $^2\text{H}$  splitting of 15 Hz, which dropped sixfold upon addition of  $\alpha$ S. Thus, it cannot be excluded that the interaction with the CPCI medium changes the conformational ensemble of  $\alpha$ S, although chemical shifts of observable residues were not significantly changed.

To further investigate the sign inversion of RDCs in the central region of  $\alpha$ S at 50 mM NaCl (Figure 1b), we constructed a 30 000-structure ensemble for a polyalanine fragment of 10 amino acid residues. Charges of  $+5e$  and  $-5e$  were placed on the N- and C-terminus, respectively, and RDCs were predicted using models of both steric<sup>[11]</sup> and electrostatic alignment<sup>[6]</sup> (Figure 2a). In the steric case, all RDCs were positive and showed the characteristic bell-shaped pattern.<sup>[12]</sup> In the electrostatic prediction, on the other hand, average RDC values turned negative, thus indicative of a preferential alignment perpendicular to the magnetic field and in agreement with a dipole-like behavior of the amino acid fragment. Furthermore, predictions at different salt

concentrations demonstrated that shielding of charges leads to more steric alignment.

Previously, we showed that the large RDCs in the C-terminal region of  $\alpha$ S are a result of long-range interactions involving the C- and N-terminal domains and the NAC region.<sup>[4]</sup> When steric alignment was assumed, enforcement of a long-range interaction between residues 1–20 and 120–140 in an ensemble of structures generated by flexible-meccano resulted in an increase in the RDC magnitude predicted for residues 2–30 and 110–140 and better agreement with RDCs measured in both sterically and electrostatically aligning media. The situation turns out to be more complicated when electrostatic alignment dominates (Figure 2b). Although RDCs for residues 116–121 were slightly increased upon enforcing the long-range contact, average RDCs that were predicted for the N-terminal region were strongly reduced. Thus, two opposing effects have to be taken into account. Owing to the long-range interaction the protein backbone becomes more rigid, potentially leading to larger RDCs, but at the same time the proximity of the negatively charged C-terminal region partially compensates the positive charges in the N-terminus, thus causing a decrease in the RDC magnitude.

This report demonstrates that molecular alignment of intrinsically unstructured and other disordered proteins in charged nematic media strongly depends on electrostatic interactions between the protein and the alignment medium. A simple electrostatic alignment model, however, reliably predicts RDCs under different sample conditions. Electrostatic effects have to be taken into account when using RDCs for the interpretation of residual structure in disordered proteins. At the same time, however, charge modulation of alignment provides an independent set of RDCs in disordered proteins, potentially improving the structural characterization of these systems. These findings have important consequences for the RDC-based interpretation of the structure and dynamics of the unfolded state.

Received: June 9, 2006  
Published online: September 28, 2006

**Keywords:** molecular alignment · NMR spectroscopy · protein structures · residual dipolar couplings

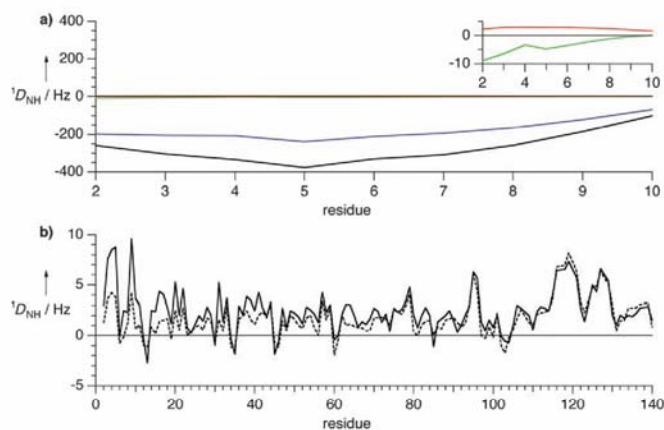


**Figure 2.** a)  $^1\text{H}$ ,  $^{15}\text{N}$  RDCs in a polyalanine fragment of 10 amino acid residues, predicted using a steric (red) and an electrostatic alignment model with salt concentrations of 50 mM (black), 100 mM (blue), and 500 mM (green) and charges of  $+5e$  and  $-5e$  at the N- and C-terminus, respectively. Inset: enlarged excerpt. b)  $^1\text{H}$ ,  $^{15}\text{N}$  RDCs in 15 mg mL<sup>-1</sup> Pf1 phage at 100 mM NaCl, predicted with (dashed line) and without (solid line) enforcing a long-range interaction between residues 1–20 and 120–140.

- [1] C. Tanford, K. Kawahara, S. Lapanje, *J. Biol. Chem.* **1966**, *241*, 1921–1923.
- [2] A. K. Jha, A. Colubri, K. F. Freed, T. R. Sosnick, *Proc. Natl. Acad. Sci. USA* **2005**, *102*, 13 099–13 104.
- [3] P. Bernado, L. Blanchard, P. Timmins, D. Marion, R. W. Ruigrok, M. Blackledge, *Proc. Natl. Acad. Sci. USA* **2005**, *102*, 17 002–17 007.
- [4] C. W. Bertoncini, Y. S. Jung, C. O. Fernandez, W. Hoyer, C. Griesinger, T. M. Jovin, M. Zweckstetter, *Proc. Natl. Acad. Sci. USA* **2005**, *102*, 1430–1435.
- [5] P. Bernado, C. W. Bertoncini, C. Griesinger, M. Zweckstetter, M. Blackledge, *J. Am. Chem. Soc.* **2005**, *127*, 17 968–17 969.
- [6] M. Zweckstetter, G. Hummer, A. Bax, *Biophys. J.* **2004**, *86*, 3444–3460.

- [7] M. R. Hansen, L. Mueller, A. Pardi, *Nat. Struct. Biol.* **1998**, *5*, 1065–1074.
- [8] R. S. Prosser, J. A. Losonczi, I. V. Shiyankovskaya, *J. Am. Chem. Soc.* **1998**, *120*, 11010–11011.
- [9] K. Zimmermann, H. Hagedorn, C. C. Heuck, M. Hinrichsen, H. Ludwig, *J. Biol. Chem.* **1986**, *261*, 1653–1655.
- [10] M. Zweckstetter, *Eur. Biophys. J.* **2006**, *35*, 170–180.
- [11] M. Zweckstetter, A. Bax, *J. Am. Chem. Soc.* **2000**, *122*, 3791–3792.
- [12] M. Louhivuori, K. Paakkonen, K. Fredriksson, P. Permi, J. Lounila, A. Annala, *J. Am. Chem. Soc.* **2003**, *125*, 15647–15650.

## Appendix B. Chemical shift lists

### Chemical shift list of $^{13}\text{C}$ -CON of h $\beta$ 2m

	pH 2.5		pH 3.6	
	N	C'	N	C'
Ile 1	124,23	175,47	124,21	175,47
Gln 2	125,63	175,52	125,63	175,53
Arg 3	123,74	176,03	123,74	176,02
Thr 4	117,96		117,95	
Pro 5		176,54		176,52
Lys 6	121,88	176,38	121,90	176,37
Ile 7	122,54	175,84	122,57	175,83
Gln 8	125,30	175,27	125,30	175,25
Val 9	122,00	175,65	122,03	175,63
Tyr 10	124,34	175,59	124,39	175,57
Ser 11	117,86	173,95	117,90	173,94
Arg 12	122,81	175,67	122,71	175,67
His 13	120,02		120,16	
Pro 14		176,50		176,49
Ala 15	124,59	177,72	124,50	177,72
Glu 16	119,67	175,67	119,89	175,67
Asn 17	120,09	175,63	120,16	175,67
Gly 18	109,30	174,13	109,28	174,15
Lys 19	120,60	176,69	120,57	176,69
Ser 20	116,40	174,13	116,39	174,15
Asn 21	120,60	174,83	120,57	174,86
Phe 22	120,14	175,36	120,16	175,38*
Leu 23	122,50	176,51	122,40*	176,64
Asn 24	118,32	174,98	118,72	175,00
Cys 25	118,43		118,36	
Val 27		175,75		
Ser 28	118,67	174,96		174,93
Gly 29	110,56	173,38	110,50	173,36
Phe 30	120,29	174,89	120,18	174,83
His 31	122,35		122,34	



	pH 2.5		pH 3.6	
	N	C'	N	C'
Pro 32		176,75		176,75
Ser 33	115,69	174,41	115,51	174,38
Asp 34	120,66	175,04	121,12	175,18*
Ile 35	119,98	175,90	119,94*	175,92*
Glu 36	123,36	176,12	123,35*	176,23
Val 37	120,39	176,00	119,96	176,08
Asp 38	121,39	175,24	121,85	
Leu 39	122,61	177,47		177,55
Leu 40	121,53	177,87	121,43	178,06
Lys 41	120,87	176,82	120,66	176,83
Asn 42	118,87	175,88	118,84	175,88
Gly 43	108,47	174,19	108,42	174,19
Glu 44	119,54	175,69	119,65	175,69
Arg 45	121,53	176,12	121,47	176,17
Ile 46	121,85	176,01	121,87	176,04
Glu 47	123,73	175,78	123,61	175,86
Lys 48	121,82	176,25	121,64	176,28*
Val 49	121,43	176,08	121,28*	176,05
Glu 50	123,47	175,81	123,52	175,81
His 51	118,78	174,23	118,70	174,24
Ser 52	115,89	174,15	116,20	174,07
Asp 53	121,04	175,13	121,43	175,25
Leu 54	122,33	177,28	122,03	177,41
Ser 55	115,59	174,28	115,58	174,36
Phe 56	121,58	175,82	121,42	175,81
Ser 57	116,04	175,02	115,74	175,06
Lys 58	122,07	176,69	122,20	176,81
Asp 59	118,54		118,30	
Trp 60		176,62		176,74
Ser 61	115,39		115,25	
Phe 62		175,96		
Tyr 63	119,12	176,04		176,34
Leu 64	119,65		119,60	
Thr 68		174,58		
Glu 69	120,52	174,62		

	pH 2.5		pH 3.6	
	N	C'	N	C'
Phe 70	120,72			
Thr 73		175,18		175,16
Glu 74	121,37		121,40	
Glu 77		176,01		176,00
Tyr 78	119,47		119,23	
Ala 79		177,53		177,73
Cys 80	117,35		116,90	
Val 82		175,52		175,59
Asn 83	122,57	174,72	121,78	174,73
His 84	119,31	173,90	118,97	173,94
Val 85	121,92	175,90	121,52	175,88
Thr 86	119,45	174,14	119,07	174,19
Leu 87	125,74	176,98	125,52	177,01
Ser 88	116,97	173,92	116,78	173,92
Gln 89	122,99		122,94	
Pro 90		176,54		176,50
Lys 91	121,53	176,27	121,29	176,20
Ile 92	122,72	175,90	122,50	175,85
Val 93	125,13	175,70	124,88	175,54
Lys 94	125,00	175,82	124,92	175,74
Trp 95	122,17	175,72	122,52	175,65
Asp 96	120,93	174,60	121,28	174,91
Arg 97	120,63	175,60	120,37	175,61
Asp 98	119,03	174,64	119,63	174,56
Met 99	121,32		123,25	

\* - resonance not observable at pH 3.6; chemical shift value corresponds to pH 2.9

### Chemical shift list of h $\beta$ 2m in 4M GdnSCN

	N	H <sup>N</sup>	C $\alpha$	C $\beta$
Ile 1	124,17	8,65	61,85	39,47
Gln 2	125,55	8,63	56,18	30,03
Arg 3	124,05	8,58	56,67	31,63
Thr 4	117,00	8,38	59,95	70,34
Pro 5			63,76	32,72
Lys 6	122,47	8,48	57,05	33,43
Ile 7	122,03	8,20	61,71	39,26
Gln 8	125,15	8,52	56,19	29,85
Val 9	121,82	8,22	62,98	33,39
Tyr 10	123,86	8,36	58,46	39,37
Ser 11	117,55	8,31	58,53	64,79
Arg 12	123,16	8,39	57,05	31,38
His 13	119,18	8,51	53,74	29,10
Pro 14			64,15	32,63
Ala 15	124,84	8,62	53,29	19,59
Glu 16	119,99	8,47	56,37	29,12
Asn 17	119,72	8,58	53,69	39,43
Gly 18	109,95	8,53	46,00	
Lys 19	121,32	8,36	56,95	33,60
Ser 20	116,76	8,47	58,69	64,45
Asn 21	121,35	8,56	53,72	39,31
Phe 22	120,71	8,33	58,58	39,94
Leu 23	122,65	8,38	55,61	42,80
Cys 25	119,39	8,44	53,70	39,29
Tyr 26	123,33	8,35	58,63	39,28
Val 27	121,29	8,26	63,15	33,32
Ser 28	119,38	8,43	58,82	64,66
Gly 29	111,05	8,43	45,64	
Phe 30	121,11	8,32	58,47	40,25
His 31	122,15	8,35	53,45	29,21
Pro 32			63,58	32,59
Ser 33	116,43	8,59	58,81	64,59
Asp 34	121,53	8,63	53,68	38,75
Ile 35	120,49	8,15	61,91	39,13

	N	H <sup>N</sup>	C $\alpha$	C $\beta$
Glu 36	124,25	8,44	56,54	29,08
Val 37	120,65	8,19	63,17	33,23
Asp 38	122,29	8,59	53,58	38,56
Leu 39	123,10	8,32	55,83	42,74
Leu 40	121,98	8,25	55,83	42,65
Lys 41	121,81	8,36	56,95	33,58
Asn 42	119,19	8,49	53,69	39,23
Gly 43	109,59	8,49	46,10	
Glu 44	120,09	8,36	56,47	29,36
Arg 45	122,42	8,46	56,49	31,19
Ile 46	122,14	8,29	61,95	39,17
Glu 47	124,14	8,44	56,54	29,05
Lys 48	123,53	8,40	56,74	33,58
Val 49	121,48	8,27	63,16	33,48
Glu 50	123,58	8,50	56,53	29,15
His 51	119,41	8,58	55,98	29,31
Ser 52	116,90	8,53	58,83	64,63
Asp 53	121,78	8,74	53,68	38,77
Leu 54	122,49	8,33	55,78	42,59
Ser 55	116,28	8,32	58,85	64,40
Phe 56	122,45	8,31	58,57	40,01
Ser 57	116,97	8,30	58,63	64,69
Lys 58	123,25	8,35	57,05	33,16
Asp 59	119,56	8,48	53,59	
Trp 60	122,14	8,19	58,42	30,04
Ser 61	116,49	8,13	58,91	64,33
Phe 62	122,80	8,16	59,61	39,81
Tyr 63	120,22	8,08	59,19	39,28
Leu 64	121,90	8,07	56,18	42,69
Leu 65	121,68	8,07	56,18	42,69
Tyr 66	119,60	8,08	58,98	39,33
Tyr 67	120,29	8,17	58,95	39,18
Thr 68	114,20	8,07	62,05	70,66
Glu 69	122,22	8,31	56,69	29,15
Phe 70	121,66	8,36	58,32	40,34
Thr 71	118,71	8,15	59,80	70,55

	N	H <sup>N</sup>	C $\alpha$	C $\beta$
Pro 72			63,99	32,58
Thr 73	113,76	8,31	62,27	70,62
Glu 74	122,57	8,43	57,00	29,25
Lys 75	121,99	8,43	57,20	33,43
Glu 77	120,93	8,34	56,90	29,05
Tyr 78	120,36	8,29	58,47	39,13
Ala 79	124,30	8,27	53,54	19,89
Cys 80	117,48	8,42	55,78	41,01
Val 82	120,67	8,24	63,11	33,28
Asn 83	122,31	8,51	53,69	39,49
His 84	119,58	8,55	55,67	29,51
Val 85	121,75	8,39	63,20	33,29
Thr 86	118,93	8,44	62,09	70,59
Leu 87	125,42	8,43	55,45	42,85
Ser 88	116,96	8,42	58,59	64,58
Gln 89	122,79	8,49	54,13	29,41
Pro 90			63,87	32,92
Lys 91	122,58	8,47	56,95	33,38
Ile 92	122,80	8,23	61,63	39,13
Val 93	124,69	8,22	62,55	33,23
Lys 94	125,33	8,33	57,20	33,48
Trp 95	121,62	8,11	57,55	30,01
Asp 96	120,36	8,37	53,38	38,68
Arg 97	121,41	8,24	57,10	30,99
Asp 98	119,59	8,53	53,69	38,73
Met 99	122,51	8,25	55,83	33,12

**Chemical Shift list of humPrP<sub>23-173</sub> in 2M GdnSCN**

	N	H <sup>N</sup>	C $\alpha$	C $\beta$
Lys 23	125,65	8,53	56,26	29,88
Lys 24	126,06	8,47	56,20	33,43
Arg 25	123,66	8,35	54,30	30,73
Pro 26			63,52	32,76
Lys 27	122,58	8,35	54,52	32,76
Gly 30	109,20	8,36	45,58	
Trp 31	121,38	8,15	57,89	30,10
Gly 35	109,20	8,36	45,58	
Ser 36	115,82	8,35	58,85	64,13
Arg 37	123,03	8,37	56,74	31,27
Gly 40	109,26	8,19	45,59	
Gln 41	120,03	8,31	56,32	29,74
Gly 42	110,54	8,57	45,46	
Ser 43	116,87	8,31	56,48	63,63
Pro 44			64,07	32,15
Gly 45	109,31	8,49	45,58	
Gly 46	109,09	8,30	45,65	
Asn 47	119,19	8,44	53,31	38,21
Gly 54	109,20	8,36	45,58	
Gly 55	109,20	8,36	45,58	
Gly 56	109,09	8,30	45,65	
Trp 57	121,38	8,15	57,89	30,10
Gly 58	110,93	8,44	45,80	
Gln 59	120,56	8,15	54,10	29,30
Pro 60			63,64	32,30
His 61	118,39	8,58	55,60	29,22
Gly 62	110,26	8,48	45,72	
Gly 63	109,20	8,36	45,58	
Gly 64	109,20	8,36	45,58	
Trp 65	121,38	8,15	57,89	30,10
Gly 66	110,79	8,40	45,47	
Gln 67	120,56	8,15	54,10	29,30
Pro 68			63,64	32,30
His 69	118,39	8,58	55,60	29,22

	N	H <sup>N</sup>	C $\alpha$	C $\beta$
Gly 70	110,26	8,48	45,72	
Gly 71	109,20	8,36	45,58	
Gly 72	109,20	8,36	45,58	
Trp 73	121,38	8,15	57,89	30,10
Gly 74	110,79	8,40	45,47	
Gln 75	120,56	8,15	54,10	29,30
Pro 76			63,64	32,30
His 77	118,39	8,58	55,60	29,22
Gly 78	110,26	8,48	45,72	
Gly 79	109,20	8,36	45,58	
Gly 80	109,20	8,36	45,58	
Trp 81	121,38	8,15	57,89	30,10
Gly 82	110,79	8,40	45,47	
Gln 83	120,56	8,15	54,10	29,30
Pro 84			63,64	32,30
His 85	118,39	8,58	55,60	29,22
Gly 86	110,26	8,48	45,72	
Gly 87	109,20	8,36	45,58	
Gly 88	109,20	8,36	45,58	
Trp 89	121,38	8,15	57,89	30,10
Gly 90	111,01	8,44	45,76	
Gln 91	119,88	8,29	56,66	28,68
Gly 92	110,43	8,56	45,60	
Gly 93	109,20	8,36	45,58	
Gly 94	109,20	8,36	45,58	
Thr 95	113,32	8,23	62,13	70,12
His 96	120,43	8,59	55,81	28,91
Ser 97	116,82	8,39	58,96	63,98
Gln 98	122,28	8,56	56,40	29,37
Asn 100			52,67	39,33
Lys 101	122,58	8,06	54,69	33,01
Pro 102			63,44	32,36
Ser 103	116,55	8,43	58,35	64,32
Lys 104	124,02	8,34	54,63	33,05
Pro 105			63,51	32,62
Lys 106	122,09	8,48	56,93	33,31

	N	H <sup>N</sup>	C $\alpha$	C $\beta$
Thr 107	114,61	8,21	61,78	70,66
Asn 108	121,40	8,48	52,70	39,34
Lys 110	122,96	8,40	56,73	33,67
His 111	118,84	8,45	55,88	28,87
Ala 113	125,81	8,49	53,29	19,45
Gly 114	108,88	8,44	45,65	
Ala 115	124,24	8,26	53,02	19,54
Ala 116	123,03	8,36	52,93	19,38
Ala 117	123,16	8,22	52,77	19,37
Ala 118	123,15	8,28	53,09	19,42
Gly 119	108,09	8,37	45,46	
Ala 120	124,03	8,17	52,71	19,67
Val 121	119,61	8,19	62,63	32,97
Val 122	124,19	8,28	62,97	33,01
Gly 123	113,03	8,54	45,53	
Gly 124	109,20	8,36	45,58	
Leu 125	121,93	8,35	55,98	42,69
Met 129	121,68	8,37	56,17	33,24
Leu 130	123,05	8,17	56,03	42,58
Gly 131	110,01	8,47	45,81	
Ser 132	115,86	8,31	58,70	64,23
Ala 133	125,95	8,50	53,37	19,38
Met 134	118,50	8,30	56,08	33,22
Ser 135	116,79	8,26	58,38	64,20
Arg 136	123,53	8,28	54,49	30,68
Ile 139	124,80	8,08	61,36	39,00
His 140	122,65	8,44	55,05	29,33
Phe 141	122,47	8,40	58,45	39,96
Gly 142	111,01	8,45	45,71	
Ser 143	115,82	8,35	58,85	64,13
Asp 144	120,81	8,59	53,53	38,07
Glu 146	120,77	8,28	56,39	28,82
Asp 147	118,97	8,31	53,68	38,09
Tyr 149	120,05	8,13	59,26	38,78
Tyr 150	120,85	8,02	59,31	39,01
Asn 153	118,75	8,34	39,13	53,97



	N	H <sup>N</sup>	C $\alpha$	C $\beta$
His 155	119,01	8,49	55,72	29,06
Arg 156	121,76	8,20	56,42	31,52
Pro 158	117,75	8,47	63,92	32,18
Asn 159	117,84	8,47	53,76	39,03
Val 161	121,03	8,11	62,99	33,07
Tyr 162	123,45	8,17	58,02	39,49
Tyr 163	122,58	8,11	58,01	39,47
Arg 164	124,37	8,13	54,23	30,93
Pro 165			63,59	
Met 166	119,97	8,43	56,32	32,65
Asp 167	122,44	8,50	52,71	39,79
Tyr 169	120,40	8,20	58,04	39,04
Ser 170	116,61	8,21	58,42	64,06
Asn 171	121,14	8,52	53,62	39,19
Gln 172	120,37	8,42	56,22	29,89

## Appendix C. H/D exchange data of humPrP<sub>23-159</sub>

### Changes in signal intensity during the back-exchange process of humPrP<sub>23-159</sub> after 3 days of H/D exchange

	I <sub>24h</sub> /I <sub>0</sub>		I <sub>24h</sub> /I <sub>0</sub>		I <sub>24h</sub> /I <sub>0</sub>
Lys 24	1,67	Gly 74	1,82	Gly 114	1,08
Arg 25	5,08	Gln 75	1,52	Ala 115	0,95
Lys 27	3,29	His 77	1,43	Ala 116	1,15
Gly 30	1,31	Gly 78	1,59	Ala 117	0,98
Trp 31	2,15	Gly 79	1,38	Ala 118	1,01
Gly 35	1,27	Gly 80	1,47	Gly 119	1,30
Ser 36	1,75	Trp 81	2,10	Ala 120	1,45
Arg 37	1,43	Gly 82	1,82	Val 121	0,77
Gly 40	2,69	Gln 83	1,52	Val 122	0,68
Gln 41	1,96	His 85	1,43	Gly 123	0,78
Ser 43	1,42	Gly 86	1,59	Gly 124	0,83
Gly 45	1,86	Gly 87	1,38	Leu 125	0,84
Gly 46	1,26	Gly 88	1,47	Gly 126	0,92
Asn 47	1,80	Trp 89	2,10	Gly 127	0,85
Gly 54	1,45	Gly 90	1,83	Met 129	0,76
Gly 55	1,31	Gln 91	1,91	Leu 130	0,65
Gly 56	1,31	Gly 92	1,88	Ser 132	0,69
Trp 57	2,20	Gly 93	1,33	Ala 133	0,68
Gly 58	1,83	Gly 94	1,47	Met 134	0,76
Gln 59	1,52	Thr 95	1,43	Ser 135	0,74
His 61	1,43	His 96	1,32	Arg 136	0,66
Gly 62	1,59	Ser 97	1,92	Ile 139	0,55
Gly 63	1,38	Gln 98	1,83	His 140	1,16
Gly 64	1,47	Lys 101	2,32	Phe 141	1,04
Trp 65	2,10	Ser 103	1,51	Gly 142	1,08
Gly 66	1,82	Lys 104	1,98	Ser 143	1,34
Gln 67	1,52	Lys 106	1,75	Asp 144	1,46
His 69	1,43	Thr 107	2,65	Glu 146	1,22
Gly 70	1,59	Asn 108	1,27	Asp 147	1,49
Gly 71	1,38	Lys 110	1,07	Tyr 149	4,68
Gly 72	1,47	His 111	1,14	His 155	1,46
Trp 73	2,10	Ala 113	1,10	Arg 156	2,82

## Appendix D. CS-Rosetta output table

### Ten best 9-residue fragments selected by CS-Rosetta in hybrid mode for the Met112-Phe141 input sequence.

Legend:

Q1,QN – first and last residue of query sequence

Q\_SEQ – query sequence

PDB – name of pdb file containing the found fragment

R1, RN – first and last residue of found fragment in the pdb file

ROS – raw Rosetta score

SEC\_ST – secondary structure of found fragment in pdb (L: loop, H: helix, E: extended)

SEQ – sequence of found fragment

CS – chemical shift based score

Q1	QN	Q_SEQ	PDB	R1	RN	ROS	SEC_ST	SEQ	CS
1	9	MAGAAAAGA	2YVV.pdb	255	263	1,69	LLLLLLLLL	GAGTAAQGI	1,66
1	9	MAGAAAAGA	1KVE.pdb	16	24	1,88	LLLLLLLLL	IAGCSGAAT	2,59
1	9	MAGAAAAGA	1KQF.pdb	978	986	2,28	LLLLLLLLL	FEGVARKGY	2,70
1	9	MAGAAAAGA	1OQV.pdb	146	154	2,35	LLLEHHHLL	SAAAETGV	2,81
1	9	MAGAAAAGA	1U7G.pdb	86	94	2,30	LLLLLEELL	IELTAVMGS	3,01
1	9	MAGAAAAGA	2AXC.pdb	25	33	2,28	LLLLLELLL	VAAPMAFGF	3,07
1	9	MAGAAAAGA	1TMO.pdb	404	412	1,68	LLLLLLLLL	SSGAAAPGA	3,19
1	9	MAGAAAAGA	1KVE.pdb	11	19	2,35	LLLLLLLLL	TTIAAIAGC	3,20
1	9	MAGAAAAGA	1IO1.pdb	344	352	2,35	LLLLLLLLL	LAEAAATTT	3,23
1	9	MAGAAAAGA	1TMO.pdb	146	154	2,17	LLLLLLLLL	QTGWRTGQ	3,31
2	10	AGAAAAGAV	2YVV.pdb	256	264	1,92	LLLLLLLLL	AGTAAQGIY	1,86
2	10	AGAAAAGAV	2QWU.pdb	64	72	2,24	LLLLLELEE	ADSATAAAS	2,32
2	10	AGAAAAGAV	1TMO.pdb	405	413	1,87	LLLLLLLLL	SGAAAPGAF	2,47
2	10	AGAAAAGAV	1ZJA.pdb	536	544	2,46	LLLLLLEEE	APAAGAASL	2,48
2	10	AGAAAAGAV	2QO3.pdb	514	522	2,06	HLLLLLLE	AGAATADAV	2,53
2	10	AGAAAAGAV	2Q7D.pdb	336	344	2,47	LLLLLLLLL	TAMAATGDV	2,60
2	10	AGAAAAGAV	1W79.pdb	202	210	2,50	LLLLLLEEE	AGSANTLVI	2,63
2	10	AGAAAAGAV	1KQF.pdb	979	987	2,34	LLLLLLLLL	EGVARKGYI	2,64
2	10	AGAAAAGAV	1YQ5.pdb	127	135	2,03	LLLLLELLE	DGAALSNYI	2,72
2	10	AGAAAAGAV	1S7M.pdb	26	34	1,78	LLLLLLEEE	AGANNANTI	3,07
3	11	GAAAAGAVV	1TYV.pdb	338	346	2,49	LLLLLLEEE	DCAGSGAYL	1,63
3	11	GAAAAGAVV	1PMH.pdb	122	130	2,21	ELLLLLEEE	ITANAGKKV	1,90

Q1	QN	Q_SEQ	PDB	R1	RN	ROS	SEC_ST	SEQ	CS
3	11	GAAAAGAVV	2J5V.pdb	271	279	2,48	LLLLLLEEE	GAPPAGEIT	2,08
3	11	GAAAAGAVV	2YVV.pdb	257	265	1,84	LLLLLLLLL	GTAAQGIYI	2,09
3	11	GAAAAGAVV	2QWU.pdb	65	73	2,35	LLLLLEEEE	DSATAAASV	2,38
3	11	GAAAAGAVV	1TMO.pdb	406	414	2,52	LLLLLLLLL	GAAAPGAFP	2,38
3	11	GAAAAGAVV	1XDN.pdb	100	108	2,39	LLLLLLEEE	GLSRVGRVLV	2,46
3	11	GAAAAGAVV	1YQ5.pdb	128	136	1,41	LLLELLLEE	GAALSNIYI	2,65
3	11	GAAAAGAVV	2B2A.pdb	119	127	2,16	LLEEELLEE	GTTTIGFYV	2,65
3	11	GAAAAGAVV	1XC3.pdb	69	77	2,45	LLLLLLELL	TSQTYGTIT	3,02
4	12	AAAAGAVVG	1HX6.pdb	58	66	2,47	LLLLLEEEE	PANVGIVKKG	1,42
4	12	AAAAGAVVG	1TYV.pdb	339	347	2,66	LLLLLEEEE	CAGSGAYLL	1,63
4	12	AAAAGAVVG	1PMH.pdb	123	131	1,95	LLLLLEEEE	TANAGKKVK	1,83
4	12	AAAAGAVVG	2A5Z.pdb	221	229	2,50	LLLLLEEEE	ADNATAHIG	2,45
4	12	AAAAGAVVG	1XC3.pdb	70	78	2,62	LLLLLLELL	SQTYGTITA	2,70
4	12	AAAAGAVVG	1J30.pdb	71	79	2,65	LLLLLLELL	DPATDKPIG	2,72
4	12	AAAAGAVVG	1YQ5.pdb	129	137	2,49	LLELLLEEE	AALSNIYIN	2,74
4	12	AAAAGAVVG	2QWU.pdb	66	74	2,60	LLLELEEEE	SATAAASVI	2,77
4	12	AAAAGAVVG	2AXT.pdb	450	458	2,33	HHLLLLLLL	AAAAGFEKG	3,07
4	12	AAAAGAVVG	1YO6.pdb	141	149	2,59	LLLLLEEEE	SVSRAAVIT	3,08
5	13	AAAGAVVGG	1HX6.pdb	59	67	2,76	LLLLLEEEE	ANVGIVKGF	1,10
5	13	AAAGAVVGG	1PMH.pdb	124	132	2,74	LLLLLEEEE	ANAGKKVKI	1,54
5	13	AAAGAVVGG	1TC5.pdb	164	172	2,77	LLLLLEEEL	KYNSRVISG	2,03
5	13	AAAGAVVGG	2POH.pdb	178	186	2,75	LLLLLLLLL	AATGTANKG	2,28
5	13	AAAGAVVGG	1K7I.pdb	338	346	2,76	LLLLLEEEL	VTIENAIGG	2,37
5	13	AAAGAVVGG	1WXC.pdb	110	118	2,80	LLLLLEELL	STDGRVMDG	2,49
5	13	AAAGAVVGG	1CL8.pdb	121	129	2,58	HHLLLLLEL	IRNGLLVGK	2,63
5	13	AAAGAVVGG	1M1Z.pdb	8	16	2,65	LLLLLEEEE	AAFGLFLASA	2,81
5	13	AAAGAVVGG	1RUT.pdb	153	161	2,82	LLLLLEELL	VGEPTLMGG	2,87
5	13	AAAGAVVGG	1QOY.pdb	196	204	1,22	LLLLLEEELH	AAAGVVVGP	2,93
6	14	AAGAVVGGGL	1P5VB.pdb	36	44	2,74	LLLLLEEEE	DTELLVGTL	1,91
6	14	AAGAVVGGGL	1CL8.pdb	122	130	2,75	HLLLLLELL	RNGLLVGKR	2,49
6	14	AAGAVVGGGL	3TDT.pdb	159	167	2,77	LLLLLEELL	SGGVGIGGV	2,56
6	14	AAGAVVGGGL	1BO4.pdb	83	91	2,10	ELLEEEEE	DQEAVVGAL	2,71
6	14	AAGAVVGGGL	3TDT.pdb	203	211	2,70	LLLLLEELL	SMGVYLGQS	2,78
6	14	AAGAVVGGGL	1C5E.pdb	39	47	2,24	LLLLLEEEE	TDGAAVGIL	2,84
6	14	AAGAVVGGGL	1ZQ1.pdb	110	118	2,60	LLLLLEEEL	ETGAVYPAF	2,96
6	14	AAGAVVGGGL	1X38.pdb	49	57	2,86	LLLLLEEEL	FIGSLLSGG	3,04
6	14	AAGAVVGGGL	1QRE.pdb	185	193	2,69	LLLLLEEEL	EPRSAAIGV	3,07
6	14	AAGAVVGGGL	1IM3.pdb	19	27	1,79	EEEEEEEL	ARGSIVGNM	3,08
7	15	AGAVVGGGLG	1K7I.pdb	340	348	2,79	LLEEELLLL	IENAIGGSG	1,50
7	15	AGAVVGGGLG	2QSK.pdb	83	91	2,83	LLEEELLLL	SGFCQGTAG	1,62
7	15	AGAVVGGGLG	1ZKJ.pdb	262	270	2,74	ELLEELLLL	VGGMTQGLG	1,62
7	15	AGAVVGGGLG	2B4W.pdb	300	308	2,60	LLLEELLL	HGTIIGDLH	1,87
7	15	AGAVVGGGLG	2C1L.pdb	331	339	2,64	LLEELLLL	AVSFIGNRG	1,89

Q1	QN	Q_SEQ	PDB	R1	RN	ROS	SEC_ST	SEQ	CS
7	15	AGAVVGGLG	2FFY.pdb	259	267	2,76	ELLEEEELL	TGDMYQGLG	1,89
7	15	AGAVVGGLG	1BF2.pdb	726	734	2,33	LLEEEELL	SETLIGGAG	1,92
7	15	AGAVVGGLG	1CL8.pdb	123	131	2,48	LLLLLELLL	NGLLVGKRG	1,93
7	15	AGAVVGGLG	2Z8X.pdb	404	412	2,81	LEEEELL	YNVILGGAG	1,99
7	15	AGAVVGGLG	2EHP.pdb	8	16	2,59	LLLEEEELL	EGKVEGVP	2,04
8	16	GAVVGGLGG	1XEZ.pdb	629	637	2,07	LLLEELL	DLLVGGNGG	1,56
8	16	GAVVGGLGG	1BO4.pdb	85	93	2,46	LEEEEEEEE	EAVVGALAA	1,68
8	16	GAVVGGLGG	2YVT.pdb	133	141	2,48	LEEEEEELL	EFEVIGFGG	1,72
8	16	GAVVGGLGG	1VPS.pdb	210	218	2,83	EEEEELL	GNYTGGTTT	2,14
8	16	GAVVGGLGG	1IM3.pdb	21	29	2,18	EEEEELL	GSIVGNMSR	2,14
8	16	GAVVGGLGG	2EHP.pdb	9	17	2,67	LLEEEELL	GKVEGVP	2,22
8	16	GAVVGGLGG	1GVP.pdb	67	75	2,98	HEEEELL	SFKVGF	2,24
8	16	GAVVGGLGG	1XR4.pdb	387	395	2,12	LLELELL	GVLRGASGG	2,41
8	16	GAVVGGLGG	2HS1.pdb	44	52	1,31	EEEEELLE	PKMIGGIGG	2,41
8	16	GAVVGGLGG	1BF2.pdb	727	735	2,86	LEEEELL	ETLIGGAGT	2,46
9	17	AVVGGLGGY	2BMZ.pdb	53	61	3,02	EEEEELL	RHYGGSGGT	0,87
9	17	AVVGGLGGY	1IM3.pdb	22	30	2,60	EEEEELL	SIVGNMSRF	1,07
9	17	AVVGGLGGY	1XEZ.pdb	630	638	2,21	LLEELL	LLVGGNGGS	1,37
9	17	AVVGGLGGY	2YVT.pdb	134	142	2,31	EEEEELLE	FEVIGFGGL	1,58
9	17	AVVGGLGGY	1UF3.pdb	108	116	2,30	EEEEELLE	YLVAGVGGE	1,59
9	17	AVVGGLGGY	1BO4.pdb	86	94	2,49	EEEEEEEE	AVVGALAA	1,62
9	17	AVVGGLGGY	1V0W.pdb	265	273	2,86	EEEEELL	IAVGGLGVG	1,64
9	17	AVVGGLGGY	1IG0.pdb	187	195	2,24	EEELL	LALGGIGGR	1,65
9	17	AVVGGLGGY	2HS1.pdb	45	53	0,57	EEEEELLE	KMIGGIGGF	1,72
9	17	AVVGGLGGY	1TT7.pdb	244	252	3,04	EELL	AVSGLTGGG	1,72
10	18	VVGGLGGYM	1IM3.pdb	23	31	2,50	EEELL	IVGNMSRFV	1,23
10	18	VVGGLGGYM	1XEZ.pdb	631	639	2,50	LEELL	LVGGNGGSL	1,30
10	18	VVGGLGGYM	2HAH.pdb	55	63	2,94	EEEELEEE	MIGGIGGFI	1,46
10	18	VVGGLGGYM	1G7S.pdb	265	273	2,97	EEEELL	AMMTSKDVI	1,80
10	18	VVGGLGGYM	1TYV.pdb	186	194	2,75	EEELL	PSGGKDGII	1,84
10	18	VVGGLGGYM	1HRU.pdb	165	173	2,78	LLLLLL	VPGETGGRL	1,92
10	18	VVGGLGGYM	2HS1.pdb	46	54	0,12	EEEELEEE	MIGGIGGFI	1,96
10	18	VVGGLGGYM	1K7I.pdb	343	351	3,06	EELL	AIGGSGNDI	1,99
10	18	VVGGLGGYM	1G6S.pdb	74	82	2,74	EEELL	EIIGNGGPL	2,01
10	18	VVGGLGGYM	2YVT.pdb	135	143	1,98	EEEEELLE	EVIGFGGLL	2,06
11	19	VGGLGGYML	1IM3.pdb	24	32	3,19	EELLLEEE	VGNMSRFVF	0,99
11	19	VGGLGGYML	1XEZ.pdb	632	640	2,51	EELLLEEE	VGGNGGSLS	1,23
11	19	VGGLGGYML	2Z43.pdb	137	145	3,06	HLLLLLEEE	KGGLSGKAV	1,52
11	19	VGGLGGYML	1QQP.pdb	76	84	2,77	LLLLLL	FSGLFGALL	1,52
11	19	VGGLGGYML	1K7I.pdb	344	352	3,13	ELLLEEE	IGGSGNDIL	1,60
11	19	VGGLGGYML	1HX6.pdb	61	69	2,97	LLEEEEEEE	VGIVKGFLV	1,66
11	19	VGGLGGYML	1S1D.pdb	156	164	3,19	EELLLEEE	VGGLGKEWT	1,74
11	19	VGGLGGYML	1UUN.pdb	152	160	3,06	LLEELL	TGAAGGVLL	1,75

Q1	QN	Q_SEQ	PDB	R1	RN	ROS	SEC_ST	SEQ	CS
11	19	VGGLGGYML	2Z8X.pdb	408	416	3,13	ELLLLLLEE	LGGAGNNTL	1,92
11	19	VGGLGGYML	1TYV.pdb	187	195	2,99	EELLLLLEE	SGGKDGIIIT	1,94
12	20	GGLGGYMLG	2ARC.pdb	34	42	3,25	LLLLLEEEE	LGMKGYILN	1,86
12	20	GGLGGYMLG	1UUN.pdb	153	161	3,24	LEELLLLLL	GAAGGVLLR	2,09
12	20	GGLGGYMLG	1UYN.pdb	59	67	3,34	LLLLLEEEE	GGVEGKMRG	2,12
12	20	GGLGGYMLG	2PGC.pdb	159	167	1,48	LLLLLEEEE	SNVGNVLLG	2,14
12	20	GGLGGYMLG	1IKP.pdb	549	557	3,23	LLLLLEEEE	GGRLETILG	2,25
12	20	GGLGGYMLG	1WRJ.pdb	127	135	3,14	LLLLLLLLL	KSLGGYSRG	2,43
12	20	GGLGGYMLG	2BKX.pdb	124	132	3,27	LLLLLEEEEL	GDTDIQLLG	2,50
12	20	GGLGGYMLG	1U6E.pdb	182	190	3,30	LLELLLLLE	QGIGPTVAG	2,55
12	20	GGLGGYMLG	1QFG.pdb	636	644	3,04	LLLLLEEEE	GPLSGLTLG	2,71
12	20	GGLGGYMLG	1A73.pdb	33	41	2,99	LLEEEEEEE	GGLQGTLC	2,72
13	21	GLGGYMLGS	2IHO.pdb	241	249	3,18	ELLEEEEE	IFCGVMLGV	0,96
13	21	GLGGYMLGS	1TYV.pdb	319	327	3,16	LLLLLEEEE	GVGFGMDGK	0,98
13	21	GLGGYMLGS	1KKO.pdb	352	360	3,17	LLEEEELLL	GMEAYQGGT	1,47
13	21	GLGGYMLGS	2PGC.pdb	160	168	1,70	LLLLLEEEE	NVGNVLLGV	1,58
13	21	GLGGYMLGS	1TYV.pdb	341	349	3,19	LLLLLEEEE	GSGAYLLTH	1,58
13	21	GLGGYMLGS	2FOK.pdb	437	445	3,29	LLEEEELLL	GYRGKHLGG	1,83
13	21	GLGGYMLGS	1A73.pdb	30	38	3,19	EEELLEEEE	PLGGGLQGT	1,91
13	21	GLGGYMLGS	1U6E.pdb	183	191	2,86	LELLLEEEE	GIGPTVAGS	1,91
13	21	GLGGYMLGS	1G6S.pdb	77	85	2,79	LLLLLLLLL	GNGGPLHAE	1,97
13	21	GLGGYMLGS	1TYV.pdb	420	428	2,93	LLLLLLLLL	GLGNIRANS	2,13
14	22	LGGYMLGSA	2PGC.pdb	161	169	1,65	LLLLLEEEE	VGNVLLGVG	1,62
14	22	LGGYMLGSA	1TYV.pdb	205	213	3,15	LLLLLEEEE	KGNVYVIGGR	1,63
14	22	LGGYMLGSA	1ZXX.pdb	63	71	2,87	LLLLLLLLL	VSGTFLYSA	1,87
14	22	LGGYMLGSA	2DEX.pdb	433	441	2,92	LLLLLEEEEL	LGRILFGDS	1,90
14	22	LGGYMLGSA	1WDD.pdb	165	173	3,32	LLLLLEEELE	YGRPLLGCT	1,96
14	22	LGGYMLGSA	2IHO.pdb	242	250	2,64	LLEEEEEEL	FCGVMLGVN	1,97
14	22	LGGYMLGSA	1N7V.pdb	526	534	2,64	LLEEEEEEL	GGVMFIGSA	1,98
14	22	LGGYMLGSA	2HIG.pdb	164	172	3,06	LLLLLLLLL	YGGTILGSS	2,02
14	22	LGGYMLGSA	2B4U.pdb	274	282	3,06	LLLLLLLLL	IGGFYYGEF	2,05
14	22	LGGYMLGSA	2R2C.pdb	78	86	3,07	LLLLLLLLLE	LEGNTLPKS	2,50
15	23	GGYMLGSAM	1VPR.pdb	245	253	3,10	LLEEEEEEE	GNLLGVVW	1,73
15	23	GGYMLGSAM	1WDD.pdb	166	174	3,01	LLLEEELEL	GRPLLGCTI	1,79
15	23	GGYMLGSAM	2PGC.pdb	162	170	2,49	LLEEEEEEE	GNYLLGVGY	1,92
15	23	GGYMLGSAM	1N7V.pdb	527	535	2,52	LEEEEEEEL	GVMFIGSAR	2,35
15	23	GGYMLGSAM	1V8C.pdb	116	124	3,02	LEEEELLEE	GVYRLPGAV	2,36
15	23	GGYMLGSAM	1TYV.pdb	206	214	3,23	LLEEEEEEE	GNYVIGGRT	2,60
15	23	GGYMLGSAM	1DGS.pdb	65	73	3,03	LLLLLLLLL	GARPLEPTF	2,92
15	23	GGYMLGSAM	1HX6.pdb	125	133	2,82	LLLLLLLLL	GAPFLSSMV	2,92
15	23	GGYMLGSAM	1EA5.pdb	118	126	2,13	LLLLLLLLL	GGFYSGSST	2,93
15	23	GGYMLGSAM	2PS1.pdb	115	123	3,21	LEEEEEEEL	GGIIVGSAL	2,97
16	24	GYMLGSAMS	2DLB.pdb	3	11	2,86	LLLLLLLLL	GYLNNIALN	1,28

Q1	QN	Q_SEQ	PDB	R1	RN	ROS	SEC_ST	SEQ	CS
16	24	GYMLGSAMS	1ZK5.pdb	108	116	3,04	EEELLLLL	GWCVGNYVS	2,05
16	24	GYMLGSAMS	1GVE.pdb	75	83	2,80	LLLLLLLL	APMFGKTLK	2,67
16	24	GYMLGSAMS	1EOK.pdb	150	158	2,82	LLLLLLLL	GWYSGSMAA	2,76
16	24	GYMLGSAMS	1UN7.pdb	316	324	2,56	LLELELLL	GTLGSILK	2,83
16	24	GYMLGSAMS	2CME.pdb	27	35	2,24	EEELLLLL	ILRLGSNLS	2,84
16	24	GYMLGSAMS	1SKZ.pdb	12	20	2,66	LLLLLELL	GCPEGSACN	2,89
16	24	GYMLGSAMS	1I4M.pdb	9	17	0,30	LLEELLLL	GYMLGSAMS	3,12
16	24	GYMLGSAMS	2IHO.pdb	244	252	2,67	EEEEEEELL	GVMLGVNKA	3,14
16	24	GYMLGSAMS	1ORO.pdb	109	117	3,18	LLEEELLLL	GNLVGSALQ	3,23
17	25	YMLGSAMSR	1BCP.pdb	50	58	3,18	EEEEEEELL	FCFGKDLKR	2,31
17	25	YMLGSAMSR	2O3I.pdb	166	174	3,10	EEELLLLL	VELGVRMPP	2,37
17	25	YMLGSAMSR	2I0X.pdb	63	71	3,10	EEELLLLL	YKLRSMPPR	2,50
17	25	YMLGSAMSR	1X00.pdb	228	236	2,97	LEELLLLL	VAAPSATSQ	2,72
17	25	YMLGSAMSR	2NW5.pdb	264	272	3,12	EEELLLLL	FVLNTYKSR	2,97
17	25	YMLGSAMSR	2EDM.pdb	103	111	2,77	EEELLLLL	NIKGTMSN	2,98
17	25	YMLGSAMSR	2FJ0.pdb	461	469	2,94	LLLLLLLL	SMLGGHASF	3,03
17	25	YMLGSAMSR	2CME.pdb	28	36	2,17	ELLLLLLL	LRLGSNLSL	3,05
17	25	YMLGSAMSR	1WTH.pdb	356	364	3,19	EEEEELLLL	YMFTNATKL	3,05
17	25	YMLGSAMSR	1QNX.pdb	119	127	3,13	EEEEELLLL	ALTGSTAAK	3,15
18	26	MLGSAMSRP	1VLY.pdb	263	271	3,08	EEELLLLL	LAGSASRLP	1,74
18	26	MLGSAMSRP	1QB5.pdb	80	88	2,99	EEELLLLL	MCASPASSP	2,01
18	26	MLGSAMSRP	2O3I.pdb	167	175	3,15	EEELLLLL	ELGVRMPPP	2,10
18	26	MLGSAMSRP	1BCP.pdb	51	59	3,11	EEEEELLLL	CFGKDLKRP	2,11
18	26	MLGSAMSRP	2FJ0.pdb	462	470	2,91	LLLLLLLL	MLGGHASF	2,67
18	26	MLGSAMSRP	1SV6.pdb	165	173	3,12	EEELLELL	VIGGPAQRP	2,70
18	26	MLGSAMSRP	1K5N.pdb	7	15	2,98	EEEEEEELL	YFHTSVSRP	2,76
18	26	MLGSAMSRP	2HWK.pdb	169	177	3,02	EEELLLLL	VVGEKLSVP	3,02
18	26	MLGSAMSRP	1BHP.pdb	32	40	2,90	EEELLLLL	KLTSGLSCP	3,02
18	26	MLGSAMSRP	1GVH.pdb	347	355	2,89	HLLLLLLL	KLEGAFSDP	3,11
19	27	LGSAMSRPI	1TTU.pdb	169	177	3,19	EEEEELLLL	IGGFVSQRI	2,07
19	27	LGSAMSRPI	1LOW.pdb	100	108	3,11	EEELLLLL	LAEAKTPPF	2,19
19	27	LGSAMSRPI	1YM5.pdb	145	153	2,56	HLLLLLLL	IGLKFIKPP	2,22
19	27	LGSAMSRPI	1PSW.pdb	174	182	2,84	LLLLLLLL	FSLSSERPM	2,31
19	27	LGSAMSRPI	2I2C.pdb	191	199	2,26	LLLLLLLL	VYRTIGSPL	2,35
19	27	LGSAMSRPI	2PZM.pdb	262	270	2,39	HLLLLLLL	VGATLAEPV	2,41
19	27	LGSAMSRPI	1RVK.pdb	345	353	2,93	LELLLLLL	YLKSLSDPM	2,52
19	27	LGSAMSRPI	2GSJ.pdb	106	114	2,40	LLLLLLLL	GGRSSSRPL	2,70
19	27	LGSAMSRPI	2PH5.pdb	178	186	2,87	LLLLLLLL	NGLTINRPK	2,81
19	27	LGSAMSRPI	1UNL.pdb	138	146	2,63	HLLLLLLL	MGNEISYPL	2,82
20	28	GSAMSRPII	1EV2.pdb	104	112	2,90	LLLLLLEE	ERSPHRPIL	1,70
20	28	GSAMSRPII	1WWM.pdb	82	90	2,89	LLLLLLEE	GASPSAPVH	1,76
20	28	GSAMSRPII	1QHO.pdb	493	501	2,86	LLLLLLEE	STSASAPQI	1,77
20	28	GSAMSRPII	1VAV.pdb	108	116	2,75	LLLLLLEE	NSGQAAPLV	2,12

Q1	QN	Q_SEQ	PDB	R1	RN	ROS	SEC_ST	SEQ	CS
20	28	GSAMSRPII	2I2C.pdb	192	200	1,96	LLLLLLLLEE	YRTIGSPLV	2,20
20	28	GSAMSRPII	1PSW.pdb	175	183	2,56	LLLLLLLLEE	SLSSERPMI	2,27
20	28	GSAMSRPII	2P1J.pdb	116	124	2,87	LLLLLLLLEE	GLDWERPVI	2,37
20	28	GSAMSRPII	2PZM.pdb	263	271	2,50	LLLLLLLLLL	GATLAEPVP	2,42
20	28	GSAMSRPII	1NZI.pdb	73	81	2,91	LLLLLLLLLL	SNNPHSPIV	2,54
20	28	GSAMSRPII	1URH.pdb	226	234	2,90	LLLLLLLLEE	GVSYDKPII	2,61
21	29	SAMSRPIIH	2CEO.pdb	342	350	2,87	LLLLLLEEE	NTFLHPPIQ	1,16
21	29	SAMSRPIIH	1EV2.pdb	105	113	2,67	LLLLLLEEL	RSPHRPILQ	1,62
21	29	SAMSRPIIH	1PPR.pdb	152	160	2,76	LLLLLLLLLL	TSAAGPATV	1,74
21	29	SAMSRPIIH	1VAV.pdb	109	117	2,94	LLLLLEEEE	SGQAAPLVK	2,18
21	29	SAMSRPIIH	1ZK5.pdb	121	129	2,94	EEEEEEEEEL	SVHVRPVIL	2,23
21	29	SAMSRPIIH	1Q2L.pdb	240	248	2,79	LLLLLLLLLL	PEITVPVVT	2,28
21	29	SAMSRPIIH	1VLP.pdb	11	19	2,66	LLLLLLLLLL	HHMSEPVIK	2,39
21	29	SAMSRPIIH	2O28.pdb	23	31	2,75	LLLLLLLLLL	TATFSPAIS	2,39
21	29	SAMSRPIIH	1VRB.pdb	180	188	2,56	LLLLLLLLLL	ENVSNPMQH	2,42
21	29	SAMSRPIIH	2DXC.pdb	226	234	2,78	LLLLLLLLLL	VNAKRPVLK	2,43
22	30	AMSRPIIHF	1VI9.pdb	208	216	2,82	EEEEELLLL	HISRPLVDF	1,47
22	30	AMSRPIIHF	2CEO.pdb	343	351	2,77	LLLLLEEEL	TFLHPPIQI	1,56
22	30	AMSRPIIHF	1OHV.pdb	212	220	3,07	LLLLLEELL	SFDWPIAPF	1,70
22	30	AMSRPIIHF	1EV2.pdb	106	114	2,76	LLLLLEELL	SPHRPILQA	1,76
22	30	AMSRPIIHF	1D02.pdb	65	73	2,34	HLLLLLLLH	EIFNPLIDL	1,82
22	30	AMSRPIIHF	2E67.pdb	70	78	3,07	LLLLLLLLLL	PRMRPLTEG	1,95
22	30	AMSRPIIHF	1JQN.pdb	435	443	2,72	HLLLLLLLLL	NSKRPLLPR	2,06
22	30	AMSRPIIHF	2O8B.pdb	735	743	3,17	LEELLEELL	PMCRPVILL	2,22
22	30	AMSRPIIHF	1JFL.pdb	95	103	3,08	HLLLLLELLH	AIKIPIISM	2,24
22	30	AMSRPIIHF	2IJE.pdb	148	156	2,97	LLLLLEELL	NCDPPCVPY	2,37



# Curriculum vitae

## Personal information:

Name: Lukasz Stanislaw Skora  
Date of birth: November 28, 1981  
Place of birth: Gdansk, Poland  
Nationality: Polish

## Education:

2000 – 2004 Undergraduate studies in biotechnology at the Faculty of Chemistry, Gdansk University of Technology, Gdansk, Poland

2004 Exchange student at the Department of Molecular Biology and Genetics, Istanbul Technical University, Istanbul, Turkey

2004 - 2005 Diploma thesis at the Department of Biochemistry and Drug Technology, Gdansk University of Technology, Gdansk, Poland (Dr. A. Skladanowski)  
subject: *Telomerase activity in A549 cells undergoing drug-induced premature senescence.*  
degree: Master of Science (with honors)

2005 – 2009 Ph. D. thesis at the Department of NMR-based Structural Biology, Max Planck Institute for Biophysical Chemistry, Goettingen, Germany (Prof. C. Griesinger & Prof. M. Zweckstetter)  
Subject: *High-resolution characterization of structural changes involved in prion diseases and dialysis-related amyloidosis.*

## Publications

Watzlawik J, Skora L, Frense D, Griesinger C, Zweckstetter M, Schulz-Schaeffer WJ, Kramer ML. (2006). Prion protein helix1 promotes aggregation but is not converted into beta-sheet. *J. Biol. Chem.* **281**, 30242-30250.

Skora L, Cho MK, Kim HY, Becker S, Fernandez CO, Blackledge M, Zweckstetter M. (2006). Charge-induced molecular alignment of intrinsically disordered proteins. *Angew. Chem. Int. Ed. Engl.* **45**, 7012-7015.

Skora L, Schulz-Schaeffer WJ, Griesinger C, Becker S, Zweckstetter M. (2009). Solvent protection of amyloid fibrils of human prion protein provides insight into the pathology of prion diseases. *In preparation.*

Skora L, Becker S, Zweckstetter M. (2009). Observation of flexible regions in amyloid fibrils of human beta-2-microglobulin. *In preparation.*

Skora L, Becker S, Zweckstetter M. (2009). Structure and dynamics of molten globule amyloid precursor states determine the fibril morphology of human beta-2-microglobulin. *In preparation.*